Universität Hamburg
DER FORSCHUNG | DER LEHRE | DER BILDUNG

CHyN
Centre for Hybrid Nanostructures

Labelling of cells with different materials for cell magnetic sorting and X-ray fluorescence imaging studies

Dissertation

zur Erlangung des Doktorgrades

der Naturwissenschaften

(Dr.rer.nat)

dem

Fachbereich Chemie

der Universität Hamburg

vorgelegt von

Bo Peng

Aus

Hubei, China

Hamburg, 2024

The presented work was conducted under the supervision of Prof. Wolfgang Parak at the Center for Hybrid Nanostructures (CHyN) of the University of Hamburg, Germany (from November 2020 to October 2024).

First Evaluator: Prof. Dr. Wolfgang Parak

Second Evaluator: Dr. Florian Schulz

Disputation date:

Examination commission members:

Prof. Dr. Wolfgang Parak (Chair)

Prof. Dr. Wolfgang Maison

Prof. Dr. Nadja Bigall

Date: 21 Feb 2025

Place: Lecture Hall B,

Martin-Luther-King-Platz 6

Index

Abstract

Iron oxide nanoparticles are great promising material in medical application based on its magnetic responsiveness, such as being adsorbed in a magnetic field, and generating heat energy in an alternating magnetic field. Polyelectrolyte capsule is versatility, in microscale the empty core for cargo loading, the polyelectrolyte wall for modify with nanoparticles, the surface for link biomolecular or functional groups. Modified iron oxide nanoparticles on the wall of capsule, used in cell sorting, which is significance in medical treatment and diagnosis, especially the enrichment of rare cells for accurate diagnosis, and overcomes the aggregation of magnetic nanoparticles caused by biological complex environment. In the thesis, the first project, iron oxide NPs were immobilized into the shell of polyelectrolyte capsules, then uptake by Hela cells which used as target cells, and mixed with some cells that do not uptake these capsules, and in these mix cells system the target cells can be separated by magnet adsorption. Two different dyes were loaded into the cavity of the capsule and were uptake by cells for labeling, respectively, and detected by flow cytometer to figure out the target cells ratio. Results indicated capsule-calcein and capsule-cy5 uptake by Hela cells, used as cell label detected by flow cytometer; Capsule-iron oxide nanoparticles uptake by Hela cells, which providing the cells with magnetic properties, can be specifically adsorbed by the magnet from mix cells.

X-ray fluorescence imaging (XFI) is a powerful tool for tracing metal elements, in situ without label. Metal nanoparticles are being developing for cancer treatment and diagnosis, based on the unique physicochemical properties and in nanoscale designs. but there has some limitation in clinical application, the biodistribution after administration and the interaction of nanoparticles with cells. So, in situ assay the location of metal nanoparticles to cellular compartments by XFI is an essential for future nanomedicines[1]. In the thesis, the second project, four different cells: human cervical cancer cell (Hela), rat kidney cell (NRK), mouse fibroblast cell (3T3) and human breast cancer cell (MCF-7), uptake four different metal nanoparticles: gold nanoparticles, iron oxide nanoparticles, sodium yttrium tetrafluoride nanoparticles and titanium dioxide nanoparticles respectively, for XFI

to study metal nanoparticles used as cell label. The results indicated iron and yttrium has a good XFI in cellular, located in cytoplasm; and the location of gold is vague, probably in the nucleus; and titanium is missing the XFI signal by our experimental method. This study proved the XFI technology is hopefully and feasible in study the interaction between metal nanoparticles and cells.

Based on XFI is situ without extra modification in metal elements detection, in the thesis, the third project, we study the in cellular location of metal -based drug by XFI. Cell viability results provide the information of these metal drugs safety treatment concentration for cell; cell uptake results give the metal amount per cell after 24 hours incubate with cell, which provide the guidance for later cell XFI of metal-based drugs.

Zusammenfassung

Eisenoxid-Nanopartikel sind aufgrund ihrer magnetischen Reaktionsfähigkeit ein vielversprechendes Material für medizinische Anwendungen, da sie beispielsweise in Magnetfeldern adsorbiert werden und in alternierenden Magnetfeldern Wärmeenergie erzeugen. Polyelektrolytkapseln sind vielseitig einsetzbar, im Mikromaßstab der leere Kern zum Beladen, die Polyelektrolytwand zum Modifizieren mit Nanopartikeln und die Oberfläche zum Anbinden biomolekularer oder funktioneller Gruppen. Modifizierte Eisenoxid-Nanopartikel an der Wand von Kapseln werden zur Zellsortierung verwendet, was in der medizinischen Behandlung und Diagnose von Bedeutung ist, insbesondere zur Anreicherung seltener Zellen für genaue Diagnosen, und sie überwinden die Aggregation magnetischer Nanopartikel, die durch eine komplexe biologische Umgebung verursacht wird. Im ersten Projekt dieser Arbeit wurden Eisenoxid-NPs in der Hülle von Polyelektrolytkapseln immobilisiert, dann von Hela-Zellen aufgenommen, die als Zielzellen verwendet wurden, und mit einigen Zellen vermischt, die diese Kapseln nicht aufnehmen. In diesem gemischten Zellsystem können die Zielzellen durch magnetische Adsorption getrennt werden. Zwei verschiedene Farbstoffe wurden in die Kapselhöhle geladen und von Zellen zur Markierung aufgenommen und mit einem Durchflusszytometer nachgewiesen, um das Verhältnis der Zielzellen zu ermitteln. Die Ergebnisse zeigten, dass Kapsel-Calcein und Kapsel-Cy5 von Hela-Zellen aufgenommen wurden, die als Zellmarkierung verwendet und mit einem Durchflusszytometer nachgewiesen wurden; Kapsel-Eisenoxid-Nanopartikel wurden von Hela-Zellen aufgenommen, was den Zellen magnetische Eigenschaften verleiht und spezifisch vom Magneten aus Mischzellen adsorbiert werden kann.

Die Röntgenfluoreszenzbildgebung (XFI) ist ein leistungsstarkes Werkzeug zum Aufspüren von Metallelementen in situ ohne Markierung. Metallnanopartikel werden aufgrund ihrer einzigartigen physikochemischen Eigenschaften und in nanoskaligen Designs für die Krebsbehandlung und -diagnose entwickelt. Es gibt jedoch einige Einschränkungen bei der klinischen Anwendung, der Bioverteilung nach Verabreichung und der Interaktion von Nanopartikeln mit Zellen. Daher ist die In-situ-Untersuchung der Lokalisierung von

Metallnanopartikeln in Zellkompartimenten durch XFI für zukünftige Nanomedizin von entscheidender Bedeutung1. In der Abschlussarbeit, dem zweiten Projekt, nehmen vier verschiedene Zellen – menschliche Gebärmutterhalskrebszellen (Hela), Rattennierenzellen (NRK), Mausfibroblastenzellen (3T3) und menschliche Brustkrebszellen (MCF-7) – vier verschiedene Metallnanopartikel auf: Goldnanopartikel, Eisenoxidnanopartikel, Natriumyttriumtetrafluoridnanopartikel und Titandioxidnanopartikel, um Metallnanopartikel, die als Zellmarkierung verwendet werden, mit XFI zu untersuchen. Die Ergebnisse zeigten, dass Eisen und Yttrium ein gutes XFI in Zellen haben, nämlich im Zytoplasma, und dass die Position von Gold vage ist, wahrscheinlich im Zellkern, und dass bei Titan mit unserer experimentellen Methode das XFI-Signal fehlt. Diese Studie hat bewiesen, dass die XFI-Technologie vielversprechend und durchführbar ist, um die Wechselwirkung zwischen Metallnanopartikeln und Zellen zu untersuchen.

Basierend auf XFI in situ ohne zusätzliche Modifikation bei der Erkennung von Metallelementen untersuchen wir in der Abschlussarbeit, dem dritten Projekt, die Position von metallbasierten Medikamenten in Zellen mit XFI. Die Ergebnisse zur Zelllebensfähigkeit geben Aufschluss über die Sicherheitskonzentrationen der Metallmedikamente bei der Behandlung von Zellen. Die Ergebnisse zur Zellaufnahme geben Aufschluss über die Metallmenge pro Zelle nach 24-stündiger Inkubation mit der Zelle und dienen als Orientierung für die spätere Zell-XFI von Medikamenten auf Metallbasis.

1. Introduction

1.1. Iron oxide nanoparticles used in cell sorting

Iron is one of metals to building living organisms, also an important element for various biological process, as a part of hemoglobin to carry oxygen, a part of certain enzymes or protein in cell, such as peroxidase, catalase, and play an important role in biocatalysts and electron transfer in the respiratory chain[2-3]. Iron atoms are not stable in nature and they always exist as oxide form, Iron oxide compound has different types in nature, such as Goethite, Lepidocrocite, Akageneite, Feroxyhyte, Hematite, Ferrihydrite, Magnetite, Maghemite[4]. Among these different forms, hematite (α-Fe_2O_3), magnetite (Fe_3O_4) and maghemite (γ-Fe_2O_3) are popular, and as representatives of ferrimagnetic nanoparticles[4-5], the crystal structures as shows in Figture1-1[6].

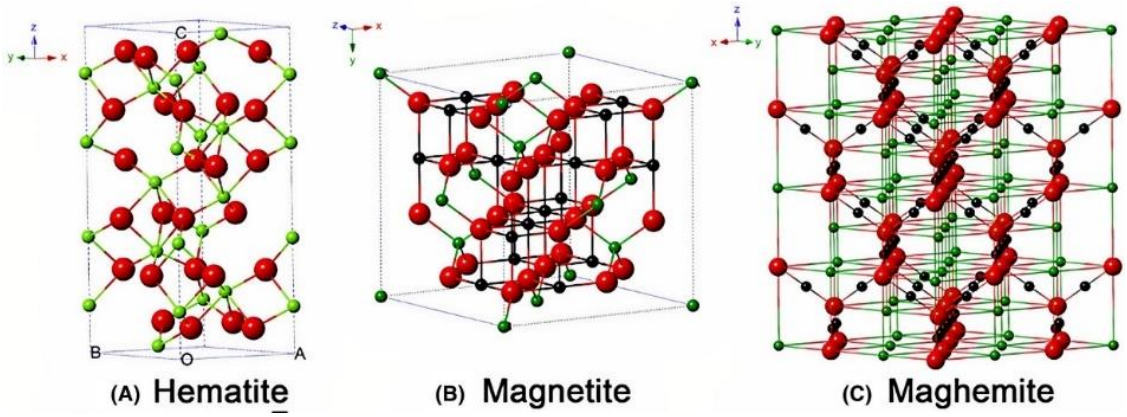

Figure 1-1: Crystal structure of the hematite, magnetite and maghemite, the black ball is Fe^{2+}, the green ball is Fe^{3+} and the red ball is O^{2-}. The figure was extracted from reference[6].

Iron oxide nanoparticles (IONP) as nanocrystals usually are between 1 and 100nm of diameter. In the past decade there has developed various different methods of synthesis shape- and size-controlled, uniform, stability, and monodisperse IONP, reference from [7], these methods mainly include three kinds: chemical synthesis, physical synthesis and biological synthesis. The biological method is using living organisms to synthesize IONPs, this kind living organisms including plants and microorganisms (bacteria[8] and fungi). The physic method includes ball milling method and laser evaporation, the balling milling method is a

top-bottom approach by broking bulk materials into nanoscopic IONPs, and this method is difficult to get desired uniform shape and size particles, the laser evaporation is a bottom-up approach by evaporating a raw material under the focused of laser beam to produce vapor, then the vapors are cooled down in a gas or liquid phase, and lead to the formation of IONPs. The most common methods used in chemistry lab is chemical synthesis, include coprecipitation, microemulsion, sol-gel method, hydrothermal and solvothermal synthesis, and thermal decomposition[7, 9]. The coprecipitation is a method of Fe^{2+} and Fe^{3+} ions coprecipitate to get the Fe_3O_4 nanoparticles. and thermal decomposition method is using iron acetylacetonate as precursor, in an oxygen and water free condition, under high temperature induce thermal decomposition, then obtain the formation of IONPs. Reference from [10] , there has reported different size and shape IONPs, include spherical, cubic, nanoring[11], flower-like, mushroom-like particles, plate-shaped, Nanorod, star-shaped and so on [11-16]. About characterization of IONPs of magnetic properties, is measured by zero-field cooled/field cooled (ZFC/FC, M-T) and hysteresis loops (M-H) curves, based on the response type to the magnetic field, containing ferromagnetic, paramagnetic, antiferromagnetic and ferrimagnetic, and magnetization[7, 17]. Iron oxide nanoparticles stability can be achieved by electrostatic and steric repulsion, it is crucial to stable against aggregation in a biological medium and a magnetic field[18].

IONPs are promising materials for the application in various fields, such as biomedicine (including diagnosis and therapy), biosensing, agriculture, environment, and catalysis, depends on their excellent properties, such as easy of synthesis, low-cost production, good stability, low toxicity, biocompatibility, and magnetic properties. And they have attracted scientist to explore its unique function in the biomedical, and iron oxide nanoparticles obtained the majority FDA-approved in inorganic nanomedicines[19], as contrast agent, drug delivery and thermal-based therapy[5, 20], about application in therapy field depends on its magnetic hyperthermia of superparamagnetic properties under an external alternating magnetic field, IONPs can be heated to terminate cancer cells by localized high temperature of the cancer tissue[21-22]. Diagnosis application in biomedical field depends on its magnetic property, and the biomolecular modified on the nanoparticles' surface, for detecting cells, the biomolecular can specifical bind with the membrane protein of cell, usually this protein is specific expression in cell, named cell label. The detect target also includes DNA/mRNA,

protein, enzymes, and so on. IONP can simplify the process and improve the detection ability of rare target[23].

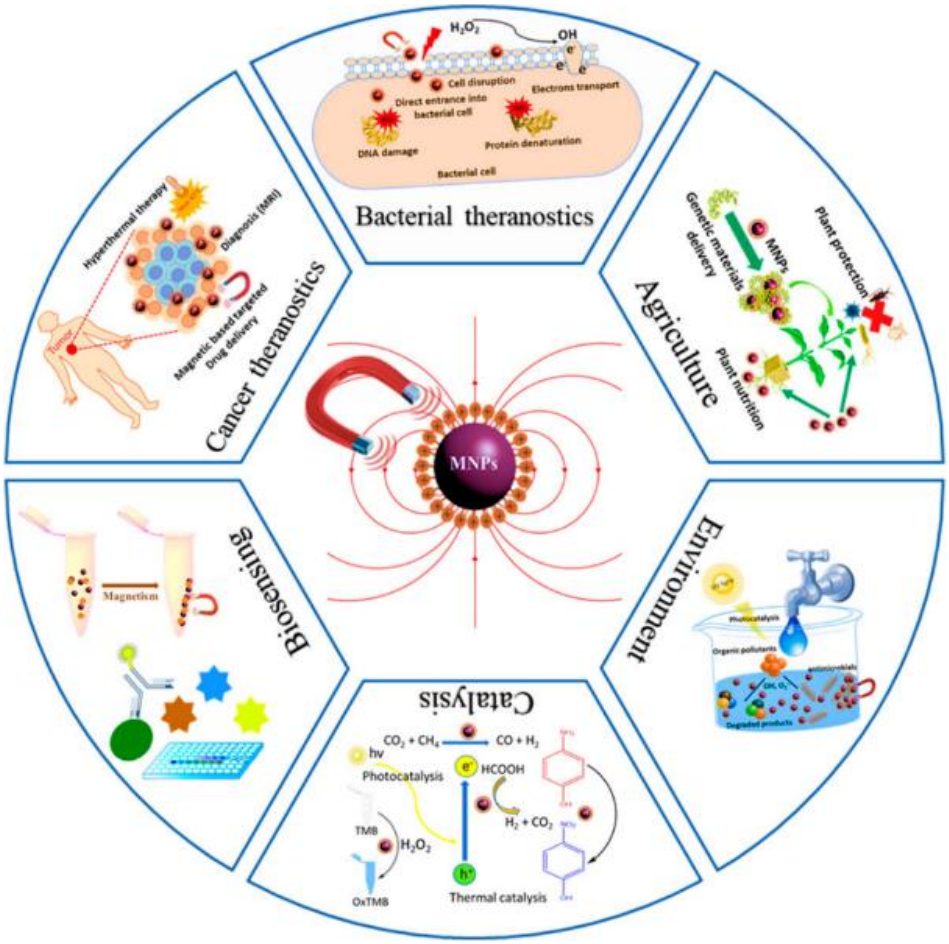

Figure 1-2: the application field of IONPs. The figure was extracted from reference [7].

Biological cells separation and purification are important application in biomedical, including disease diagnostics, cell biology and drug development. The interest cells in a heterogeneous cell population, such as circulating tumor cells in cancer patient[24] or fetal cells in pregnant[25], to isolate and analysis these rare cells is an effective method for the early diagnosis. Based on the cells' size and density sorting cells by sedimentation, filtration, and centrifugation, which is usually used to separate the cells from background media in blood sample. As for further separate cells that without significant differences in size and density, scientist employed other methods including magnetic activated cell sorting (MACS) and fluorescence activated cell sorting (FACS) [26-27]. The process of FACS is to label cells with fluorescent dye, then the labeled cells will be detected by laser beams at high speed, and the cells entrapped

in a droplet buffer will be given an electric charge and then using an external electric field to sort[28], but low throughout lead to require a long time for large sample (up to 2000 cell per second)[29], and the equipment is expensive and difficult to operate requiring highly skilled person, and the fluidic systems require a large volume leading to low sample's recovery. MASC is to entitled cell with magnet, then under magnetic field to sort. Recently, MASC is more and more integrated with microfluidic syatems[30]. Cells internalized magnetic nanoparticles can also be sorted by different internalized amount[31]. Compared with other cell separation methods, MACS have good selectivity by building antibody-antigen binding between cells and magnetic particles, MASC also have specificity by using magnetic force to retaining the target cell and applying shear stress to remove the non-target cell during flushing.

1.2. layer-by-layer assembly Polyelectrolyte capsule

The oppositely charged electrolytes alternate deposition to create a shell of multiples layers, this concept is first described in 1966[32]. In 1997, Mohwald developed the hybrid hollow spheres by polyelectrolyte layer-by-layer (LbL) assembly technique upon colloidal templating[33] and Decher developed the nano assemblies on a solid surface by multilayer polymeric fabrication[34], since that, Layer by layer attaching oppositely charged polyelectrolytes onto a core substrate, then remove the core by decomposition upon solvent, the schematic shown in Figure 1-1 (A), has received tremendous interest, and has several advantages: 1. Synthesis in entirely aqueous solutions, which is same with biomolecules, such as nucleic acids and proteins will denature in nonaqueous solutions; 2. The size and shape of the capsule can be changed by the designed template used for adsorption[35]; 3. The capsule wall can use a large range of polymers to finely tune the permeability, stability, composition and surface function of the capsule. 4. the assembly process is cheap by use simple laboratory equipment and inexpensive materials; 5. LbL assembly capsule shows a significant promise in medical application of delivery drugs[36-39], as shown in Figure 1, the cargo has two methods of encapsulation, which can be a delivery capsule.

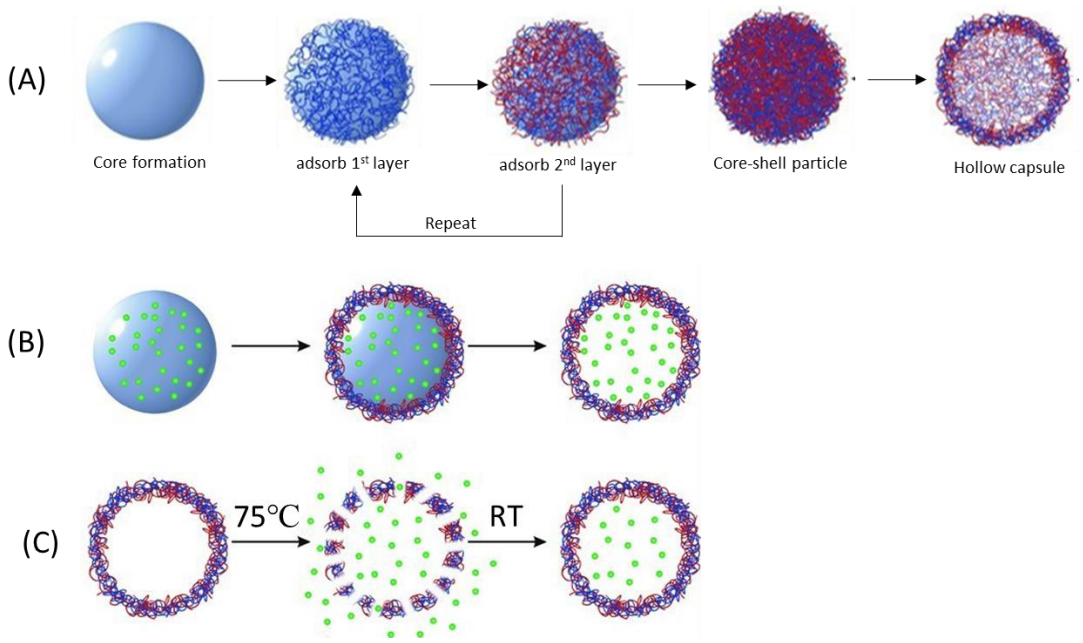

Figure1: (A) layer by layer assembly of polyelectrolyte into a hollow capsule. Cargo encapsulation within layer-by-layer capsules: (B) preloading, before layer-by-layer added dye in the core; (C) post loading, after removing the core, change temperature and increase capsule permeability, then entrapping the dye inside. The picture reference from[36].

The empty core of the capsule can be loaded with different macromolecules, such as dye, enzymes, oligonucleotides or protein, and so on. The polyelectrolyte wall of the capsule, which can modify functional molecules and nanoparticles, such as IONPs used for target sorting, and gold nanoparticles used for light-triggered cargo release. The surface of capsule can be linked with different bioactive macromolecules, such as antibodies and aptamer, which can used for cell-specific binding, reduce non-specific interaction, and polyethylene glycol (PEG) modified on the surface of the capsule can limit interaction with biological environments.

For capsules with cell, from the literature [40], shows there is no significant effect on cell viability on various cell types when incubating with capsules, and not show an increase apoptosis, and capsule used ion cell are immune compatible. And the literature [41] shows the endocytic pathway in the uptake capsule is phagocytosis, based on the electrostatic interaction inducing the nonspecific interaction of capsule with cell, then cell membrane

forms a phagocytic cup to stabilize the capsule on the membrane by actin reorganization and filopodia formation, then cytosolic invagination, then the capsule are transported to the acidic vesicles of perinuclear cytoplasm, then capsule reach the final position heterophagy lysosomes by active the phagocytic machinery. By modifying gold nanoparticles in the wall of capsule, this capsule can be transfer to a plasmonic materials, then release the cargo by triggered of ultrasound, light or microwaves[42-44]. And the literature [45], shows capsule endocytosis into cell, then transfer to endosome , then transfer to acid environment of lysosome, and these capsule work as pH-sensor in situ to monitor the pH value inside cell.

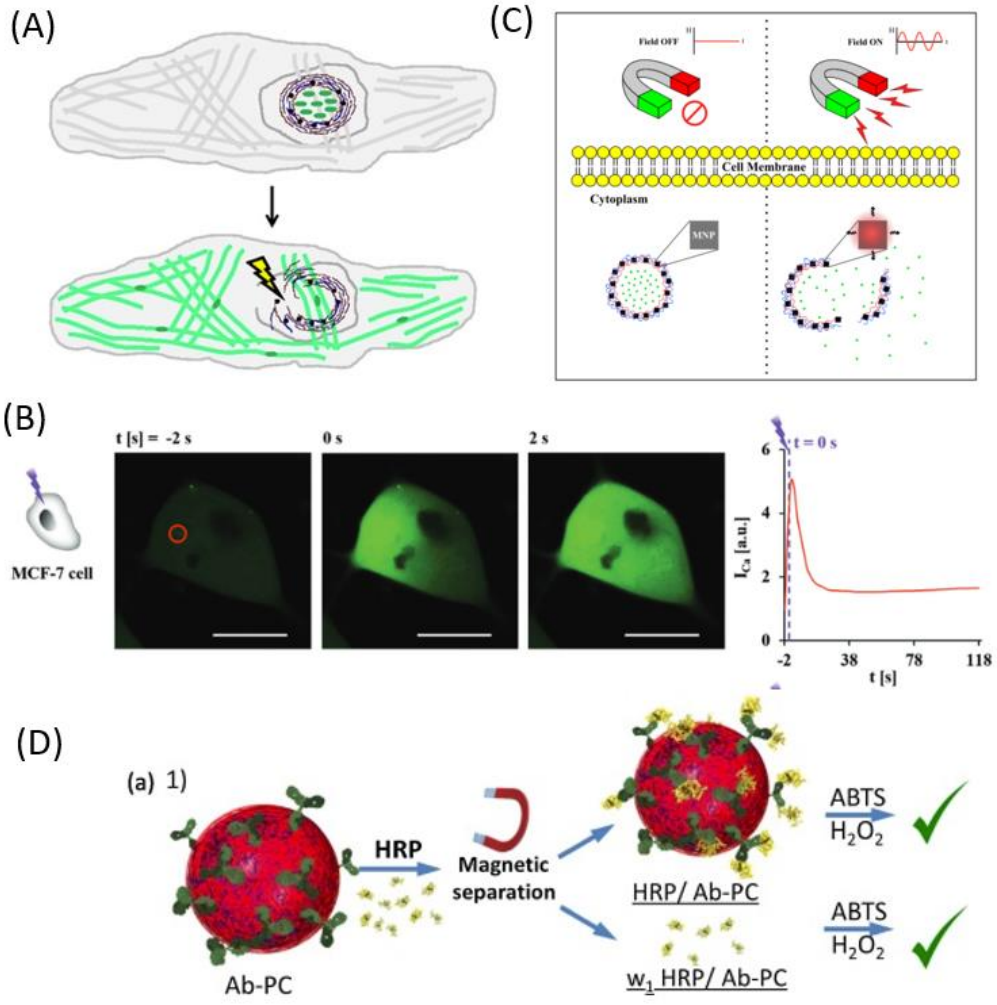

Figure: several modifications for the functional of the capsule, and their application: (A) (B) . Capsule broken of the plasmonic nanoparticles generated heat by a light trigger, then the dye will be released to stain cell; (C) capsule broken of magnetic nanoparticles generated

heat by alternating magnetic field, then the dye will be released to stain cell; (D) modified antibody on the surface and modified magnetic nanoparticle in the wall, to separate protein by a magnetic field.

(A) picture is reference from [46]; (B) picture is reference from[44]; (C) picture is done by Leroy Nack; (D) picture is reference from [47].

Polyelectrolytes used in synthetic must have a number of charged groups, as shown in Figure 1-3. The polymers are various in properties of biodegradation and stability, some can be biodegradability, such as alginate (ALGI-), dextran (DEXS-), poly-L-arginine (PARG+) and chitosan (CHI+). Some polymers cannot be in cellar degrade, include polyacrylic acid (PAA-), polyethyleneimine (PEI+), poly (allylamine hydrochloride) (PAH+), poly (styrene sulfonate) (PSS-), poly- (diallyl dimethylammonium chloride) (PDADMAC+) and poly (vinyl sulfate) (PVS-). These polyelectrolyte layers are assembled onto a solid surface by electrostatic interaction force, and highly dependent upon solution's ionic strength, pH, temperature etc physiochemistry properties. capsule's wall has high semipermeable property, when the solution's pH value become down and temperature become high, the cargo inside the capsule are easy to release, and there has high release rates for water soluble molecules with molecular weights below 5 kDa[48], and for large molecules of molecular weights above 10 kDa can stable keep inside the capsule[49]. In our lab, we usually use centrifugation method to synthesis capsule as shown in Figure 1-4.

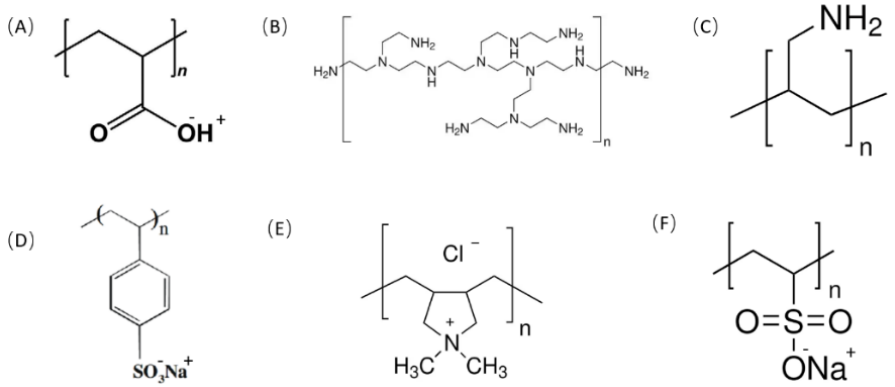

Figure 1-3: Chemical Structure of some electrolytes, (A) polyacrylic acid (PAA), (B) polyethyleneimine (PEI), (C) poly(allylamine hydrochloride) (PAH), (D) poly(styrene sulfonate) (PSS), (E) poly-(diallyl dimethylammonium chloride) (PDADMAC) and (F)

poly(vinyl sulfate) (PVS).

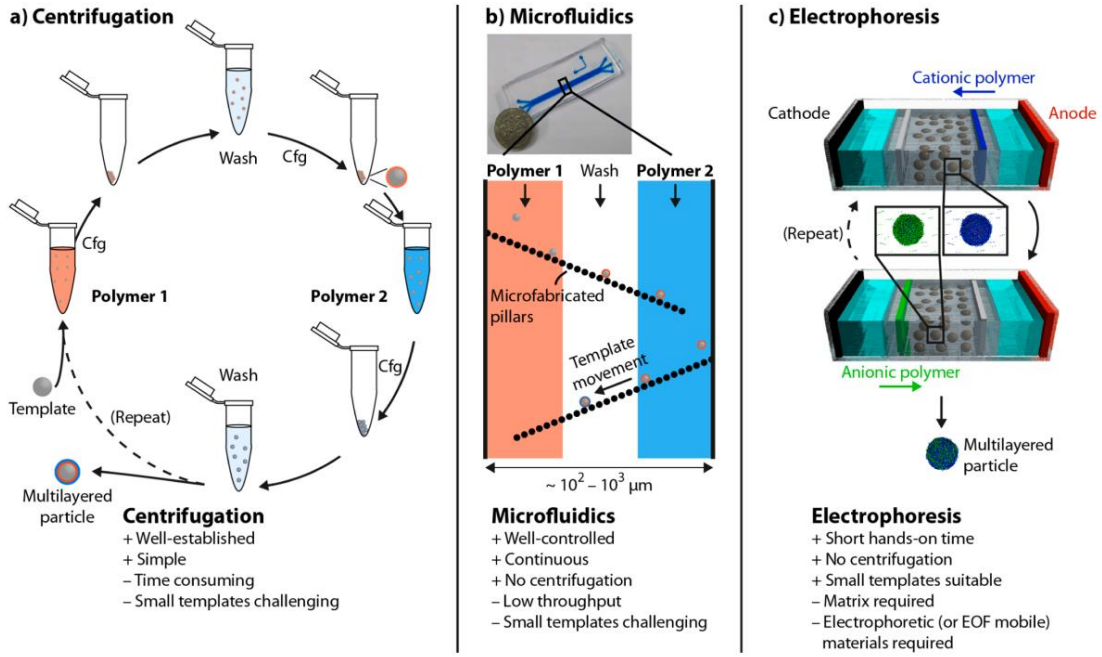

Figure 1-4: several method for layer-by-layer assembly of capsule, reference from [38].

1.3. Flow cytometry

Flow cytometry is a technology for cells or particles under fast linear flow conditions to simultaneously conduct multi-parameter, rapid quantitative analysis and sorting[50-51]. It is widely used to analyze the expression of cell surface and intracellular molecules, identify and determine cell types in heterogeneous cell populations, evaluate the purity of isolated populations, and analyses cell size and heterogeneity. And it can analyze multiple parameters of single cells simultaneously[52]. The work principle is to measure the fluorescence intensity produced by fluorescently labeled antibodies or fluorescently molecular to detect proteins/ DNA. So, it is important to stain cells with fluorescence material, and prepare a single cell suspension from cell culture and tissue samples. Then the sheath fluid brings the cell suspension pass through the laser beam one cell at a time, then the detector detects the forward and side scattered light, as well as the fluorescence emitted by the stained cell. The forward scattered light is detected in the form of FSC, which is related with cell's size, and the side scattered light is detected in the form of SSC, which is related

with the granularity of the cell. Fluorescently stained cells or particles are detected individually. The forward and side scattered light and the fluorescence emitted by stained cells are separated into predetermined wavelengths and assigned channels by a set of filters and mirrors in the flow cytometer. The fluorescence is filtered so that each sensor detects only fluorescence of a specific wavelength. These sensors are called photomultiplier tubes (PMTs). Present in the computer is dot plot, each dot represents a single cell detected by the flow cytometer[53-55].

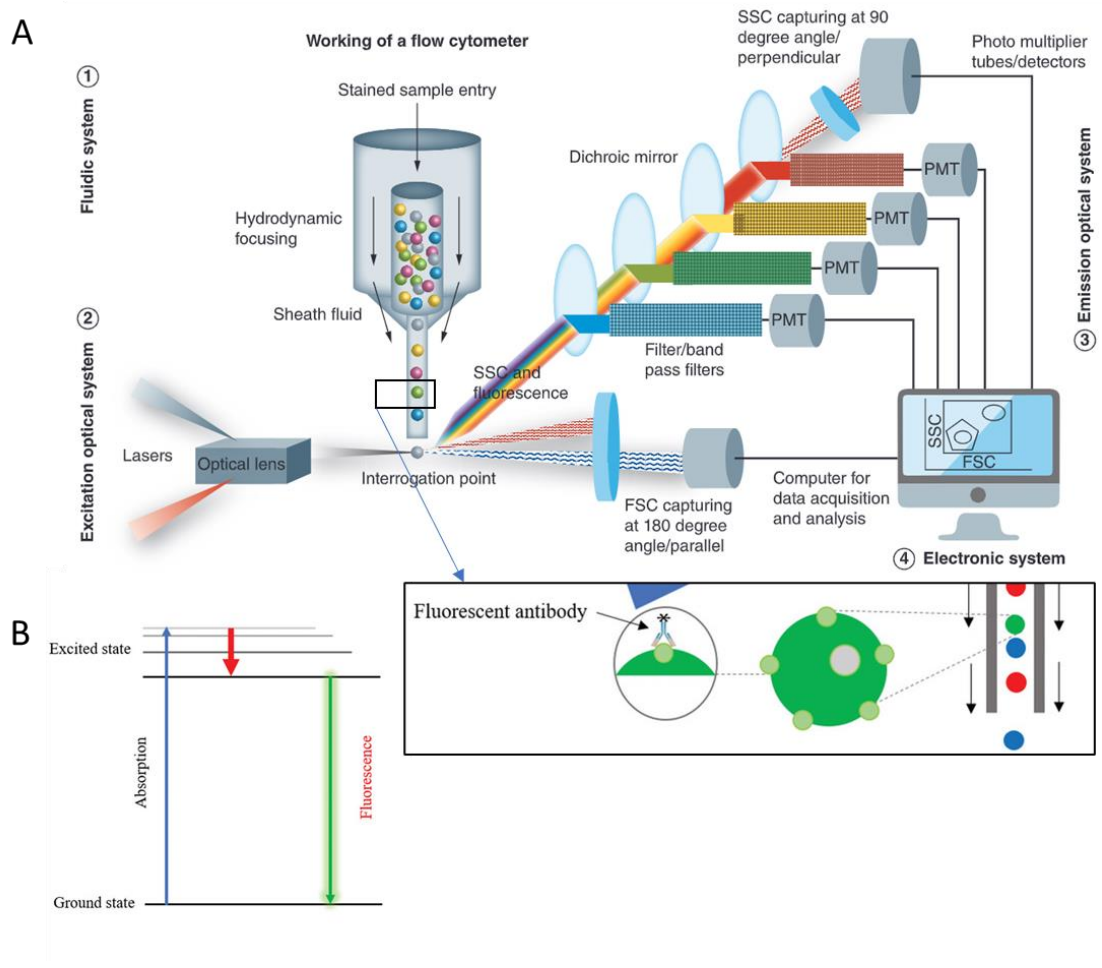

Figure: (A) the principle of a flow cytometer; (B) the principle of fluorescence emission: after being excited by light absorption (blue arrow), the electron transits to an excited state of lower energy (red arrow), then emits photons when it drops down to the ground state (green arrow). the picture is reference from [51] [50].

1.4. Inductively coupled plasma mass spectrometry measurements

For fast multi element determination of heavy metals in different sample matrices, ICP-MS is one of the most sensitive analytical techniques in trace and ultra-trace concentrations. ICP-MS including, a liquid sampler, pump, nebulizer, spray chamber, argon gas torch inlets, torch, sampler cone, skimmer cone, ion lenses, quadrupole mass analyzer, electron multiplier detector and data collection, shown in Figure 1-4. Pump, nebulizer and spray chamber is used for introducing liquid samples into the plasma by pneumatic nebulization[56-57]. Argon will produce plasma under torch, which's temperature ranges from 6 to 10*10^3 K, suitable for atom excitation and elemental ionization. Sampler cone and skimmer cone extracted these ions into the low-pressure mass spectrometer interface. Ion lenses, quadrupole mass analyzer and electron multiplier detector make up the mass spectrometer, ion lenses are used for focus ions on the mass analyzer, quadrupole mass analyzer are used for separate these positively charged ions according to their mass to charge ratio, electron multiplier detector will detect the ions and collected the signals. ICP-MS can used for determine the amount of elemental present in vitro based uptake studies, also can used for determine the amount of elemental released from NPs.

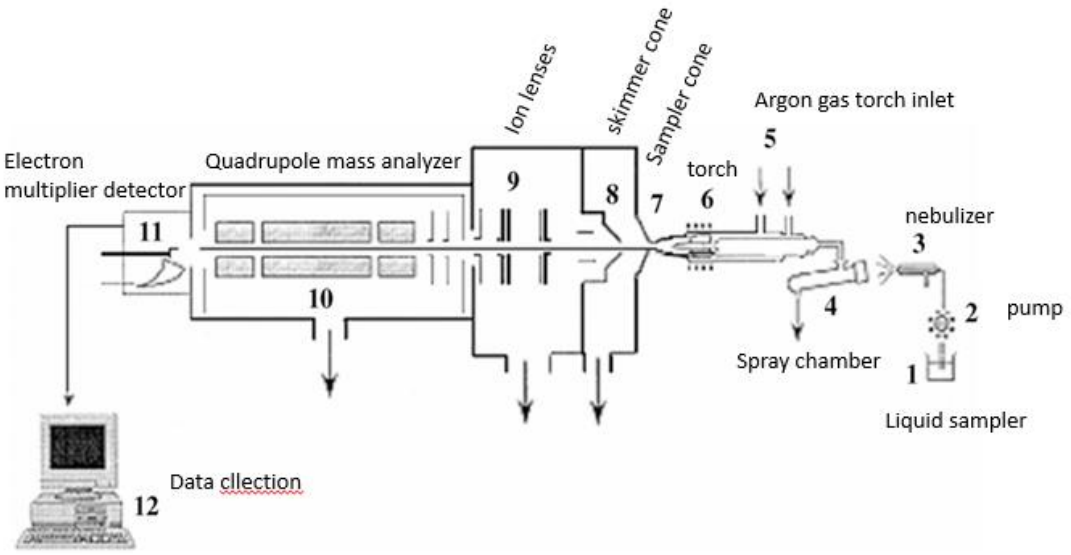

Figure 1-4: schematic diagram of inductively coupled plasma-mass spectrometer, The figure was extracted from reference[57].

For sample preparation, collected samples was digested by performed with freshly prepared aqua-regia (HCl: HNO_3 = 3:1) for overnight or longer, then added 3mL 2% HNO_3 solution to

digested samples, used for ICP-MS analysis.

For sample analysis, using a freshly prepared serial dilution of element to construct a calibration curve, different element concentrations starting from 0 ppb to 2500 ppb or 0 ppb to 500 ppb. The auto-tuning solution (Agilent for ICP-MS 7500cs) with a standard concentration of 1 μg/L of Ce, CO, Li, Mg, Ti, and Y, which was used to set the general background, also to calibrate the strength and frequency of electrical field of lenses and the quadrupole field. After the sample goes through a series of processes, it is finally counted by the detector, then using the calibration curve transferred the count values into elemental concentrations, multiplied by the dilution factor to get the actual elemental concentration in sample.

1.5. X-ray fluorescence imaging for cell

The nature of X-rays is high-energy electromagnetic radiation with wavelength ranging from 10 nm to 0.01nm, and photon energy ranging from 0.1keV to 100keV. The diameter of atoms is ranging from 0.05nm to 0.5nm. electromagnetic waves with high photon energy (above 5-10keV) and shorter wavelength (below 0.2-0.1nm) are called hard X-ray, and those with lower energy and longer wavelength are called soft X-ray[58]. So hard X-ray can be used for atom level research. And Hard X-ray has penetrating ability, are widely used to image the inside of the object, have good biological penetration depth for large cells, tissue and organisms, e.g. computed tomography (CT)[59] and airport security, this technique is depend on the X-ray attenuation is different in different elemental composition and subject density, for CT tissue image principle, C, H, O and N elemental is the mostly of biology tissue, and bones contain high Ca and high density.

In detail, as shown in Figure 1-5, X-ray can carry enough energy to excite electrons located in orbitals of heavy elements atoms, and electronic transitions between valence orbital generate optical signal[60], then detect the signal of element specific X-ray emission.

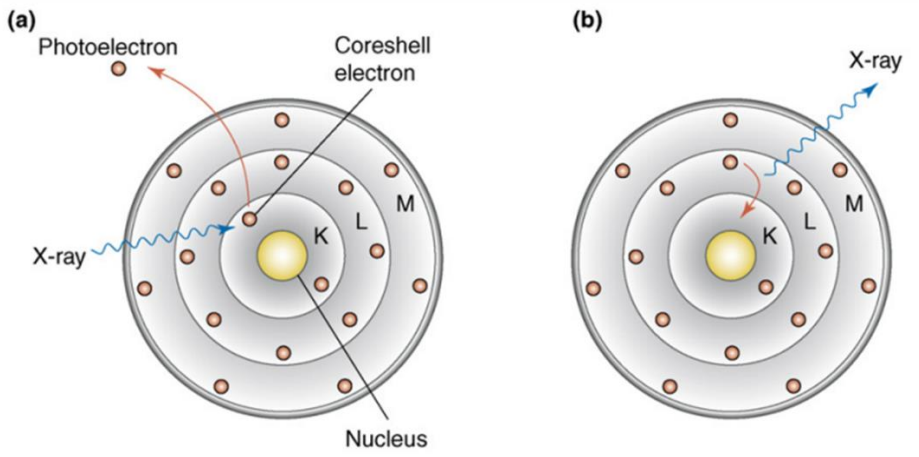

Figure 1-5: principle of X-ray fluorescence generation illustrates by Bohr atomic model: an electron ejects from an atom by X-ray excitation, another electron from a higher shell fills this vacancy, resulting a photon emission. This picture is reference from [60].

So based on X-ray technique, XFI (X-ray fluoresce imaging), can used for directly detection of the elemental components of nanoparticles in situ/in vivo[61], to study the biodistribution and Fate of nanoparticles (degradation) in biological samples, also including NP-based drugs location, qualification, state, and supramolecular arrangement for provide important information. There are some limitations for X-ray application in biological samples: large biological samples absorb and scatter the signal, slow acquisition (especially for high resolution and large field of view), resolution depends on the size of the beam, hard to detect cell organelles (now only distinguish nuclear and cytoplasm); for the advantages, it's a good imaging method for mental nanoparticles, and the emission signal is elemental specific, it reflects the original signal of material in suit and in vivo. The XFI can be used for observing the colloidal properties of nanoparticles[62], and the biotransformation of nanoparticles[63] [64-65]in biological environment, and study the nanoparticles distribution in plant combined with mass spectroscopy[66], and tracking immune cell in vivo in situ in mice[67-68] . So, the X-ray will have an important, fundamental roles in the nanomedicine toward its maturity[69].

Animal cell will division[70] , gene expression of functional control, senescence and apoptosis, these activities are the life of cells. Bio membranes composed of lipids divide cells into different compartments, the element consist of animal cell are mainly C, H, O and N, the

molecular are mainly protein, nucleic acid, lipids and sugars. And some metal cations are trace amount in cell but are also an important component that is essential for life activities: Na+(maintaining membrane potential) 、 K+ (Participates in protein and some enzyme synthesis) 、 Ca2+(component of calmodulin, actomyosin, and ATPase) 、 Fe2+ or Fe3+ (Components of hemoglobin, cytochrome, peroxidase and ferritin) 、 Zn2+ (compound of Zn-finger proteins of many transcription factors) 、 Cu2+ (Component of tyrosinase, ascorbate oxidase) and so on. For trace metal elements in animal cell with an x-ray fluorescence imaging, which is belong to the field of inorganic physiology[71]. And zinc ion stabilizes the structure of DNA and RNA, so it is present in the chromosomes, cell nucleus and nucleolus[72], and it is also tightly bound with the enzymes of DNA and RNA synthesis, RNA polymerase[73], reverse transcriptase and transcription factor[72], form different structures of functional importantly for the enzyme[74-75]. Zn emission intensity will change at different stages of the cell cycle by cell XFI, from this literature[76]. So, scientists use Zn signal marker the location of nucleus. Potassium ion intracellular is necessary for ribosomal integrity[77], and stimulates in corporation of amino acids into polypeptides[78], so it is important in the control cell differentiation[79], and decrease of Potassium ion concentration intracellular will induce call apoptosis[80-81], ribosome is stay in cytoplasm for synthesis polypeptide, so scientist use K signal marker the location of cytoplasm. From the report of I L Cameron et al.[82], the different cell type has different elemental X-ray spectroscopy of concentration, which allow to distinguish the cell type[82], and the elemental concentration has high relationship with the cytoplasmic regions' ultrastructure[82].

(A)

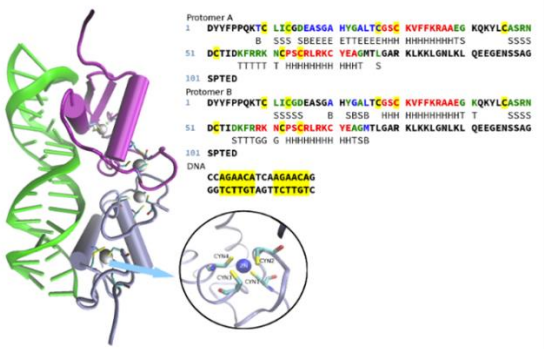

(B)

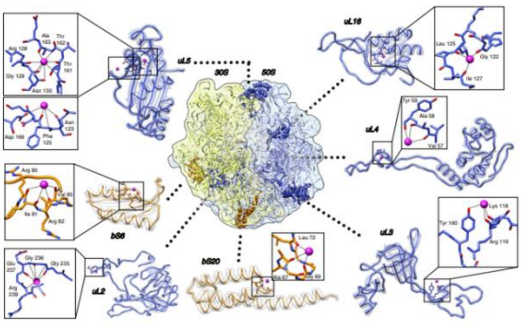

Figure 1-6: （A) Zinc finger complex structure, zinc ion (silver ball) coordinate with four cysteine residues stabilizes the protein-DNA binding complex. this picture is reference from[83]. (B) Potassium ions (red ball) as structural support element to interact with the subunit of ribosome. this picture is reference from[84].

1.6. Motivation of this study

Nanoparticles have been extensively studied in the past few decades and are now being developed for the diagnosis and treatment of diseases. Cancer cell lines are used as models in basic research to study the interaction between nanoparticles and cells, laying the foundation for the development of nanomedicine.

1.6.1. application of polyelectrolyte capsule for target cells magnetic sorting.

Scientists have conducted extensive research on magnetic iron oxide nanoparticles over the past few decades, using various methods: surface modification[85], size control, and adjustment of particle components[86] to enhance their stability, dispersibility, and biocompatibility in biological systems. Ultimately, it is expected that these nanoparticles can be used in medical diagnosis and treatment[87]. Polyelectrolyte capsules assembled by electrostatic interaction are a versatile carrier for biological environments[39]. Magnetic iron oxide nanoparticles are modified on the capsule wall to give the capsule magnetism. When the magnetic capsules are added to the cell culture medium, they will be internalized by the cells[88]. And our research is focus on the internalized cells, to explore whether these cells can be captured in a magnetic field and whether they can be captured in a complex mixed cell system, and to provide some basic research for the use of magnetic nanoparticle-modified capsules in future biomedical diagnosis and treatment.

1.6.2. label cell with different nanoparticles for x-ray fluorescence imaging.

In cell biology, studying the structure and function of cells can reveal some of the fundamental principles of life at the micro, nano and molecular levels. Microscopy is an important imaging technology to explore microscopic structures. To research the

intracellular distributions of nanoparticles in cancer cell lines is essential for improve the nanomedicine design. The energy of Hard X-rays is 5 keV and higher, they are highly penetrating. X-rays with energies of about 15 keV can penetrate more than 1 cm of tissue. X-ray with strong energy to excite the inner electron of metal element, then detect the fluorescence emission energy, reflect the element information. so, for in suit and in vivo analysis nanoparticles position intracellular it is necessary using X-ray fluorescence imaging. Cell-labeling nanoparticles in biological imaging and diagnosis has aroused great interest. Different cells labelling with different nanoparticles can be used to simultaneously identify and distinguish multiple cell types in the same image. This multi-labeling capability is particularly important for studying cell heterogeneity and interactions in complex biological systems. It can provide new experimental methods and tools for exploring complex problems in cell biology, such as cell signaling, cell-cell interactions, etc.

1.6.3. label cell with drug-based drug for XFI.

Metal-based drugs, because metal groups have high X-ray absorption capacity and unique X-ray fluorescence spectra, can provide high-contrast images in X-ray fluorescence imaging, label cell with metal-based drug for XFI can monitor the distribution of drugs in cells in suit, by studying the location of metal-bearing drugs in cells, we can gain insight into the biological processes inside cells, such as how drugs affect cell function and metabolism. Such studies help reveal the mechanisms and interactions of cells. They can also help study the mechanism of action of drugs. For example, drugs may act in specific parts of cells (such as endosomes, mitochondria, etc.), and understanding these details can help reveal their biological effects, providing some information for basic scientific research, and helping optimize the design of drugs to ensure they are effective at their target sites.

we hope our study will help for find some new and make small contribution for the application of nanoparticles in the biomedical field.

2. Application of Polyelectrolyte capsule for target cells magnetic sorting

2.1. Introduction

Capsule has many advantages for its versatility, polymer can be degradable or undegradable, polyelectrolyte layers number controlling the capsule's stiffness, loading capsule with macromolecules, different bioactive molecular or functional groups linked to the surface, in the wall of capsule modifying nanoparticles with different composition and size. In here, PSS and PAH used as material of synthesis capsules, and calcein and cy5 as cargo, post loading in capsule, because these two kinds dye has different excitation and emission, which is convenient for later specific detection. Magnetic nanoparticles have magnetic responsiveness, for extract target substances. Modify diameter ca. 30nm magnetic nanoparticles in the wall of capsule, then the magnetic- capsule diameter is about 5 μm, which will more stable than only use IONPs since its easy agglomeration in salt cell medium. By the magnetic responsiveness, as a tool for controlled drug delivery and to sorting rare cell in biological environment[89-90], which will help for early cancer founding, non-invasive prenatal diagnosis and so on medical diagnosis. So, in here, we use a simple equipment and connect with flow cytometer to do magnetic-capsule for target cell sorting in a mix cell system, and target cells and background cell are modified with two different capsule-dye.
Whether there has a better magnetic responsiveness when same number of nanomagnets modified in the wall than a magnetic bead containing same number of nanomagnets? then by the same way to test the difference between magnetic-capsule and magnetic nanoparticle.

2.2. Major regents

2.2.1. Regents used for synthesis experiment

Calcium chloride (CaCl2, CAS number 10043-52-4, Sigma Aldrich), sodium carbonate (Na2CO3, Sigma Aldrich), poly (sodium 4-styrenesulfonate) (PSS, Mw: 70000, CAS number 25704-18-1, Sigma Aldrich), poly (allylamine hydrochloride) (PAH, Mw: 15000, Sigma

Aldrich), ethylenediaminetetraacetic acid disodium salt dihydrate (EDTA (disodium salt), #6381-92-6, Sigma Aldrich), used for synthesis capsule.

Calcein (CAS number 154071-48-4, Sigma Aldrich), Sulfo-Cyanin5 (Lumiprobe, German) used for synthesis capsule-dye.

Benzyl ether (CAS Number 103-50-4; Lot# SHBL6366), biphenyl-4-carboxylic acid (CAS number 92-92-2), iron (III) acetylacetonate ($Fe(acac)_3$; CAS Number 14024-18-1; Lot# MKCK7101), oleic acid (OA, CAS number 112-80-1) used for synthesis iron oxide nanoparticles.

poly (isobutylene-alt-maleic anhydride)-nitrodopamine (PMA-ND) used for coating iron oxide nanoparticles.

2.2.2. Regents used for cell experiment

Name	Company	Function
RPMI 1640 medium	Sigma aldrich	For cell culture
Phosphate buffered saline	Invitrogen	For cell experiment
bovine serum albumin	Sigma	For cell experiment
0.05% trypsin/EDTA	Thermo fisher	For cell culture
Fetal bovine serum	Biochrom	For cell culture

2.3. Abbreviations

PSS	poly (sodium 4-styrenesulfonate)
PAH	poly (allylamine hydrochloride)
EDTA	ethylenediaminetetraacetic acid
ICP-MS	inductively coupled plasma mass spectrometry

FeOx NPs	Iron oxide nanoparticles
PMA	An amphiphilic polymer based on a backbone of poly(isobutylene-alt-maleic anhydride) and a hydrophobic side chain
PBS	Phosphate buffered saline
TEM	Transmission electron microscopy
+M	Collected solution sample when attach with magnet
-M	Collected solution sample when not attach with magnet

2.4. Key instruments

Name	Model	Company	Function
Dynamic light scattering (DLS)	NANO 25	Malvern	NPs characterization
Transmission electron microscopy (TEM)	JEM-1400PLUS	JEOL	NPs characterization
Fluorescence meter	Florolog-3	Horiba Jobin Yvon	Capsule-dye characterization
Confocal microscopy	LSM 510	Carl zeiss Microscopy GmbH	Capsule-dye characterization
Indcuctively coupled plasma mass spectrometry (ICP-MS)	7700 Series studies	Agilent	get Mental content per cell
Flow cytometer	BD LSRFortessa	BD Biosciences	Get different cell ratio

2.5. experiments and methods

2.5.1 Synthesis of iron oxide nanoparticles

0.70 g (2mmol) Iron (III) acetylacetonate ($Fe(acac)_3$; CAS Number 14024-18-1; Lot# MKCK7101) as precursor, and 10.42g (52.6 mmol) benzyl ether (CAS Number 103-50-4; Lot# SHBL6366) as solvent, 1.1g (3.89 mmol) Oleic acid (OA; CAS Number 112-80-1) and 0.4g (2mmol) biphenyl-4-carboxylic acid (CAS Number 92-92-2; Lot#S29012V) as ligand. The four compounds are mixed together in a three-neck glass flask. The mixture in 90℃, at 500 rpm stirring, was degassed for 45min, remove the oxygen. Then switch to nitrogen atmosphere for 1min, and repeat this for 3 times for remove residual oxygen. Then the mixture was heated from 90℃ to 292℃, at a rate of 20℃ per min, simultaneous continuous under nitrogen atmosphere. Then kept it reflux at 292℃ for 30 min. Then wait it cold down to room temperature, before this temperature not remove the nitrogen system. Then add 70mL acetone (CAS Number 67-64-1) in the particle solution, done centrifuge at 6000rpm for 5min, kept the precipitate and discarded the supernatant, repeat this for 3 times, then dissolved in 25mL chloroform (CAS Number 67-66-3). The glass used in synthesis iron oxide nanoparticles was first rinsed with aqua regia and then with Millipore water before use.

2.5.2. Iron oxide nanoparticles transfer from organic to water solvent

Before this we do ICP-Ms got the concentration of iron element, is 4mg Fe per milliliter solution. Then I took out 5mL iron oxide nanoparticles including of 20mg Fe, which were mixed with 15mL ethanol, done centrifuge at 9000 rpm for 5min, kept the precipitate and discarded the supernatant. Then the precipitate dissolved in 1mL tetrahydrofuran (THF), simultaneous prepared 33.33mg poly (isobutylene-alt-maleic anhydride)-nitrodopamine (PMA-ND) in 2mL THF. Then mixed the two solutions, and for better dispersion, before and after mixed, putted the iron oxide nanoparticles in sonication for 5min. Then add 5mL ethanol in mixture system, then kept it shaking for 3 hours. Then the solution was added 20mL n-hexane and centrifuged for 1 min at 4000rpm, discarded the supernatant, and resolved the precipitate in 3mL (2M) NaOH, and redispersed by sonication, then centrifuged at 5000rpm for 3:30min, kept the precipitate, added 3mL Millipore water, centrifuged at 5000rpm for 3:30min to wash this for 2 times. Finally, dissolved the iron oxide nanoparticles

in 5mL water in a glass vial for store.

2.5.3. Synthesis of capsule

10 mg/mL Poly (allylamine hydrochloride) (PAH, Mw ≈ 17.5 kDa, CAS Number 71550-12-4) in 0.05M NaCl (and control the solution at 6.4 Ph) as positively charged polymer, 10mg/mL poly (sodium 4-styrenesulfonate) (PSS, Mw ≈ 70 kDa, CAS Number 25704-18-1) IN 0.05M NaCl (and control the solution at 6.4 Ph) as negatively charged polymer. Mixed 1mL Na_2CO_3 (0.33M) and 1mL $CaCl_2$ (0.33M) under kept stirring at 1000rpm for 30 sec, then turned off the stirring and kept mixture still for 2:30min, then washed with Milli-Q water for three times by centrifuge and discarded the supernatant. The action of transfer the mixture from still to wash should quickly, this step is critical for the $CaCO_3$ core's size. Subsequently, layer by layer assembly of a polymer shell was by addition of oppositely charged polymer solutions to the cores. 2mL aforementioned PSS solution added into the $CaCO_3$ precipitate, then sonicated for 3min, shanked 10min, and wash three times with Milli-Q water for three times. Follow this, added 2mL aforementioned PAH solution into the precipitate, then sonicated for 3min, shanked 10min, and wash three times with Milli-Q water for three times. Repeat add 2mL PSS and 2mL PAS alternately for four times. Then add 2mL ethylenediaminetetraacetic acid (EDTA, 0.2 M, pH 7) in the precipitate for overnight, which was order to complexation of Ca^{2+}. The next day, centrifuged the mixture solution at 1700rpm for 5 min, and wash with Milli-Q water by centrifuge for 3times. Finally, the capsules are placed in 2mL water and stored at 4 ℃.

2.5.4. Synthesis of capsule-iron oxide nanoparticles

After added second 2mL PSS and 2mL PAH in the process of synthesis capsule, added 1mg the iron oxide nanoparticles decorated with PMA, in Milli-Q water solvent, instead of adding 2mL PSS, then sonicated for 3min, shanked 10min, and wash three times with Milli-Q water. Then added 2mL PAH in the precipitate, and repeat sonicated and shanked, repeat add particles and PAH once again. Finally, add 2mL EDTA for overnight to remove the $CaCO_3$ core. The next day wash the capsule-iron oxide nanoparticles with the milli-Q water to remove the EDTA.

2.5.5. Synthesis of capsule-Dye

The capsule store in the water, and transfer to dye solution, kept in room temperature for 1 hours and avoided light, then put the mixture solution in the metal bath for 90min at 75℃. Then wash with Milli-Q water to remove the free dye.

2.5.6. Use Miltenyi MS column to separate target cells which uptake capsules-iron oxide NPs

The first day, count the Hela cells and culture 300 000 cells in each well in 6-well plate; The second day, change the medium, and capsule-magnetic NPs are added to the Hela, the addition amounts of capsule-magnetic NPs is the different ratios of capsules per cell: 0, 1:1, 2:1, 4:1, and 8:1. The capsule-magnetic NPs were added to the Hela cells and incubated for 24 h at 37 ℃ / 5% CO2; The third day, wash cells with PBS for three times , then detached them with 500µL 0.05% Trypsin (2 min at 37 ℃). Trypsin was stopped with 500µL medium+ and the number of cells counted with a counting chamber (initial number of cells, I);

Prepare MS Column by rinsing with buffer: apply 500 µL of buffer (PBS with 0.1% BSA) on top of the column and let the buffer run through. And attach the MS column vertically to the magnet;

Repeatedly pipetting the above cells to suspend and disperse the cells, and add the above cells onto the prepared MS Column respectively.

Then wash MS Column with 3×500 µL buffer, collect the effluent solution, marked as +M;

Remove MS Column from the magnet and place it on a new collection tube. Pipette 1 mL buffer onto the MS Column. Immediately flush out fraction with the magnetically labeled cells by firmly applying the plunger supplied with the column. collect the solution that flows out at this point, marked as –M;

Centrifuge the +M and –M at 300 rcf and 5 min, gently take out supernatant, and pipette into 1 mL buffer, then count the cells under a microscope with a counting plate.

2.5.8. magnetic cell sorting by attach with magnet

As show in Figure 2.5.1, Usually we prepare a 600µL cell suspension and take out 100µL for

flow cytometry to detect the cell proportion. The cell suspension used for magnetic sorting is 500µL (just occupies the tip of the EP tube), and then place the tip of the EP tube containing the suspension firmly against the magnet for 10 minutes; after that, remove the liquid in the tube and add 600µL buffer wash repeat three times while the EP tube is still attaching the magnet, collected the liquid sample as +M; then remove the EP tube from the magnet and add 200 µL buffer to collect the cells sample in it, and name as -M.

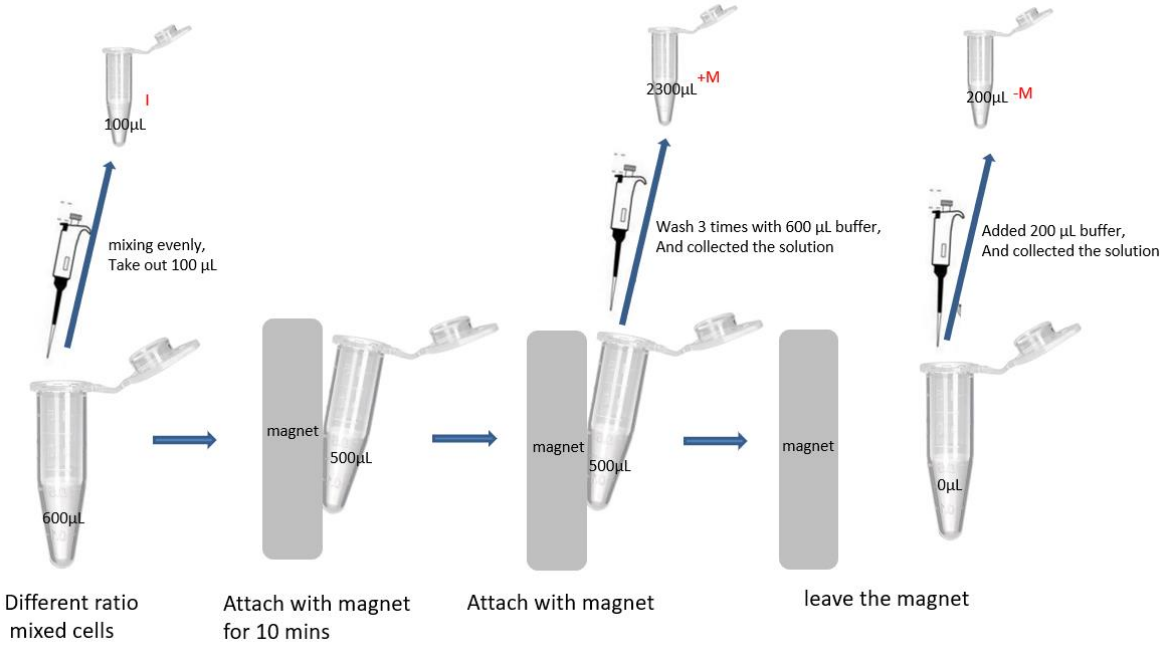

Figure 2.5.1: schematic diagram of magnetic cells sorting by attach with magnet.

2.5.8. Use magnet to absorb cells which uptake capsules- iron oxide NPs

The first day, count the Hela cells and seed 300 000 cells in each well in 6-well plate; The second day, change the medium, and capsule-magnetic NPs are added to the Hela, the addition amounts of capsule-magnetic NPs is the different ratios of capsules per cell: 0, 2, 4, 6, 8, and 10. The capsule-magnetic NPs were added to the Hela cells and incubated for 24 h at 37 ℃ / 5% CO2; The third day, wash cells with PBS for three times , then detached them with 500µL 0.05% Trypsin (2 min at 37 ℃). Trypsin was stopped with 500µL DMEM+ and the number of cells counted with a counting chamber (initial number of cells I); then attach with magnet in the way showed in Section 2.5.8, collected the +M and -M samples, count it.

2.5.9. Use magnet to separate target cells which uptake capsules- iron oxide NPs from mix cells system

The first day, count the Hela cells and culture 765 000 cells in T25 culture flask, and seeded three flasks; The second day, change the medium with 5% FBS, add 5mL new medium per flask, then 10.05 µL (1.455*10^8 capsule-cy5 per mL solution as stock) of capsule-cy5 was added to one T25 bottle, 11.7 µL (1.308*10^8 capsule-calcein per mL solution as stock) of capsule-calcein was added to the other one T25 bottle, at the same time, this bottle also added different concentration capsule-FeOx NPs (1.0775*10^8 capsule-FeOx NPs per mL solution as stock): 56.8 µL (as 8 capsule-FeOx NPs per cell), 28.4 µL (as 4 capsule-FeOx NPs per cell), 14.2 µL (as 2 capsule-FeOx NPs per cell) and 42.6 µL (as 6 capsule-FeOx NPs per cell). There is one bottle of cells just to change the medium without adding anything. Then incubated them for 24 h at 37 ℃ /5% CO2; The third day, wash cells with PBS for three times, then detached them with 500µL 0.05% Trypsin (2 min at 37 ℃). The Trypsin was then stopped with 8500µL DMEM+ and centrifuge the above 9mL of different label cells, 300rcf, 5min; then remove the supernatant, add Buffer (PBS with 0.1% BSA) to hela-capsule-calcein and Hela-capsule-cy5.

Then these two kinds cells were mixed in different ratios (I designed two rato range: less 10%, more than 10%), and the mix system solution volume is 600 µL, and the number of Hela-capsule-calcein was kept at 180 000. Then follow the way in Section 2.5.8, Pipette each mixed system evenly, and take out 100 µl in each mix system as initial number of cells (I), for flow cytometry to detect the ratio of the target cells before magnetic separation; The remaining 500 µl of the mixing system is used for magnetic sorting, repeatedly pipetting each mixed system evenly, then vertically attached to the magnet for 10min. Then add 600 µL Buffer, and gently pipet the 600 µL Buffer to wash the tube, repeat three times, and collected the solution as +M; Finally, remove the magnet, add 200 µl Buffer as -M, and pipetting the cells to count the cells under a microscope with a counting plate;

followed by flow cytometry to check the cell purity before and after magnetic separation.

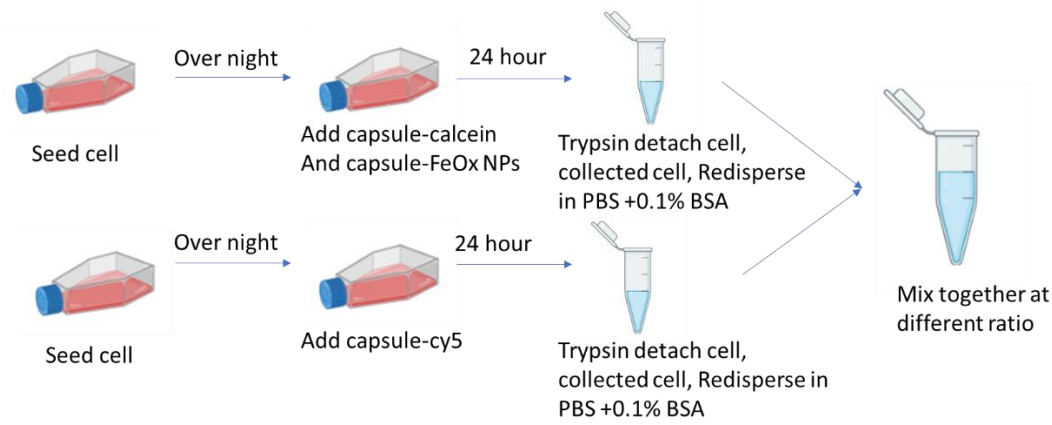

Figure 2.6.2. the schematic of prepare mix cells system, same kind cell under different capsule treatment.

2.6. the purpose of this project

We want to know the capsule modified with FeOx NPs can used for cell magnetic sorting. So, we design a mix system with two different labeled cells, by uptake two different capsule-dye (capsule-calcein and capsule-cy5), at the same time the cells which uptake capsule-FeOx NPs for magnetic sorting, at different concentration of added capsule-FeOx NPs to study the target cell capture efficiency. As show in Figure 2.6.1, firstly Let the same batch of cells be divided into two batches, one batch cells uptake capsule-calcein and capsule-NPs and another batch cells uptake capsule-cyanine 5; then detach these two kinds cells and mix them together at different ratio; then attach these mixed cells system to magnet for magnetic sorting; finally using flow cytometer to detect the change of two kinds label cells proportion before and after magnetic sorting.

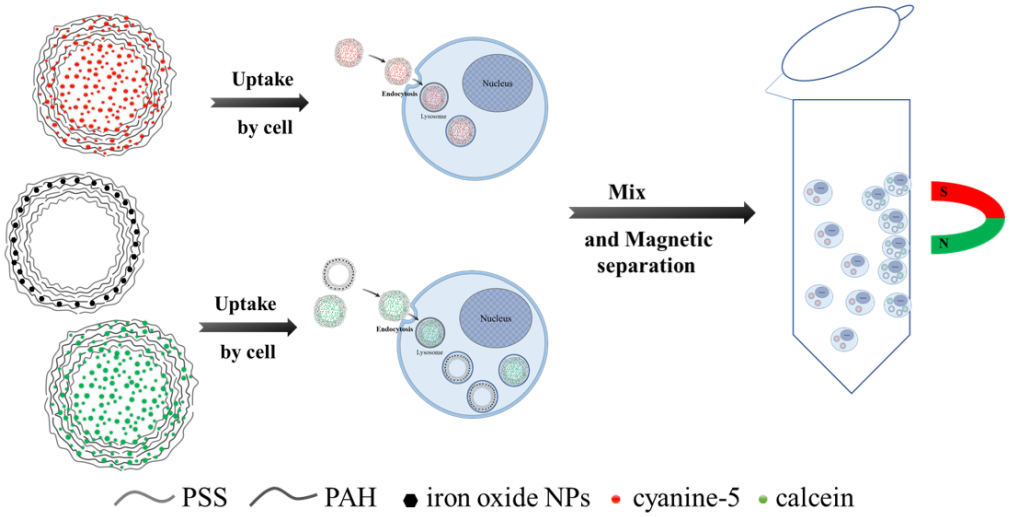

Figure 2.6.1: the schematic of capsule-FeOx NPs used for magnetic cell sorting in mix system.

2.7. results and discussion

2.7.1. characterization of iron oxide nanoparticles

As show in Figure 1 a), gained the shapes including sphere, cube, and other forms, which was determined by transmission electron microscope (TEM). Using the ImageJ software to get the Particle size distribution in the Iron oxide nanoparticles TEM image by measure 107 NPs, as show in Figure 1 b), the mean value of iron oxide nanoparticles is about 30.34nm. TEM is accelerated and concentrated electron beam onto a very thin sample, usually an ultrathin less than 100 nm thick on a grid, and the electrons collide with the atoms in the sample and change direction, so producing solid angle scattering. The size of the scattering angle is related to the density and thickness of the sample, so images with different light and dark colors can be formed, after magnification and focusing, the image will be displayed on imaging devices, such as fluorescent screens, films, photosensitive coupling components and so on.

At the same time, using dynamic light scattering (DLS) to determine the nanoparticles' hydrodynamic diameter in number and intensity distribution, as show in Figure 1 c) and d), the median of normal distribution, in number and intensity distribution, are all between 100nm and 200nm. DLS measures the diffusion of particles moving under Brownian motion,

and converts this into size and size distribution using the Stokes-Einstein relationship, and DLS are usually used to evaluate the particle size distribution of very small particles in the range 0.3nm -1nm. In here iron oxide particles has magnetic properties, so here shows a very large size value and a large range distribution, this result is correct, but do not get the true particles size. From above, we can know we synthesis the diameter of iron oxide nanoparticle is about 30nm.

And using Laser Doppler Micro-electrophoresis to measure the zeta potential, as show in Figure 1 e), in here we can get the surface charge of the iron oxide nanoparticles in water solvent is negative charge, this also shows that the surface of the nanoparticles is modified with PMA polymer.

Here we did not examine the hysteresis loops (M-H) curves of the magnetic nanoparticle to determine whether it is a superparamagnetic nanoparticle.

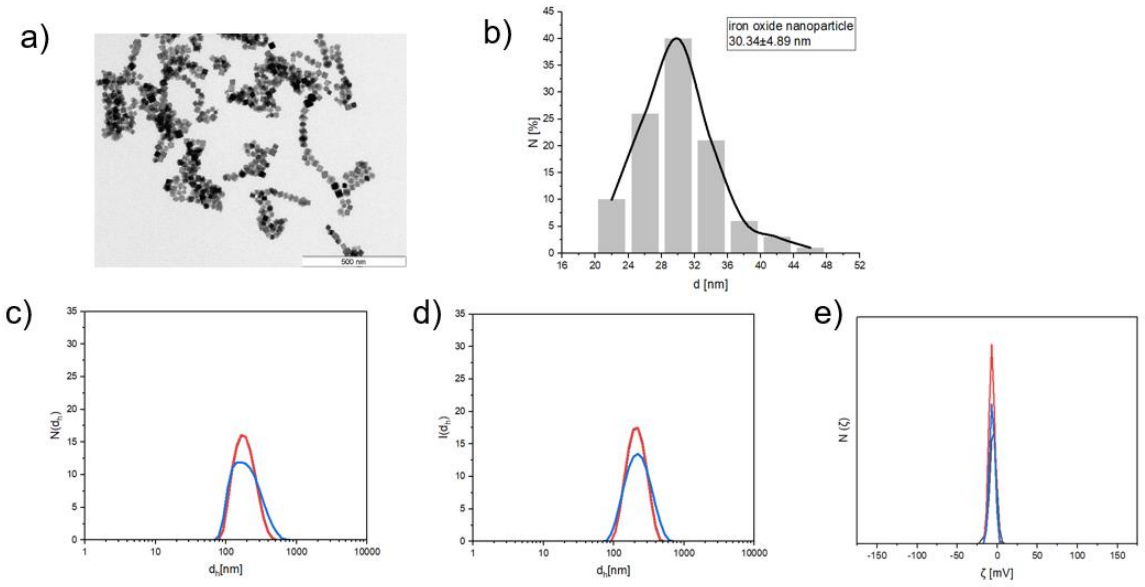

Figure 1: Characterization of IONPs coating PMA in water, a) TEM images. b) The histogram of size distribution of diameter d [nm] obtained from TEM images. The mean value ± standard deviation (SD) of iron oxide nanoparticles were 30.34 ± 4.89 nm from almost 107 iron oxide nanoparticles. (c) Number hydrodynamic distribution N (dh) of the hydrodynamic diameter dh in water. (d) Intensity distribution I(dh) of the hybrodynamic diameter dh in water. (e) ζ-potential distribution N (ζ) of the INOPs-PMA NPs in water.

2.7.2. characterization of capsule-dye

In here we loaded Calcein and Cyanine-5 inside the capsule respectively, and the excitation and emission wavelengths of calcein are 490nm and 515nm respectively, and the excitation and emission wavelengths of cyanine-5 are 650nm and 670nm respectively. As show in Figure 2 a), prepared four different calcein concentration: 0.125 mg/mL, 0.25 mg/mL, 0.5 mg/mL and 1mg/mL in Milli-Q water, and in Figure 2 b) three different cyanine-5 concentration: 0.25 mg/mL, 0.5 mg/mL and 1mg/mL, then incubate with same number capsules, follow the steps in section 2.5.5, then using Fluorescence spectra to detect the Fluorescence intensity, from these results, we can know, as the dye concentration increase, the peak value of the emission spectrum is also increasing.

Then we choose 1-2mg/mL calcein and 1-2 mg/mL cyanine-5 in Milli-Q water as the loading concentration for capsule-dye. As show in Figure 3, using confocal laser scanning microscope (CLSM) to observe the fluorescence performance of capsule-dye, we choose the corresponding excitation light and detection filter to detect the fluorescence signal, now we know we loading the dye inside the capsules successfully, and we can clearly see the capsule that emits different fluorescence and its morphology. Then using Flow cytometer to detected the signal, as show in Figure 4, in same condition to test these three different samples: non-loading capsule, capsule-calcein and capsule-cy5. In the scatter plots distribution in FITC and APC, (FITC can reflect the signal of calcein, and APC can reflect the signal of cy5), these three different capsules can be clearly distinguished.

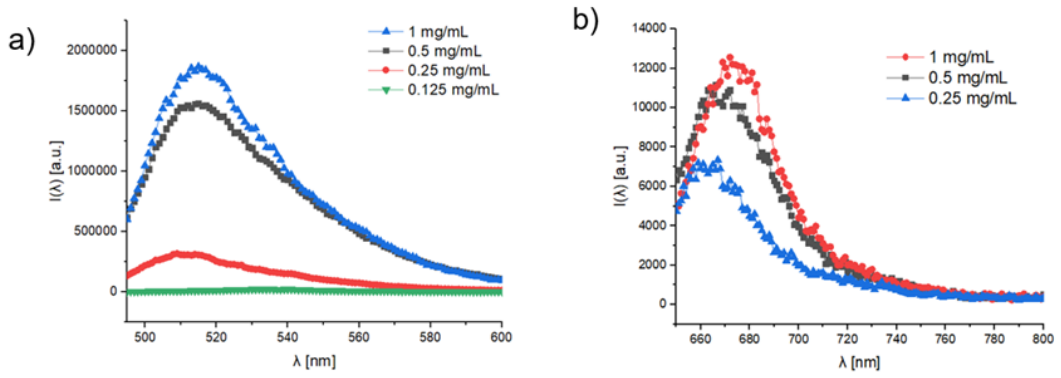

Figure 2: Fluorescence spectra I(λ) of capsule-dye, and a series of a) calcein concentrations (from 0.125 - 1 mg/mL), b) cy5 concentrations (from 0.25 - 1 mg/mL) in Millie-Q water. The number of capsules put into each concentration is 680 0000.

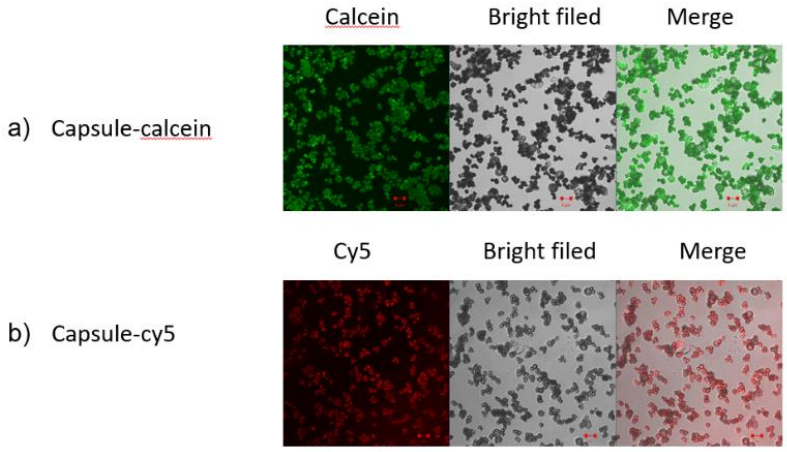

Figure 3: Confocal of a) capsule-calcein, b) capsule-cy5. the scale bar is 5 µm.

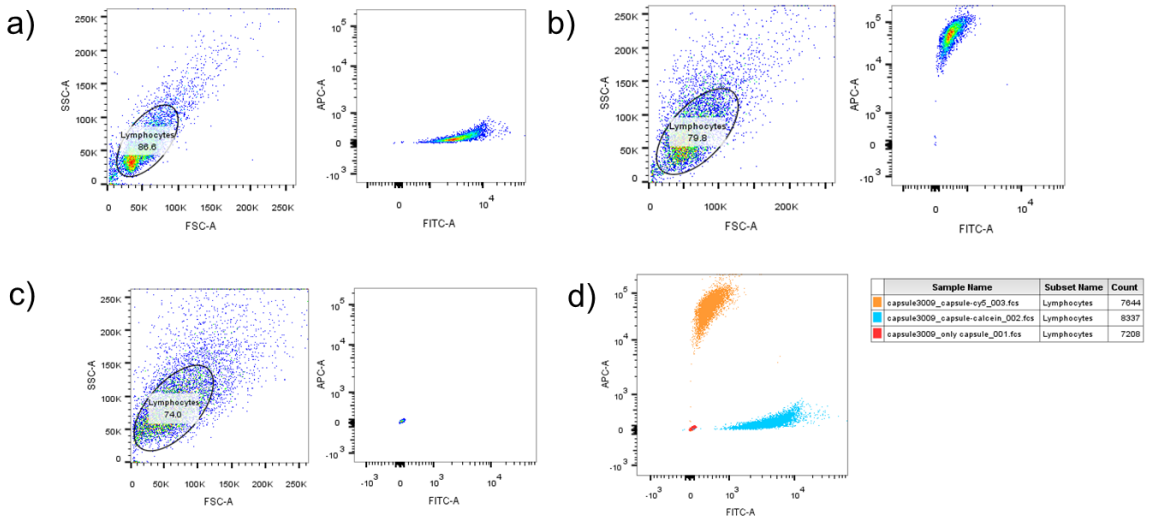

Figure 4: Scatter plots distribution of a) capsule-calcein, b) capsule-cy5 and c) capsule in SSC with FSC and in FITC with APC; d) scatter plots distribution merge of a), b) and c) in FITC with APC, they are performed under the same parameter.

2.7.3. characterization of capsule-iron oxide nanoparticles

We coated the iron oxide nanoparticles with PMA polymer, so the surface is negative charge, and change the PSS (negative polymer) with IONPs -PMA NPs during the process of layer-by-layer synthesize capsule to get the capsule-IONPs. As show in Figure 5, using confocal to observe the morphology of capsule and capsule- IONPs NPs, the scale bar is 5 µm, and the diameter of capsule and capsule- IONPs NPs is about 5 µm, and the black nanoparticle is modified on the wall of capsules. From Figure 6, we can know the capsule- IONPs has the magnetic behavior, can be adsorbed by attach to magnet.

the number of IONPs per capsule can calculated by the volume formula of a sphere and the density and mass formula of iron oxide, here we choose the density of ferric oxide (Fe_3O_4) for calculation, here we should use X-ray diffraction (XRD) technology to measure the crystal structure and phase composition of this INOPs. then we get the the number of FeOx nanoparticles per capsule is around 70000.

$m_{NP} = \rho_{NP} \times V_{NP}$

$V_{NP} = 4/3\ \pi(d/2)^3$

$N_{NP} = m_{total} / m_{NP}$

$N_{NP/CAP} = N_{NP} / N_{CAP}$

m_{total}: the total mass in capsule- IONPs sample tested by ICP-MS

m_{NP}: the mass of single nanoparticles

ρ_{NP}: the density of nanoparticles, here we choose the density of Fe_3O_4 (5.17g/mL)

V_{NP}: the volume of nanoparticles

So, $N_{NP/CAP} = [\ m_{total} / (\rho_{NP} \times 4/3\ \pi(d/2)^3)]/N_{CAP}$

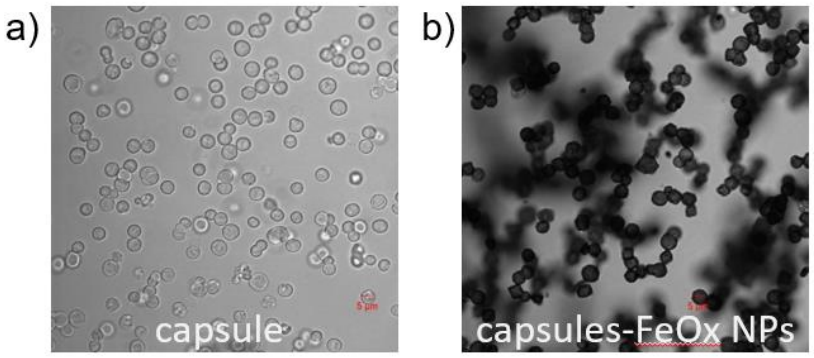

Figure 5: Confocal of a) capsule, b) capsules- IONPs. the scale bar is 5 µm.

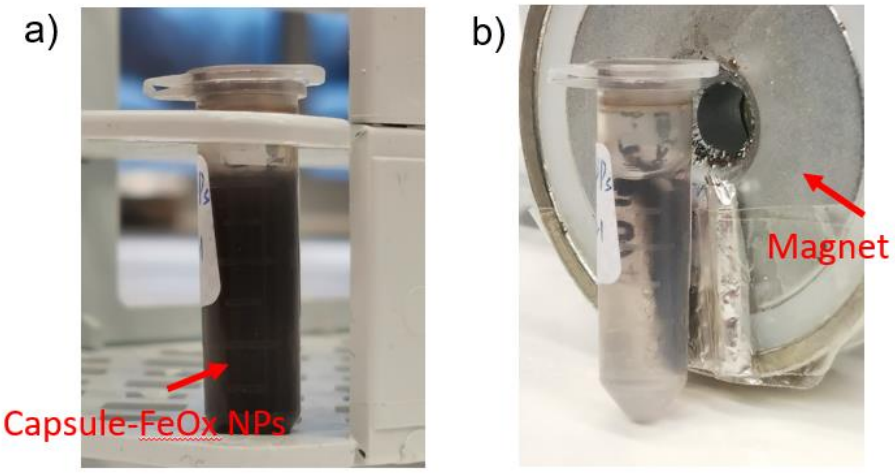

Figure 6: The magnetic behavior of capsule- IONPs is demonstrated under an external magnetic field gradient (a) before and (b) after applying the magnet.

2.7.4. experiment results of materials with cells

2.7.4.1. Hela cells with capsule-dye

Because capsule-calcein and capsule-cy5 will used in Hela cells, as cell labels. In here, we use flow cytometer to detected whether these two materials can used as cell's label. Firstly, three different samples, including capsules, capsule-calcein and capsule-dye, were incubated with Hela cells respectively for 24 hours, and added amount is double amount of cells number. Then after 24 hours, wash three times with PBS to remove the capsule-dye that not internalized in cells, then detached these cells with trypsin, then centrifuge at 300g for 5min to collected the cells. Then using flow cytometer to test the signals. In final, we got the data show in Figure 7, in same test condition, gate the scatter plots of SSC and FSC distribution, generally, we think that the points where SSC and FSC are too small represent cell debris and some capsules that are not internalized into the cells, because FSC represents cell size and SSC represents cell heterogeneity, cell has the normal size and have some heterogeneity value as cell has organelles and nuclei in it. so, we gate the dots, SSC between 50k and 180k and FSC between 20k and 100k, for next step analysis. Then in the scatter plots distribution in FITC and APC (FITC can reflect the signal of calcein, and APC can reflect the signal of cy5), these three different Hela cells can be distinguished, as show in Figure 4 d), the blue dots are Hela-capsule-cy5, and the orange dots are Hela-capsule-calcein, and the

red dots are only Hela cells, the three kind dots are separate. So, capsule-calcein and capsule-cy5 can used for cell lables.

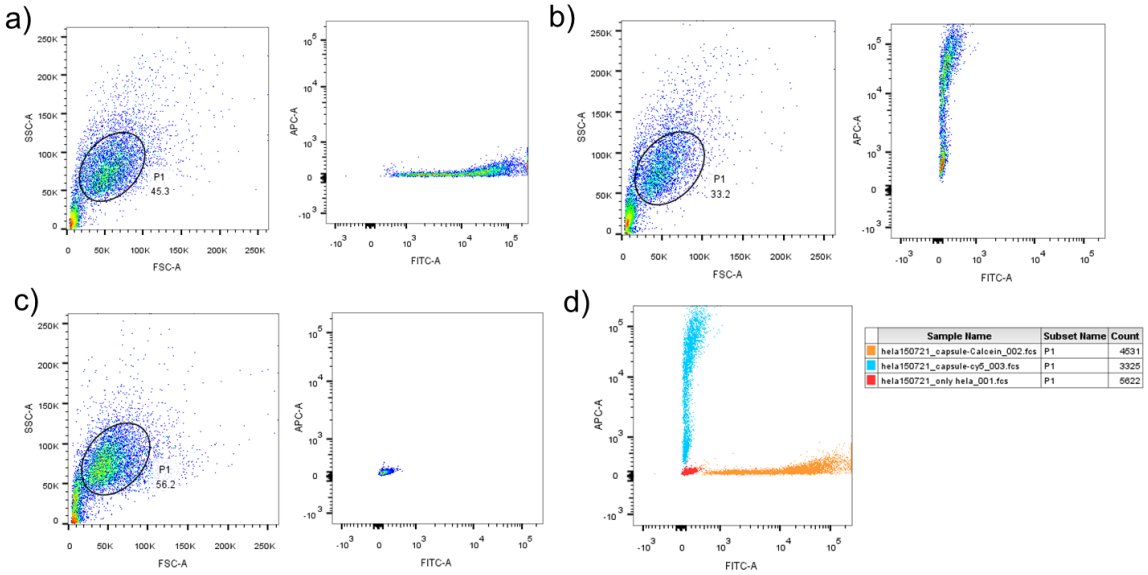

Figure 7: Scatter plots distribution of a) Hela-capsule-calcein, b) Hela-capsule-cy5 and c) capsule in SSC with FSC and in FITC with APC; d) scatter plots distribution merge of a), b) and c) in FITC with APC.

2.7.4.2. Hela cells with capsule- IONPs

Because capsule- IONPs will used in cell for magnetic sorting, in here, we studied the magnetic behavior of Hela-capsule-IONPs by applying magnet. Firstly, capsule- IONPs were incubated with Hela cells for 24 hours, and added amount is six times of cells number; then after 24 hours, wash the cells three times with PBS to remove the capsule- IONPs, that not internalized in cells, then detached these cells with trypsin, then centrifuge at 300g for 5min to collected the cells. As show in Figure 8 a), these Hela-capsule-IONPs were dispersed in PBS, appears black, then attached to a magnet, show in Figure 8 b), these black Hela- IONPs were sucked to the side with magnet.

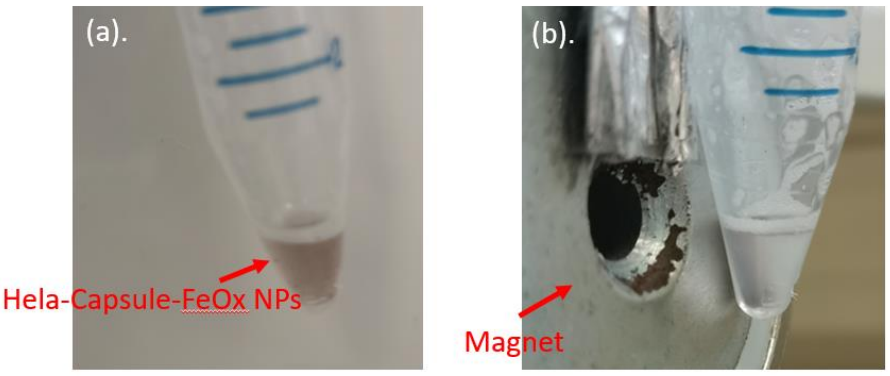

Figure 8: The magnetic behaviour of Hela-capsule-IONPs is demonstrated under an external magnetic field gradient (a) before and (b) after applying the magnet.

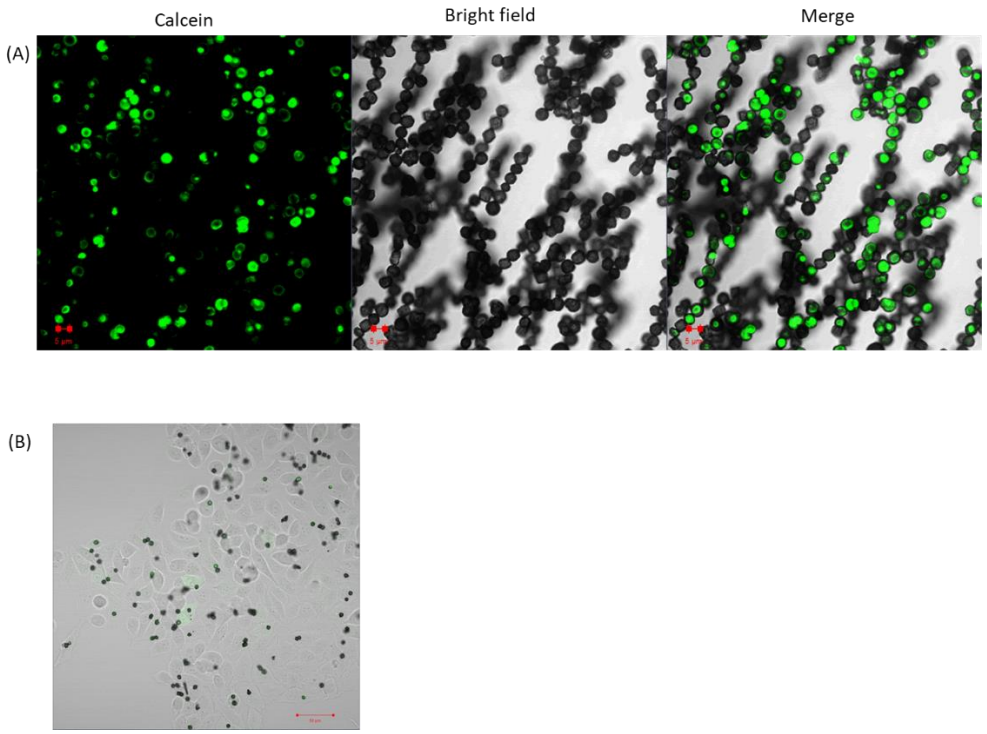

Figure 9: (A). capsule modified with IONPs, and postload Calcein dye. Observe under confocal, the scar bar is 5μm. (B). The confocal image of capsule- IONPs -calcein in Hela cell, after incubate 24 hours, the scar bar is 50μm.

2.7.5. the result of capture cells which uptake capsule- IONPs

After Hela cell uptake capsule- IONPs, we study capture efficiency of this kind cell can be adsorbed by magnet, so we count cell under a microscope to calculate the proportion of

captured cells. Different ratio capsule- IONPs were added in Hela cells, including 0, 1, 2, 4, 6, 8, 10 capsule- IONPs per cells, after 24 hours incubated with Hela cells in medium with 5% FBS, wash cells three times with PBS, then detach cells with 0.5% trypsin, centrifuge at 300g for 5min, and collect cells and dispersed in PBS with 0.1% BSA, used for capture. As show in Figure 9 a), we use Miltenyi MS column to capture cells, When the column is attached to the magnet, we add the cell solution, the number of cells at this time is recorded as I, and collect the outflowing liquid at the lower end of the column, count the cells number at this time as +M. When the column leaves the magnet, add PBS with 0.1% BSA liquid again, and collect the outflowing liquid at the tube, count the cells number at this time as -M. In Figure 9 b), as the ratio of capsule- IONPs per cell increase, the -M/I is also increase and +M/I is decrease. The detail data show in Table 2-1.

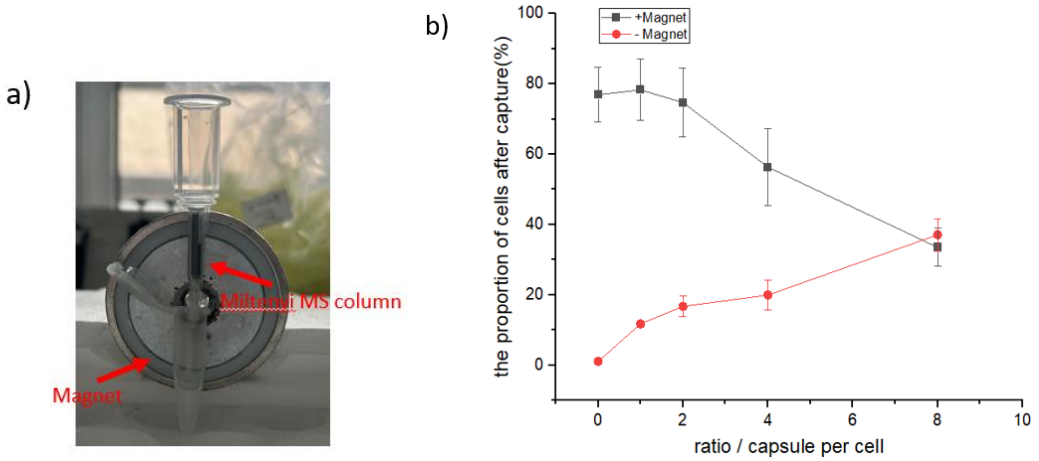

Figure 9: a) the device of Miltenyi MS column used to sort cells; b) Capture efficiency of the magnetic separation HeLa cells after incubation for 24 in DMEM+ with capsule- IONPs by Miltenyi MS column. The black curve shows the +M sample (collect while attached to the magnet), the red curve shows the –M sample (collected while NOT attached to the magnet).

Ratio (capsule-FeOx NPs /cell)	+M/I (%)	-M/I (%)	(+M/I)+(-M/I) (%)
0	76.97 ± 7.77	1.05 ± 0.75	78.02
1	78.35 ± 8.72	11.74 ± 0.97	90.09
2	74.74 ± 9.75	16.72 ± 2.88	91.46

4	56.35 ±10.96	19.94 ± 4.20	76.29
8	33.52 ± 5.41	37.08 ± 4.63	70.6

Table 2-1： Counted number of cells for the initial number of cells I, the number of cells flushed through the column while attached to the magnet +M, and the number of cells flushed thorough the column without the magnet –M. Use Miltenyi MS column to capture cells which uptake capsules-IONPs.

We also use magnet to directly capture the cells that uptake capsule- IONPs, as shown in Figure 10 a), when the tube attached to magnet, taken out the solution, and counted cells number at this time as +M, after that, the tube leaves the magnet, count the cell number as -M, as show in Figure 10 b), as the ratio of capsule- IONPs per cell increase, the -M/I is also having a growth trend and +M/I is decrease. The detail data show in Table 2-2.

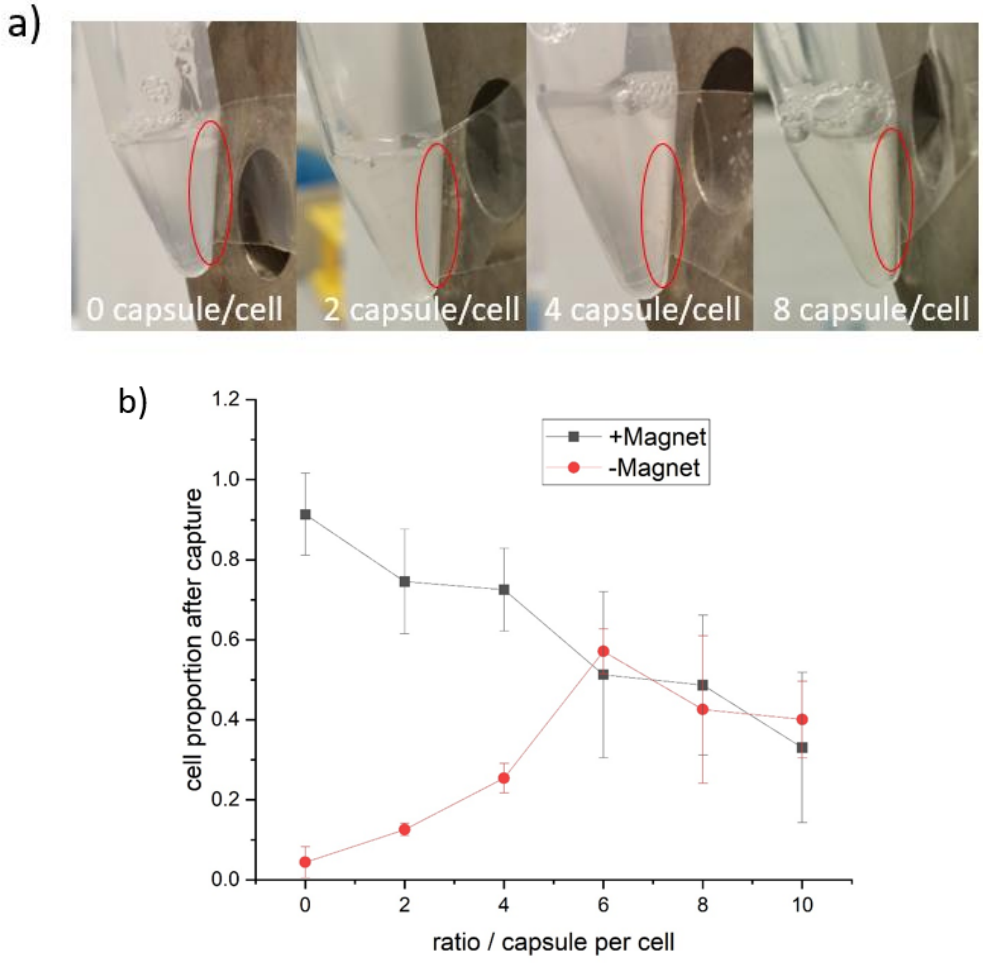

Figure 10. a) Hela cells with different ratio of capsule- IONPs per cell in tub, directly attach to magnet for cell sorting. b) Capture efficiency of the magnetic separation HeLa cells after incubation for 24 in DMEM+ with the capsules-IONPs by super magnet. The black curve shows the +M sample (collect while attached to the magnet), the red curve shows the –M sample (collected while NOT attached to the magnet). Results are presented from three individual experiment.

Ratio (capsule-FeOx NPs /cell)	+M/I (%)	-M/I (%)	(+M/I)+(-M/I) (%)
0	91.34 ± 10.23	6.64 ± 0.47	97.98
2	75.55 ± 13.02	12.56 ± 1.56	87.11
4	72.48 ± 10.39	25.42 ± 3.68	97.90
6	51.29 ±20.76	57.12 ± 5.60	108.41
8	48.65 ± 17.51	42.58 ± 19.4	91.23
10	33.03 ± 18.75	40.10 ± 9.55	73.12

Table 2-2： Counted number of cells for the initial number of cells I, the number of cells flushed through the column while attached to the magnet +M, and the number of cells flushed thorough the column without the magnet –M. Use magnet to capture cells which uptake capsules-IONPs.

When the ratio of added capsule- IONPs per cell is 8, from Figure 11, the proportion of cells retained by the magnet is 37.08 ± 4.63 % by using Miltenyi MS column,
42.58 ± 19.4 % by directly attach to magnet in tube. So, directly attaching to magnet has a better effect of cell sorting than using Miltenyi MS column, but there is a large error.
(+M/I) +(-M/I) represents the percentage of collected cells (attach to magnet and leave magnet) in the total, when the ratio of added capsule- IONPs per cell is 8, this value is 70.6 % by using Miltenyi MS column, and 91.23 % by directly attach to magnet in tube, so using Miltenyi MS column will lose more cells, which may be trapped in the column and cannot be washed down. So, to sum up, when capsule- IONPs are used for cell sorting, the effect of directly attaching to magnet is no worse than using Miltenyi MS columns, and less

cells are lost.

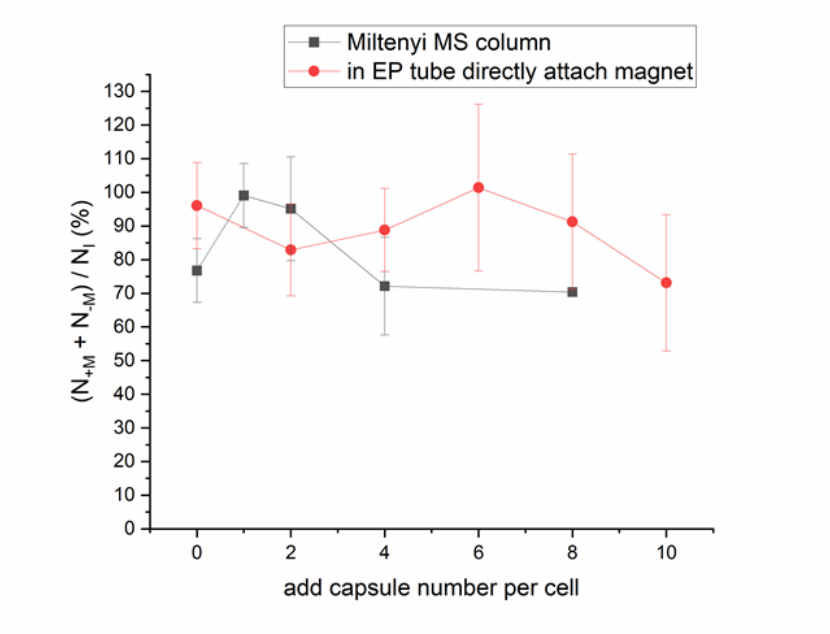

Figure 11: Comparison of cell recovery between the two capsule devices: pass the cells through the Mitenyi MS column (black line), put cells in PE tube attaching with magnet. N_{+M}: the cell number in collected sample when attach to magnet; N_{-M}: the cell number in collected sample when not attach to magnet; N_I: the cell number before cell capture.

2.7.6. the result of capture cells which uptake capsule-IONPs in a mix system

Next, explore the capture effect of target cells in the mixed system when the target cells already uptake capsule- IONPs. From the above, capsules with internalized fluorescent dyes can be used for cell labeling, so the cell internalized capsule-calcein as target cell, and the cell internalized capsule-cy5 as background cell. At the same time, added capsule-IONPs in target cell, added capsule- IONPs ratio including 8, 6, 4 and 2 times per cell (the cells number is the seed cells number in the first day), after incubate 24 hours with Hela cells in incubator, then detach these cells by trypsin, using ICP-MS to get the Fe content in each cell, as show in Figure 11, then make a range of mix system at different proportion of target cells. After that, the tubes with a mix cells system directly attached to magnet, and collected the cell when attached the magnet as +M and leaved the magnet as -M. Then used flow cytometer to detected the proportion of target cells and background cells in the initial sample of before sorting (named as I), also detected the proportion of target cells

and background cells in -M and +M. At the same time, counted the target cells before sorting and counted the cells in -M, used following *eq 2.1* to calculate the target cells capture efficiency.

Capture efficiency = N_{-M}*$Q1_{-M}$ / N_{Q1} *eq 2.1*

N_{-M}: the cells number in collected sample of leaved magnet after magnet sorting;

$Q1_{-M}$: flow cytometer detected the proportion of target cells in collected sample of leaved magnet after magnet sorting;

N_{Q1}: the number of target cells in the initial sample of before sorting.

When added 8 times capsule- IONPs per cell, scatter plot (FSC and SSC, FITC and APC) results analysis of flow cytometry shows in SI Figure 1, designed proportion of target cells including 0.2% (SI Figure 1- 1,2,3), 0.5% (SI Figure 1- 4,5,6), 1% (SI Figure 1- 7,8,9), 2% (SI Figure 1- 10,11,12), 5% (SI Figure 1- 13,14,15), 10% (SI Figure 1- 16,17,18), 20% (SI Figure 1- 19,20,21), 40% (SI Figure 1- 22,23,24) and 60% (SI Figure 1- 25,26,27). And the cells number of target cells before magnet sorting and the cell number of the total cells after magnet sorting of leave the magnet are recorded in SI Table 1, and calculated the capture efficiency.

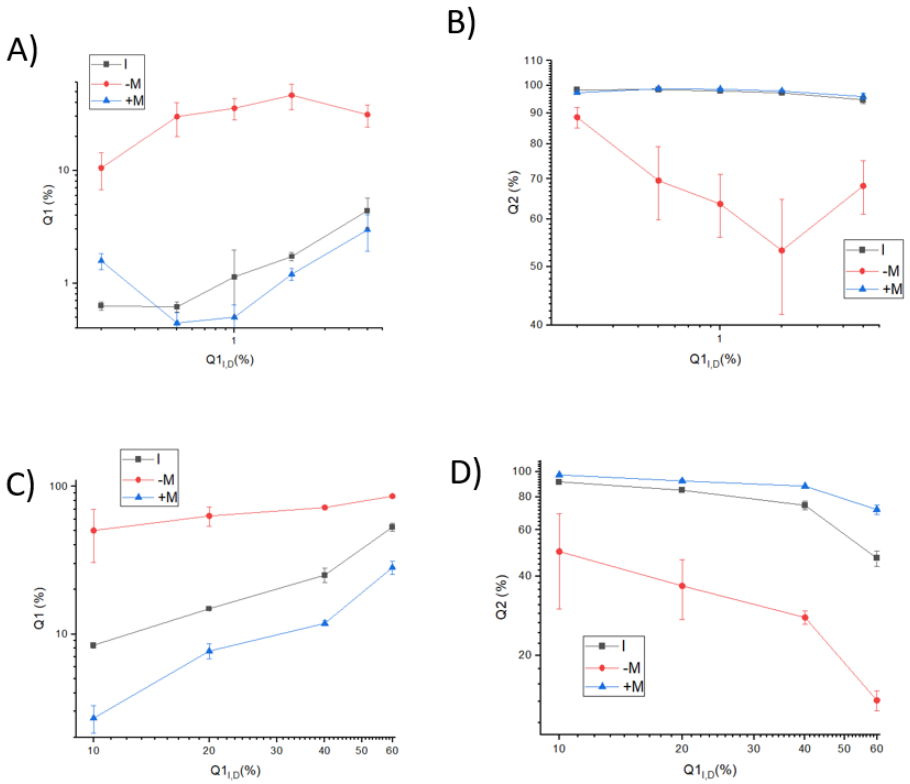

Figure 11. after added 8 times capsule- IONPs per cell for incubate 24 hours in DMEM with 5% FBS, then mix at different ratio, directly attached to magnet for cell sorting. flow cytometer detected the proportion of target cells (Q1) and background cells (Q2) in the initial sample of before sorting(I), collected sample of leaved magnet after magnet sorting(-M), and collected sample of attached to the magnet(+M). A) B): $Q1_{I,D}$ are 0.2 %, 0.5%, 1%, 2%,and 5%; C) D): $Q1_{I,D}$ are 10%, 20%, 40%, and 60%. $Q1_{I,D}$: designed the proportion of target cells in the initial sample.

When added 4 times capsule-IONPs per cell, scatter plot (FSC and SSC, FITC and APC) results analysis of flow cytometry shows in SI Figure 2, designed proportion of target cells including 0.3% (SI Figure 2- 1,2,3), 1% (SI Figure 2- 4,5,6), 10% (SI Figure 2- 7,8,9), 16% (SI Figure 2- 10,11,12), 28% (SI Figure 2- 13,14,15), 44.4% (SI Figure 2- 16,17,18), and 61.5% (SI Figure 2- 19,20,21). And target cells before magnet sorting and the total cells after magnet sorting of leave the magnet are recorded in SI Table 2, and calculated the capture efficiency.

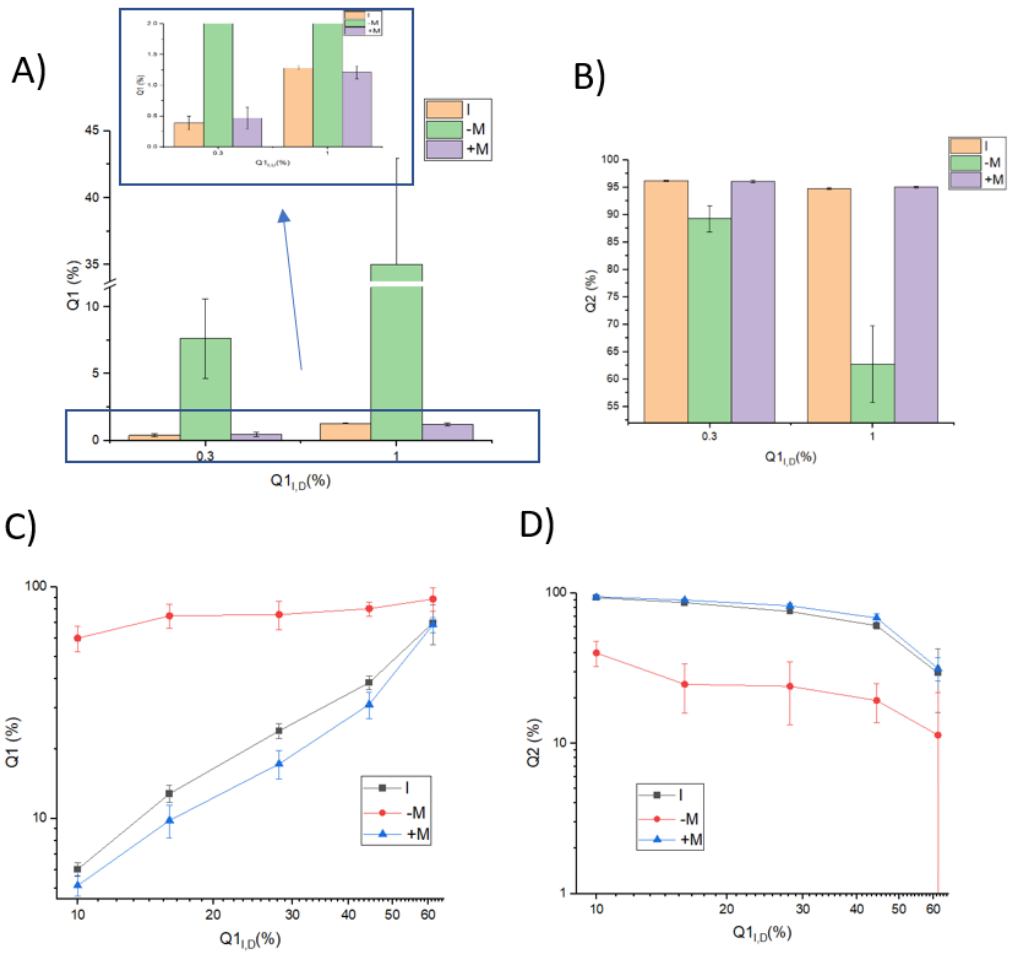

Figure 12. after added 4 times capsule-IONPs per cell for incubate 24 hours in DMEM with 5% FBS, then mix at different ratio, then directly attached to magnet for cell sorting. flow cytometer detected the proportion of target cells (Q1) and background cells (Q2) in the initial sample of before sorting(I), collected sample of leaved magnet after magnet sorting(-M), and collected sample of attached to the magnet(+M). A) B): $Q1_{I,D}$ are 0.3 %, 1%; C) D): $Q1_{I,D}$ are 10%, 16%, 28%, 44.4% and 61.5%. $Q1_{I,D}$: designed the proportion of target cells in the initial sample.

When added 2 times capsule-IONPs per cell, scatter plot (FSC and SSC, FITC and APC) results analysis of flow cytometry shows in SI Figure 3, designed proportion of target cells including 10% (SI Figure 3- 1,2,3), 16% (SI Figure 3- 4,5,6), 28% (SI Figure 3- 7,8,9), 44.4% (SI Figure 3- 10,11,12), 61.5% (SI Figure 3- 13,14,15) and 96.2% (SI Figure 3- 16,17,18). And target cells before magnet sorting and the total cells after magnet sorting of leave the magnet are recorded in SI Table 3, and calculated the capture efficiency.

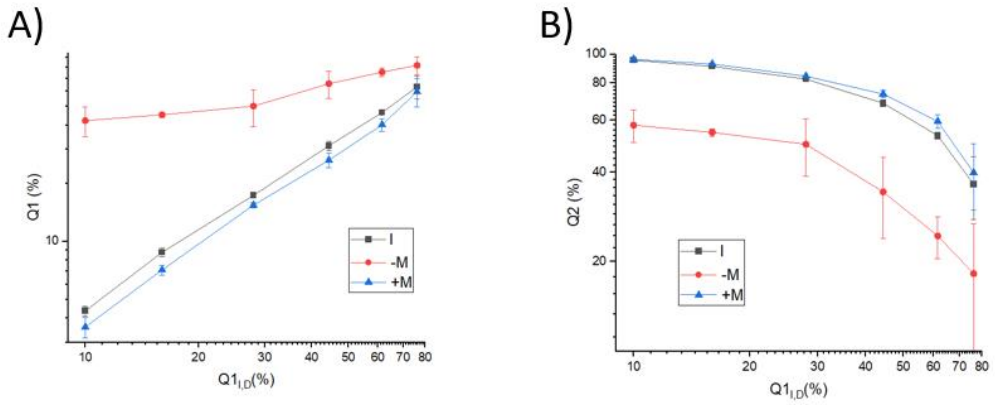

Figure 13. after added 2 times capsule-IONPs per cell for incubate 24 hours in DMEM with 5% FBS, then mix at different ratio, directly attached to magnet for cell sorting. flow cytometer detected the proportion of target cells (Q1) and background cells (Q2) in the initial sample of before sorting(I), collected sample of leaved magnet after magnet sorting(-M), and collected sample of attached to the magnet(+M). A) B): $Q1_{I,D}$ are 10%, 16%, 28%, 44.4% 61.5% and 76.2%. $Q1_{I,D}$: designed the proportion of target cells in the initial sample.

When added 6 times capsule- IONPs per cell, scatter plot (FSC and SSC, FITC and APC) results analysis of flow cytometry shows in Figure 4, designed proportion of target cells including 0.2% (SI Figure 4- 1,2,3), 0.5% (SI Figure 4- 4,5,6), 1% (SI Figure 4- 7,8,9), 2% (SI Figure 4- 10,11,12), 10% (SI Figure 4- 13,14,15), 16% (SI Figure 4- 16,17,18), 28% (SI Figure 4 - 19.20.21) and 44.4 % (SI Figure 4 - 22,23,24). And target cells before magnet sorting and the total cells after magnet sorting of leave the magnet are recorded in SI Table 4, and calculated the capture efficiency.

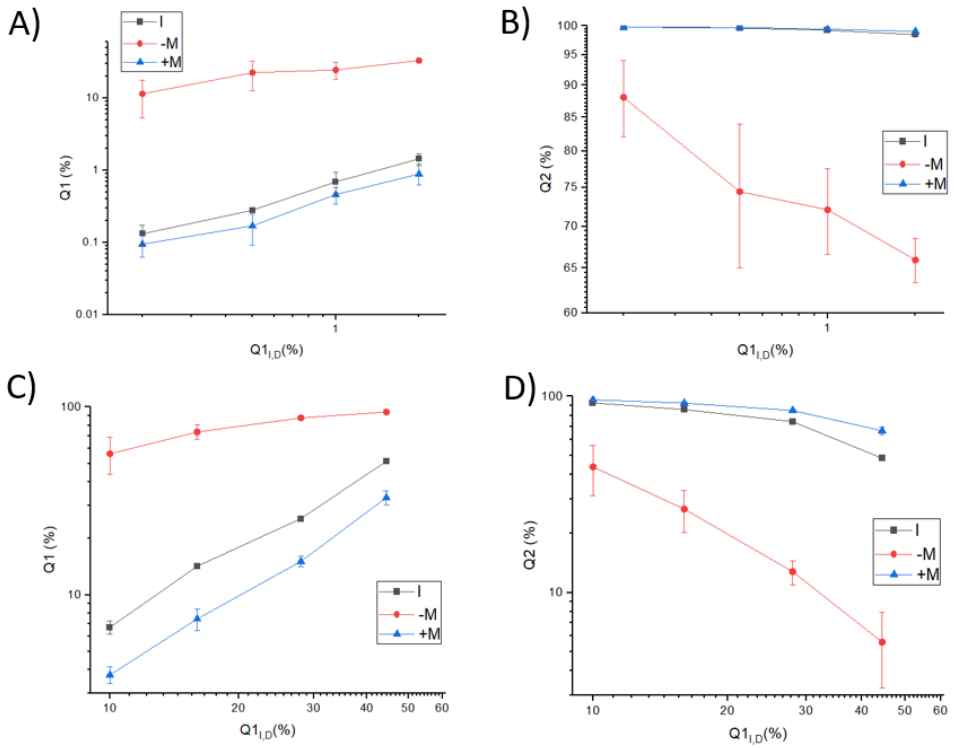

Figure 14. after added 6 times capsule-IONPs per cell for incubate 24 hours in DMEM with 5% FBS, then directly attached to magnet for cell sorting. flow cytometer detected the proportion of target cells(Q1) and background cells(Q2) in the initial sample of before sorting(I), collected sample of leaved magnet after magnet sorting(-M), and collected sample of attached to the magnet(+M). A): $Q1_{I,D}$ are 0.2%, 0.5%, 1%, 2%, and 5%; B): $Q1_{I,D}$ are 10%, 16%, 28%, and 44.4%. $Q1_{I,D}$: designed the proportion of target cells in the initial sample. Q1: flow cytometer detected the proportion of target cells.

From above data, to explore the capture efficiency at different added amount of capsule-IONPs, as show in Figure 15, as the added capsule- IONPs increasing, the capture efficiency of target cell also increasing.

Flow cytometer detected the proportion of target cells in initial sample before magnet sorting ($Q1_I$) as X-axis, as show in Figure 16, as $Q1_I$ increasing, flow cytometer detected the proportion of target cells after magnetic sorting of leaving the magnet ($Q1_{-M}$) also increasing, and the slope of the curve of added 6 capsule- IONPs per cell is greater than added 2 capsule- IONPs per cell, which meaning the added capsule- IONPs is working in magnetic sorting.

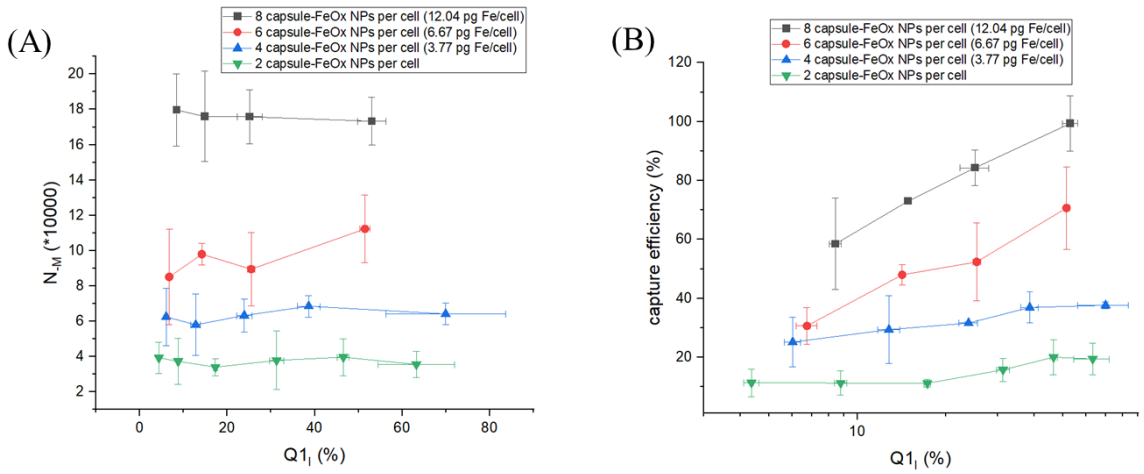

Figure 15. (A). The cells number after magnetic sorting, (B). capture efficiency in different added amount of capsule- IONPs per cell. Q1I: flow cytometer detected the proportion of target cells in initial sample before magnet sorting. N-M: the cell number in collected sample when not attach to magnet.

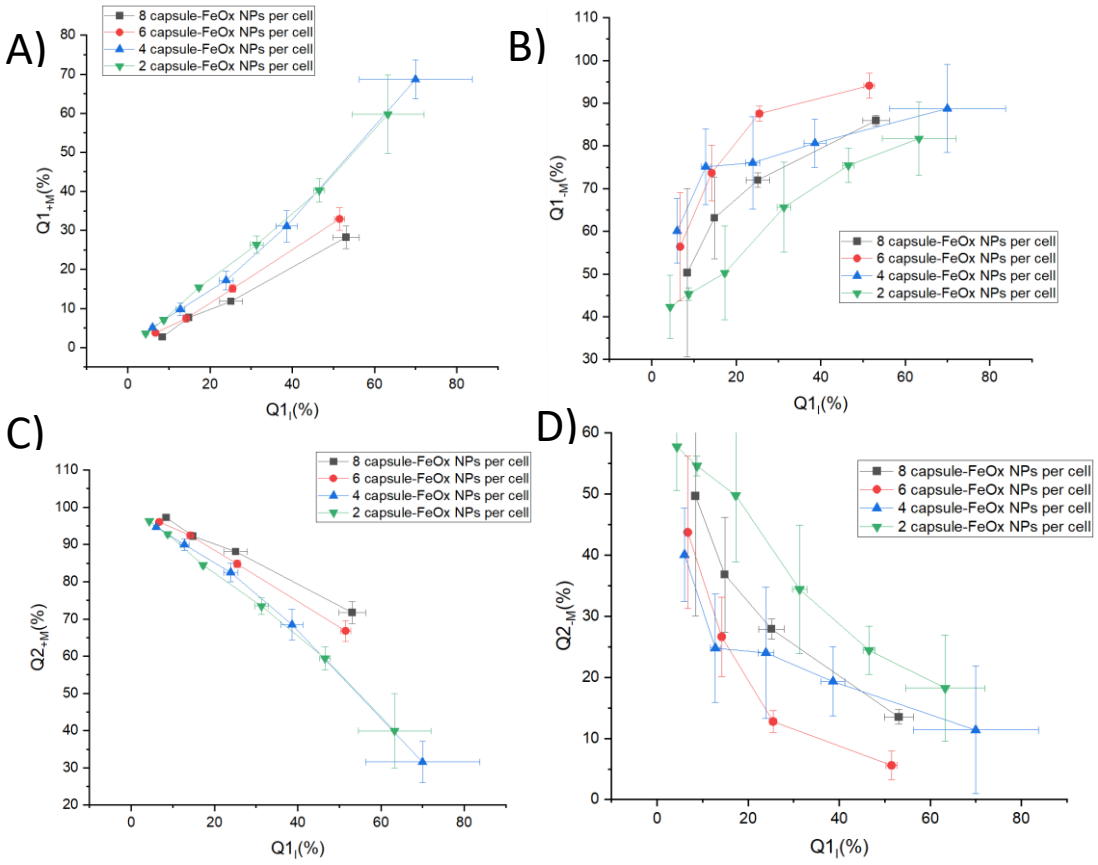

Figure 16. trend change of different capsule- IONPs added amount of 2, 4, 6 and 8 per cell, **(**A) target cell ratio in collected sample of attached to the magnet ($Q1_{+M}$), (B) target cells ratio in collected sample of leaving the magnet ($Q1_{-M}$), (C) background cell ratio in collected sample of attached to the magnet ($Q2_{-M}$), (D) background cells ratio in collected sample of leaving the magnet ($Q2_{-M}$). Each point is three individual magnetic sorting experiments.

2.7.7. the results of capture cells which uptake IONPs in a mix system

2.7.7.1. The purpose of this part

From above, we know the capsule modified with IONPs can used for magnetic sorting, and the 6 capsule- IONPs has a better capture purity than added 2 capsule- IONPs per cell. Then we want compare the capture efficiency between IONPs and capsule- IONPs when the iron content per cell is same in add capsule- IONPs and add IONPs.

Firstly, make clean the magnetic behavior between Hela and IONPs, do an uptake experiment about Hela and IONPs to see the iron content per cell after 24 hours incubate at different Fe concentration. Do a capture experiment to see it is possible of Hela that already uptake IONPs can be capture by the way of attach to magnet; Secondly, based on the above results, do a capture experiment to see it is possible of Hela that already uptake IONPs can be capture in a mix system and compare the capture efficiency and target cell ratio change in before and after magnetic sorting with the results of added capsule- IONPs; Third, based on above results, make sure the capture efficiency between capsule- IONPs and IONPs.

2.7.7.2. IONPs with Hela cell

To explore the magnetic behavior of Hela internalized IONPs s. Seeded 140 000 Hela per well in 12-well-plate, 2mL medium with 5% FBS, in incubator for 24 hours. Then change the medium and incubate with different concentration IONPs (0, 1, 2, 4, 8 and 10 μg Fe per mL medium) for 24 hours in medium in incubator, after that, Hela cells washed with PBS for three times then detach with trypsin, 100μL 2min in 37℃, then added 1mL medium with 5% FBS to stop the detach process, collected the cells and centrifuge for 5 mins at 300g, then dispersed in 1mL Buffer (PBS with 0.1% BSA), counted the cells as I, then attach with magnet for 10 min, as show in Figure 12 a), then wash with Buffer for three times, the tube still attach tightly with magnet, collected the solution as +M sample, then remove the magnet and collected the cell by added Buffer, and named as -M. Then counted the cell number in +M and -M.

As show in Figure 17 b), as the increasing of iron concentration, the cell proportion in -M

sample also increasing, and the max proportion is about 65% when the added Fe is 8 µg/mL, then there is no increase in follow concentration. So, we can know from here, the cell which uptake IONPs can be capture by attaching with magnet, and the maximum proportion of captured cells is approximately 65%.

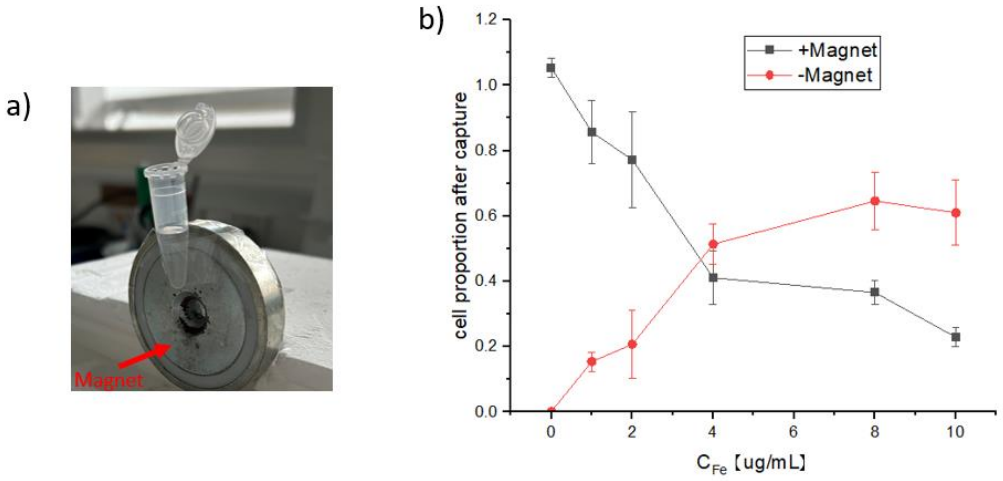

Figure 17. a) EP tubes containing cells are attached to magnets for magnetic sorting; b) Capture efficiency of the magnetic separation HeLa cells after incubation for 24 in DMEM+ with IONPs by Supermagnet. The black curve shows the +M sample (collect while attached to the magnet), the red curve shows the –M sample (collected while NOT attached to the magnet). Results are presented from three individual experiment.

To explore the uptake situation of Hela internalized IONPs. Seeded 140 000 Hela per well in 12-well-plate, 2mL medium with 5% FBS, in incubator for 24 hours. Then change the medium and incubate with different concentration IONPs (0.5, 1, 2, 4, and 8 µg Fe per mL medium) for 24 hours in medium in incubator, after that, Hela cells washed with PBS for three times then detach with trypsin, 100µL 2min in 37℃, then added 1mL medium with 5% FBS to stop the detach process, collected the cells and centrifuge for 5 mins at 300g, then dispersed in 1mL PBS, counted the cells. Then centrifuge for 5 mins at 300g, added 400uL aqua regie (HCl: HNO_3= 3:1) for overnight, then added 2mL 2%HNO_3 for ICP-MS test the concentration.

As show in Figure 18, as the increasing of iron concentration, the content of Fe elemental found per Hela cell also increasing, and when the added IONPs is 4 µg Fe per mL medium, after 24 hours incubate, found 12.89 pg Fe per call.

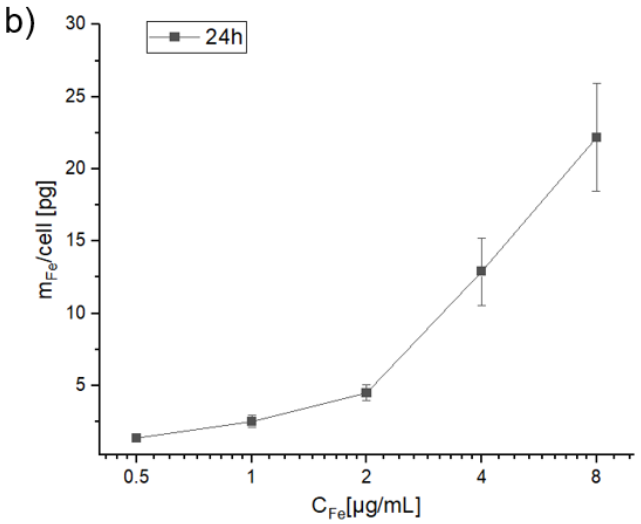

Figure 18. Amount of Fe elemental found per cell in Hela exposed to IONPs -PMA at different concentrations after 24 h by ICP-MS. Results are presented from three individual experiment.

2.7.7.3. the results of capture cells in a mix system

Then to explore the capture efficiency of target cell which uptake IONPs in a mix system, we choose added 4 μg Fe per milliliter medium, then to explore the capture efficiency. Do same experiment in Section 2.5.9, and the scatter plot (FSC and SSC, FITC and APC) results analysis of flow cytometry shows in SI Figure 5, designed proportion of target cells including 1% (SI Figure 5- 1,2,3), 2% (SI Figure 5- 4,5,6), 4% (SI Figure 5- 7,8,9), 8% (SI Figure 5- 10,11,12), 16% (SI Figure 5- 13,14,15), 28% (SI Figure 5- 16,17,18), 44.4% (SI Figure 5- 17,18,19), 61.5% (SI Figure 5- 20, 21,22) and 76.19% (SI Figure 5- 23,24,25). And the cells number of target cells before magnet sorting and the cell number of the total cells after magnet sorting of leave the magnet are recorded in SI Table 5, and calculated the capture efficiency.

As show in Figure 19, flow cytometer detected the proportion of target cells in -M sample are all higher than I samples and +M Sample, and the proportion of background cells in -M are all lower than I sample and +M sample, so, the Hela cell internalized IONPs can be magnetic sorting by attach with magnet in a mix cell system.

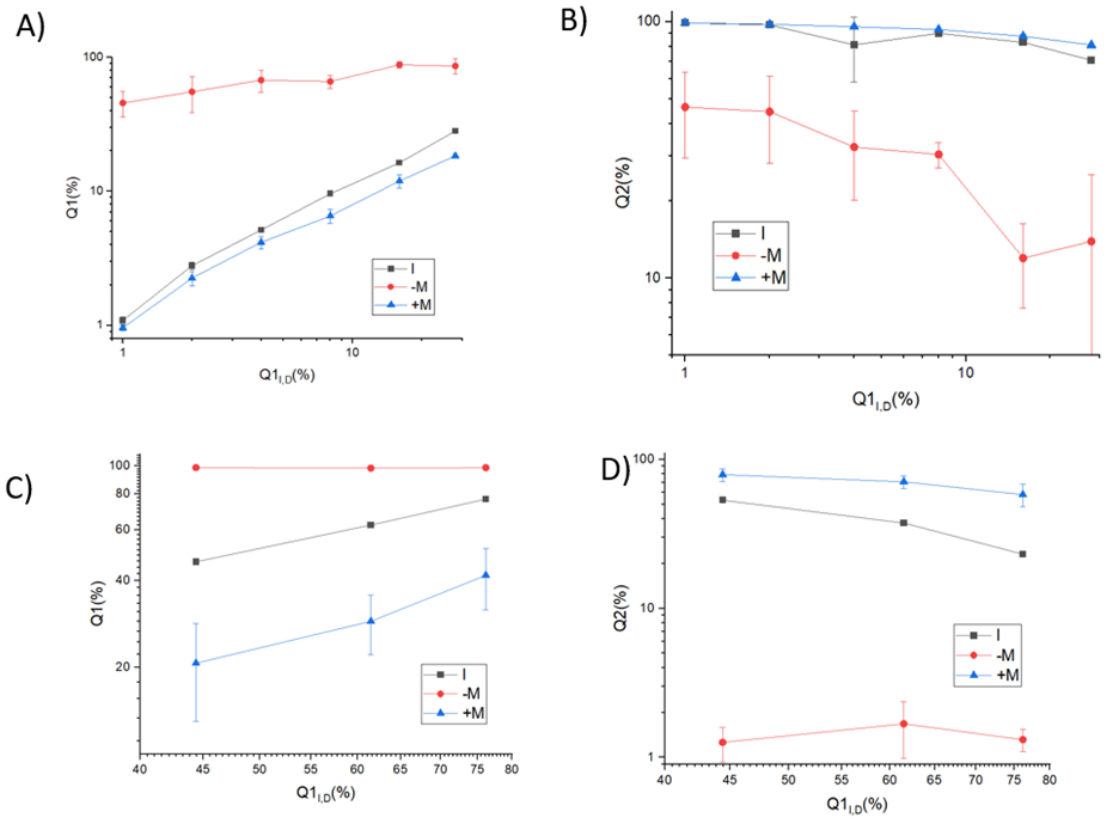

Figure 19. after added 4 μg Fe of IONPs per mL medium and incubated with Hela cells for 24 hours in DMEM with 5% FBS, then directly attached to magnet for cell sorting. flow cytometer detected the proportion of target cells (Q1) and background cells (Q2) in the initial sample of before sorting(I), collected sample of leaved magnet after magnet sorting(-M), and collected sample of attached to the magnet(+M). A) B): $Q1_{I,D}$ are 1 %, 2%, 4%, 8%, 16% and 28%; C) D): $Q1_{I,D}$ are 44.4%, 61.5%, 40%, and 76.19%. $Q1_{I,D}$: designed the proportion of target cells in the initial sample.

2.7.7.4. the results of compare the capture efficiency in a mix system between capsule-IONPs and IONPs

To further compare the capture efficiency in a mix system, when the cells uptake capsule-IONPs and IONPs respectively, and the iron content in the cells was same after 24 hours of uptake. In order to keep the magnetic sorting is same situation, we choose a DynaMag 2 (Invitrogen by Thermo fisher scientific) to do this experiment, as show Figure 20, and the tip of tube not tightly attach with the magnet.

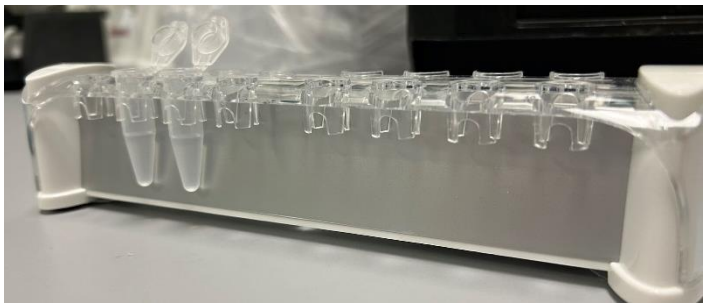

Figure 20. Magnetic sorting method in compare capsule- IONPs and IONPs. The tip of the EP tube is not tightly attached to the magnet.

So, we designed the capture experiments of adding 8 capsule- IONPs per cell and 5 μg Fe /mL medium by adding IONPs. Designed target cells ratio is 25% and 50%, the scatter plot (FSC and SSC, FITC and APC) results analysis of flow cytometry shows in SI Figure 6, designed proportion of target cells including 25% (SI Figure 6- 1,2,3), 50% (SI Figure 6- 4,5,6) when added 8 capsule- IONPs per cell, and 25% (SI Figure 6- 7,8,9), 50% (SI Figure 6- 10,11,12), when added 5 μg Fe /mL medium by adding IONPs. And the cells number of target cells before magnet sorting and the cell number of the total cells after magnet sorting of leave the magnet are recorded in SI Table 6, and calculated the capture efficiency.

Show in Figure 21 e), the capture efficiency between capsule- IONPs and IONPs are similar, and there is no significant difference when the iron content is similar between added capsule- IONPs and IONPs. In Figure 21 a), when the target cells are about 25%, the target cells ratio after magnetic sorting are no significant difference between added capsule- IONPs and added IONPs.

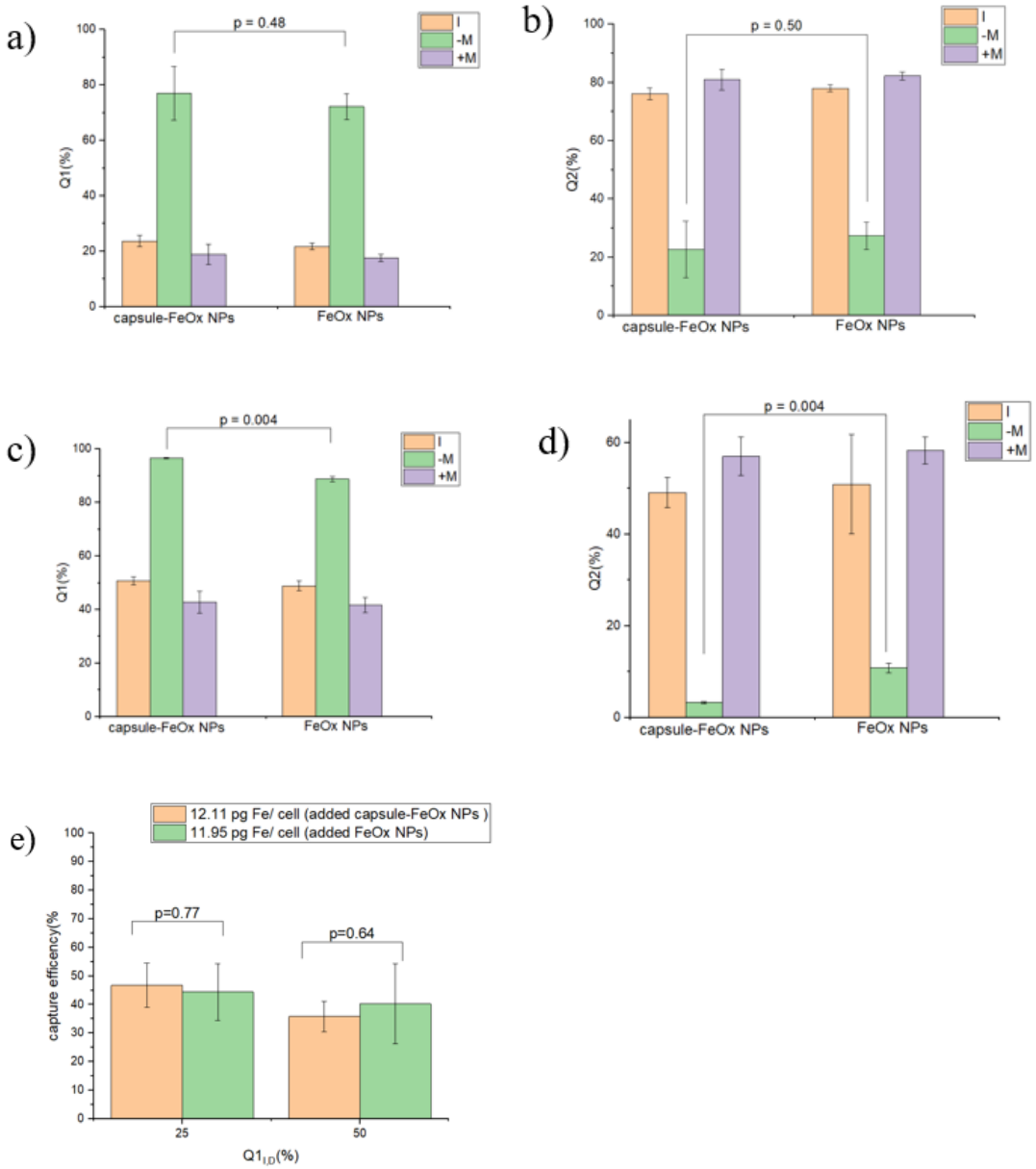

Figure 21. compare target cell ratio a) c), and background cell ratio b) d), between added capsule-IONPs and IONPs when $Q1_{I,D}$ is 25 % a) b), 50% c) d). e) compare capture efficiency between added capsule- IONPs and IONPs.

2.8. conclusion

From above results we can get following conclusion:

Different dye, here we used calcein and cy5, and the molecular weight of calcein is about 622 Da, and the molecular weight of cy5 is 657 Da, they can enter the cavity of the capsule by post-loading, incubate with capsule in 70℃ for 90 min. Then the loaded capsule can used for cell label, used for marking target cell and background cell in a mix system. And this method of labeling cells is not uniform, some cells will not uptake the capsule, some cells only attach with capsule, and some cells are uptake the capsule, they are not uniform in label cells, which is consistent with the report of Semmling et al[91]. the method of labeling cells more uniformly is to use molecules with specific affinity for biological molecules in cells, such as dye-labeled antibodies or nucleic acid aptamers. In our study, added only twice the amount of capsule-dye as the number of cells, and some target cells and background cells were not labeled with capsule-dye, but we set different proportions of target cells in mix cells system, to get the change of cell purity after capturing target cells, which is a trend that can reflect the real situation.

Capsule modified by iron oxide nanoparticles on the wall (capsule-IONP) are assembled by electrostatic interactions, the iron oxide nanoparticle is coating with PMA and the surface charge is negative, after assembling two layers of PSS/PAH, a relatively stable rigid structure has been formed, then replace PSS with these nanoparticles and continuing to assemble two layers. These Capsule-IONP can be targeted into cells under the influence of a magnetic field, from the report of Markus et al[42], and the report from Neus et al [92] reveal polyelectronic capsules will contact the cells due to gravity in the cell culture medium by considering the density and volume of the capsule. And from the cell imaging the cells can uptake capsule-IONPs, then detach these cells, and for magnetic sorting by attach with magnet and using Miltenyi MS column (the core part of the columns is the internal microporous structure, which can generate a strong local magnetic field under the action of an external magnetic field), both methods can retain cells that have been incubated with magnetic capsules, but the price of using Miltenyi MS column is more expensive than directly attaching EP tube to a magnet, directly using the EP tube to attach to the magnet to capture cells is a better

choice.

Ultimately the capsule-IONPs is used in complex clinical samples. The presence of background cells is the biggest interference in isolating target cells. Therefore, a mixed sample of two labeled cells was used for sorting experiments to explore the ability of the capsule-IONPs to capture target cells in mixed samples. Adding capsule-IONPs at 2, 4, 6, or 8 times the number of cells increased the proportion of target cells after magnetic sorting, while the proportion of background cells decreased. At the same time, it was also observed that the proportion of target cells decreased and the proportion of background cells increased in the washing waste liquid. We can get the conclusion that capsule-IONPs are effective in magnetic cell sorting.

When comparing the percentage of target or background cells in different ratio capsule-IONPs per cell, adding more capsule-IONPs will reduce the percentage of target cells in the washing waste liquid, which means that cells with more capsule-IONPs will be attracted by the magnet; in the captured sample, adding six times capsule-IONPs per cells will increase the percentage of target cells compared to adding two times capsule-IONPs per cell, which also means that cells with more capsule-IONPs will be attracted by the magnet. Adding eight times magnetic capsule per cell will result in a lower percentage of target cells than adding six times capsule-IONPs per cell, so we can get the conclusion it does not the more capsule-IONPs are added, the higher the percentage of target cells after magnetic sorting, it is maybe caused by more background cells to adhere and be retained, and more target cells to die. Therefore, the relationship between the percentage of target cells after magnetic sorting and the number of capsule-IONPs added needs to consider cells adhesion, and perhaps using a flow capture system will better in prevent cell adhesion.

In a mix system, capture efficiency and capture purity is a complex relationship. The number of captured cells increases, which increases the capture efficiency, but it does not mean that the purity of the target cells increases. Therefore, when capturing target cells, capture efficiency and capture purity should be considered together, both of which have guiding significance for clinical application.

Hela internalized iron oxide nanoparticles coating PMA also can be magnetic sorting by attach with magnet. After adding iron oxide nanoparticles to the complete culture medium of cells for 24 hours, we observed obvious aggregation of magnetic beads under the

microscope, because the magnetic nanoparticles in the salt culture medium environment will affect the surface charge of the nanoparticles, and maybe form protein coronas with the protein cytokines in culture medium, in addition, these magnetic nanoparticles themselves have magnetic interactions, which all leads to the aggregation. However, we are investigating whether iron oxide nanoparticles will have an effect on cell magnetic sorting, so there are not considering the aggregation of magnetic nanoparticles. However, we have to point out that the current use of magnetic nanoparticles for magnetic cell sorting is often incubated in a protein-free isotonic saline solution, the incubate time is determined by the ligands on the surface of the magnetic beads interact with the biomolecules on the cell surface, which is often about 10 minutes to one hour.

In a mixed sample containing target cells and background cells, the ratio of target cells is increase after magnetic sorting, and the ratio of background cells are decrease, so the iron oxide nanoparticles also are effective in magnetic sorting of cells. From my experiments, there is no significant different of capture efficiency between added capsule-IONPs and added iron oxide nanoparticles when the iron content per cell is similar.

3. Different Cell labeled by different metal nanoparticles for X-ray fluorescence imaging

2.1. Introduction

From cancer facts and figures 2024, in the worldwide, cancer is one of the leading causes of death[93], and developing some methods to effective cancer therapy and diagnosis is challenging and importantly. Nanoparticles has versatility, and has much research in the modern science, in the field of inorganic nanoparticles, there have different size, structure (including inner structure), composition and geometry, and specific physical, electrical, optical and magnetic properties, which let the nanoparticles have great potential in the application of precision therapy, medical imaging and improving drug delivery in bioenvironments. For cancer diagnosis, biomedical imaging by nanoparticles[94] which has special physical and chemistry properties[95]. For precision therapy, developing target ability of chemotherapy drugs and specific bond to the biomarker on the surface of cancer cell [96]; delivering with nanoparticles to enhanced tumor accumulation[97] and improve the stability of small molecular, for some with limited water solubility[98]. When nanoparticles used in biological environment, there has a lot of biological barriers[99-100]: excretion by macrophages, form coronas[101], and blood flow[102] when systemic administration, extravasation ability of nanoparticles to reach the target tissue[103]. Penetration ability of nanoparticles in solid tumor[104], cell uptake ability[105-106] and distribution in cell[107-108 109]when contact with cancer cell[110-111].The quantitative details are important for study the interaction between nanoparticles and cells[112-113].

In this project, we focus on metal nanoparticles, including Au-PMA NPs, IONP-PMA, NaYF4-PMA NPs, TiO2-PMA NPs, Ag-PMA NPs, CdSe-PMA NPs and Pt-PMA NPs, and different cells, including Hela, NRK, 3T3, MDA-MB-231, and MCF-7, study the interaction between these cells and nanoparticles about cells uptake and explore the metal nanoparticles distribution in cell. We use ICP-MS to make sure the uptake ability of cell for nanoparticles, X-ray inflorescence imaging is a promising detection method in situ, then to detect the metal nanoparticles signal in cell. Make and explored the metal nanoparticles as cell labeling in a

mix differently cells sample by XFI.

3.2. Major regents

Name	Purity	Company	Function
Gold (III) chloride trihydrate	≥99.9%	Sigma Aldrich	Au NPs synthesis
Sodium citrate	99.9%	Sigma Aldrich	Ag and AuNPs synthesis
tannic acid	99%	Sigma Aldrich	Ag NPs synthesis
Silver nitrate	≥99.9%	Sigma Aldrich	Ag NPs synthesis
poly (isobutylene-alt-maleic anhydride)	NA	Sigma Aldrich	For coating NPs
tetrahydrofuran	≥99.9%	Sigma Aldrich	For coating NPs
dodecylamine	97%	Alfa Aesar	For coating NPs
chloroform	100%	VWR	For coating NPs
SH-PEG-CH_3O	NA	Sigma Aldrich	For coating NPs
Resazurin	~80%	Sigma Aldrich	Cell viability
Phosphate buffered saline		Invitrogen	For cell culture
Dulbecco's modified eagle medium-High glucose		Sigma-Aldrich	For cell culture

Dulbecco's modified eagle medium,	PAN biotech	For cell culture
0.05% Trypsin/EDTA	Thermofisher	For cell culture
Fetal bovine serum	capricorn	For cell culture
Poly-L-lysine hydrobromide	Sigma	Promote cell adhesion
Fetal bovine serum	PAN biotech	For cell culture

3.3. Abbreviations

$HAuCl_4$	Tetrachloroauric acid
DDA	dodecylamine
PMA	poly (isobutylene-alt-maleic anhydride)-graft-dodecyl
$AgNO_3$	Silver nitrate
FeOx NPs	Iron oxide nanoparticles
Au-cit	Gold nanoparticle capped with citrate
PBS	Phosphate buffered saline
TEM	Transmission electron microscopy
PFA	paraformaldehyde

THF	tetrahydrofuran
DDA	Dodecylamine
PEG	Polyethylene glycol (CH_3O-PEG-SH)
Au-PMA NPs	Gold nanoparticles coating with PMA
$NaYF_4$-PMA NPs	Sodium tetrafluoro yttrium nanoparticles coating with PMA
Pt-PMA NPs	Platinum nanoparticles coating PMA
V	viability
CdSe	Cadmium selenide

3.4. Key instruments

Name	Model	Company	Function
Dynamic light scattering (DLS)	NANO 25	Malvern	NPs characterization
Transmission electron microscopy (TEM)	JEM-1400PLUS	JEOL	NPs characterization
UV-vis absorption	Cary 60 UV-Vis	Agilent	NPs characterization
microplate reader	Omega S/N 415-4273	BMG LABTECH GmbH	For cell viability

Indcuctively coupled plasma mass spectrometry (ICP-MS)	7700 Series studies	Agilent	get Mental content per cell
X-ray micro-probe beamline	P06 hutch	Desy	get the mental signal in cell

3.5. Experiments and methods

3.5.1. Synthesis of Au nanoparticles

The principle of synthesis Au NPs is reducing gold ions using sodium citrate as reducing agent and stabilizer, as described in *eq 3.1*.

$$n\ HAuCl_4\ (aq) + n\ (^-OCOCH_2)_2\ C(OH)COO^-)\ (aq) \longrightarrow$$

$$4n\ Cl^-\ (aq) + 4n\ H^+\ (aq) + Au^0{}_n + n\ (^-OCOCH_2)_2\ CO\ (aq) + n\ CO_2 \qquad eq\ 3.1$$

The first step of synthesis of ~ 100nm Au nanoparticles was synthesizing the Au-cit NPs seed. And then seeded growth of Au NPs up to 100nm[114-115], as shown in Figure 3-1.

Add 150mL a solution of 2.2mM trisodium citrate into a 250mL three-neck round bottomed flask, under vigorous stirring heated the solution with a heating metal to boiling, simultaneous utilize a condenser to prevent the evaporation of the solvent. After boiling 5min, add 1mL 25mM HAuCl4 solution, induced the solutions color changed from yellow to soft pink in 10 min, and the Au seed nanoparticles was synthesized. Then reduced heat until the solution's temperature reached 90℃, and kept the solution in 90℃, kept stirring and utilized condenser for the whole process of Au seed growth.

the growth of Au seed is repeat these steps: Add 1mL 25mM HAuCl4, then stirred for 30min, then repeat this step for twice times, then extracted 55mL solution from flask, then added 53mL Milli-Q water and 2mL 60mM trisodium citrate to dilute the solution, then wait about 20min the solution's temperature heat up to 90℃. Then continue injected 1mL 25mM $HAuCl_4$ for three times and 30 min interval. Repeat 7 cycles, we can get the Au-cit NPs with diameter about 100nm.

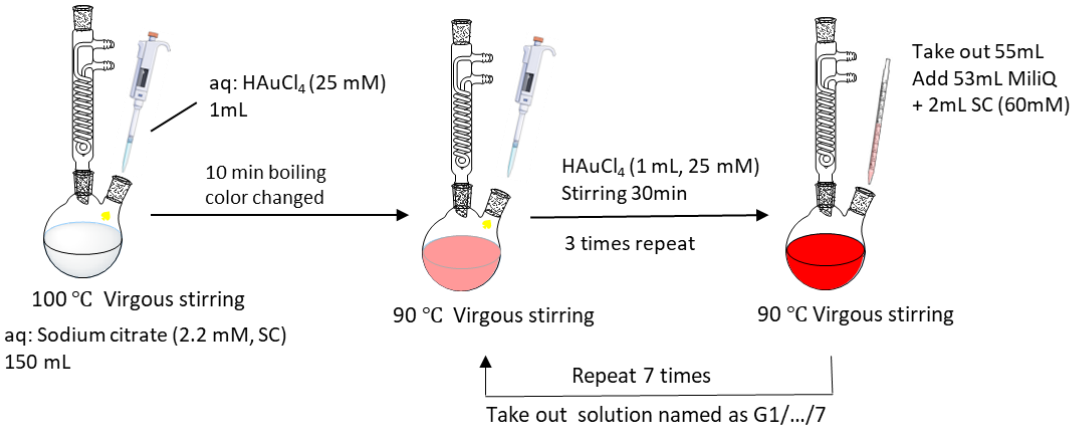

Figure 3-1: Synthesis process of 100nm Au-cit NPs.

The extracted 55mL solution in this process marked as G1, and then repeat this process, marked the extracted solution as G2, G3…, G6, G7. In order to know the size of Au NPs extracted from each cycle, we use UV-vis absorbance spectra to measure the size, because observed optical behavior change is fit with the nanoparticle's size change[116-117], also use DLS to measure the nanoparticles size [114], as show in Figure 3-2 and Figure 3-3.

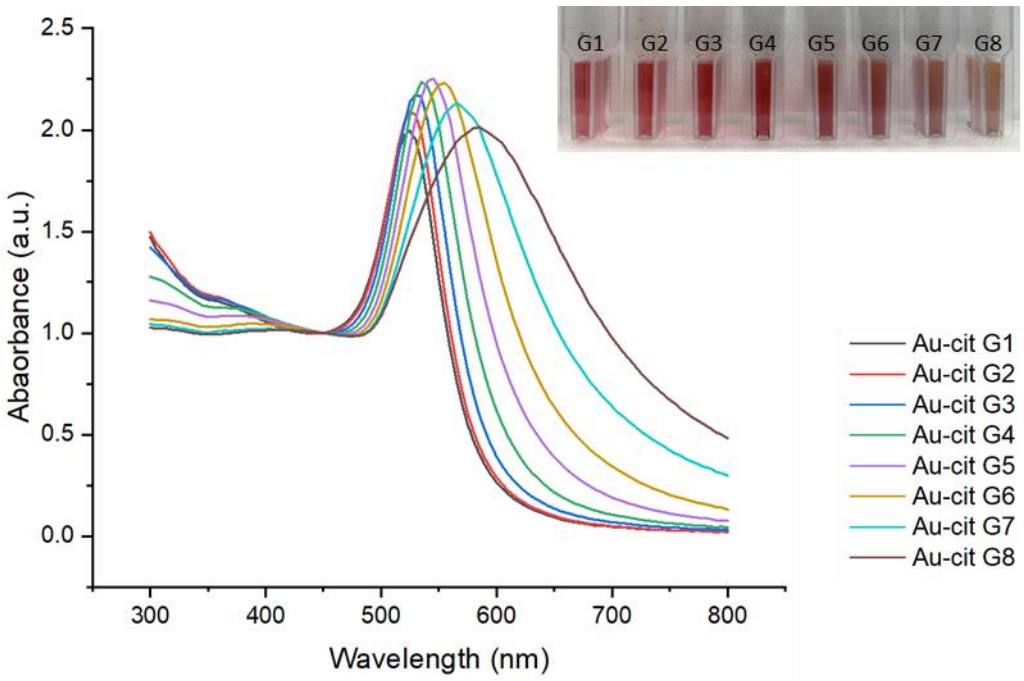

Figure 3-2: UV-vis absorption spectra of Au-cit NPs obtained after different growth steps.

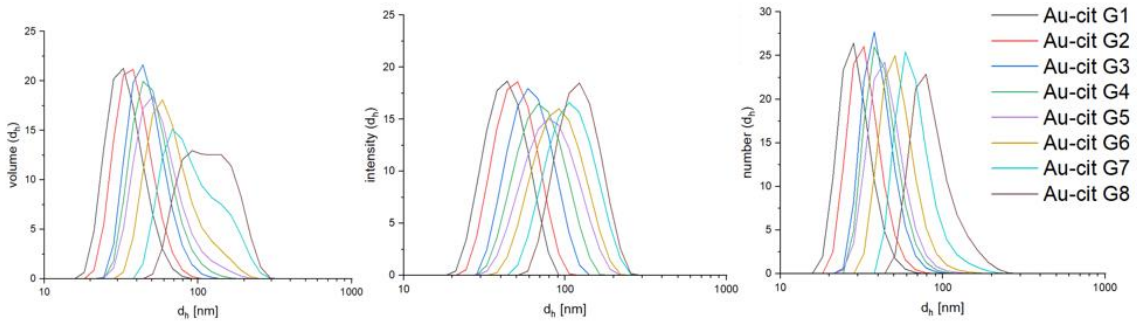

Figure 3-3: Size distribution profiles measured by dynamic light scattering of Au-cit NPs obtained after different growth steps.

Sample	λ_{SPR} [nm]	$d_{h,I}$ [nm]	$d_{h,V}$ [nm]	$d_{h,N}$ [nm]	PdI
Au-cit NP G1	525	44.43 ± 0.87	34.7 ± 1.05	29.63± 1.21	0.093
Au-cit NP G2	525	51.12 ± 0.75	39.56 ± 1.18	33.81 ± 1.58	0.087
Au-cit NP G3	529	63.27 ± 0.92	47.87 ± 0.44	40.77 ± 0.34	0.109
Au-cit NP G4	535	73.47 ± 1.05	52.85 ± 1.1	43.44 ± 1.01	0.131
Au-cit NP G5	545	85.41 ± 0.83	59.38 ± 3.2	46.13 ± 3.62	0.151
Au-cit NP G6	555	95.21 ± 1.15	71.85 ± 2.25	54.44 ± 2.81	0.112
Au-cit NP G7	564	113.47 ± 1.50	99.33 ± 1.85	69.61 ± 2.69	0.094
Au-cit NP G8	584	125.27 ± 2.18	122.97 ± 3.31	89.01 ± 5.02	0.067

Table 3-1: Characterization of Au-cit NPs from different generation. Surface plasma resonance peak (λ_{SPR}), hydrodynamic diameter ($d_{h,I}$, $d_{h,V}$ and $d_{h,N}$). Data points are given as mean value ± standard deviation (SD).

From the inference [118], the Au-cit nanoparticles size is about 100nm, and the position of the surface plasmon resonance peak is between 560nm and 580nm, so we choose G7 as the 100nm Au NPs.

We need get the molar concentration of Au NPs for next step surface modification calculation. TEM provide the diameter of NPs and the ICP-MS provide the mass concentration, for spherical Au NPs, then we can get the Au NPs molar concentration in solution system from above diameter and mass by following equations:

$c_{NP} = [C_{NP}/ (\rho_{NP} \times 4/3\ \pi(d_{NP}/2)^3)] / N_A$ *eq 3.2*

c_{NP}: molar concentration of nanoparticles

C_{NP}: mass concentration of nanoparticles

ρ_{NP}: density of this metal nanoparticles

d_{NP}: diameter of nanoparticles

N_A: Avogadro's number

Here, we use the UV-vis absorption at 450nm to calculate the molar concentration of Au NPs according to the Beer-Lambert law, eq 3.3. And the value of ε_{450} is 6.44E+10, according to the literature [118].

$c_{NP} = A_{450} / \varepsilon_{450}$ *eq 3.3*

3.5.2. synthesis of Ag nanoparticles

The principle of synthesis Ag NPs is reducing silver nitrate using sodium citrate and tannic acid as reducing agent, stabilizer and complexation agent[119], as shown in Figure 3-4.

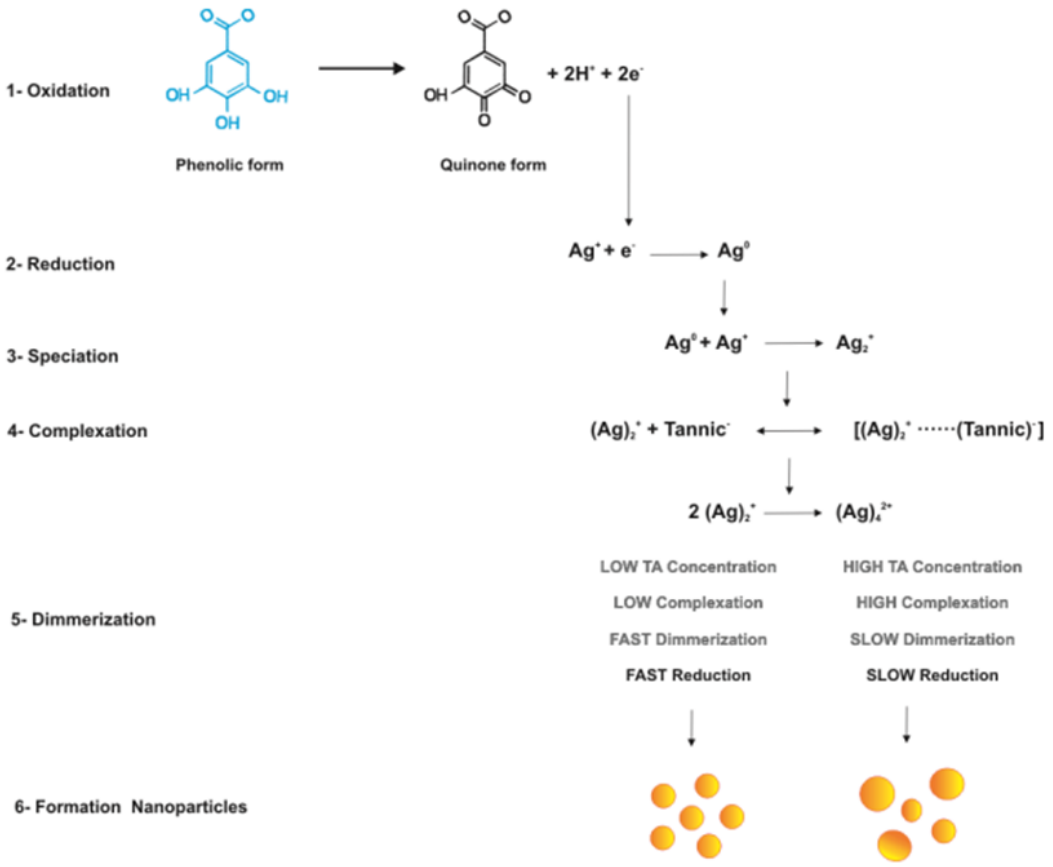

Figure 3-4: Synthesis mechanism of reducing silver ions by TA, (1) oxidation of TA to donate two electrons. (2) Ag+ received the electron and changed to Ag0. (3) (4) TA interacts Ag_2^+ and Ag^+ inducing its complexation. (5) (6) uniformly and irregular size Ag NPs form in low and high TA concentration respectively. this figure is extracted from the supporting information of reference[119].

As show in Figure 3-5, synthesizing silver nanoparticles requires first synthesizing silver seeds, and then the seeds growth. Chemicals preparation before experiment including: 147mg sodium citrate in 20mL Milli-Q water (SC, 25mM), 170mg tannic acid in 40mL Milli-Q water (TA, 2.5mM), 127mg silver nitrate in 30mL Milli-Q water ($AgNO_3$, 25mM). For synthesize seeds Ag NPs, 147mg sodium citrate in 10mL Milli-Q water to get 50mM SC, 42.5mg tannic acid in 10mL to get 2.5mM TA.

Mixed 10mL 50mM SC and 10mL 2.5mM TA to 100mL with Milli-Q water, into 500mL three-neck glass flask, heating the mixture to boiling under stirring and condenser, heated by a heating mantle, stirring by a magnetic stirrer, and condenser avoid the solvent evaporate, then added 1mL 25mM $AgNO_3$ into the solution, color immediately turned to bright yellow, and Ag NPs deeds formed. Then reduced the solution temperature to 90℃, inside solution no boiling.

The growth of Ag seeds is repeat these steps: take out 19.5mL solution, then added 16.5mL milli-Q water, 500µL 25 mM SC, and 1.5 mL 2.5 mM TA, then waited about 5-10 min the solution's temperature heat up to 90℃, then added 1mL 25mM $AgNO_3$, under stirring and heating the solution of seeds growth for 25min. Above process is one cycle of seeds growth. Then repeat seeded growth cycle for 17 times.

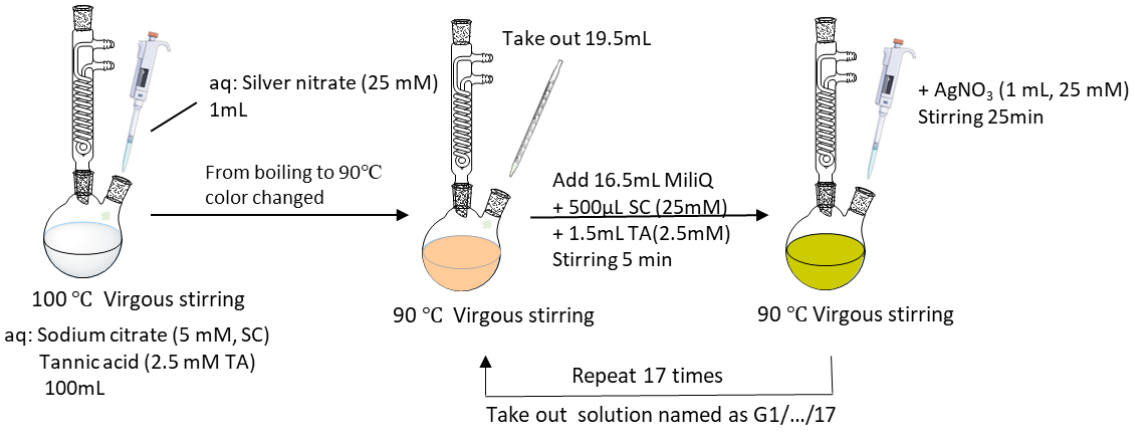

Figure 3-5: Synthesis process of 100nm Ag NPs.

The extracted 19.5mL solution in the first cycle marked as G1, and extracted solution in the next cycles marked as G2, G3…, G17. These solution cooled by putting in water or ice, the using DLS to monitor the size by test the intensity distribution of hydrated particle size, from inference[119], intensity peak value is around 116.5nm, and the Ag NPs diameter is about 100nm, and the concentration is about 5.2 x 10^10 NPs per mL. In the later surface modification, I always use this concentration to calculate.

3.5.3. Pd-PMA nanoparticles and CdSe-PMA quantum dots

The principle of synthesis Pd nanoparticles is reducing palladium acetylacetonate using morpholine borane as a reductant, oleylamine as a surfactant, and in a mixture of oleylamine and 1-octadecene[120]. After synthesis Pd NPs in organic solvent, added ethanol to wash these nanoparticles by centrifuge at 137000rcf for 30min, discard the supertant, then dispersed in chloroform, added PMA which is dispersed in chloroform for rotary evaporation to coating PMA. This part experiment is done by Sarodi Jonak.
Quantum dots with shell of CdSe, including synthesis and coating PMA, was done by Chenxi Yang.

3.5.4. Preparation of poly (isobutylene-alt-maleic anhydride)-graft-dodecyl

poly (isobutylene-alt-maleic anhydride)-graft-dodecyl is an amphiphilic polymer, which is consists of two parts: poly (isobutylene-alt-maleic anhydride) as a hydrophilic backbone and dodecylamine as hydrophobic side chains, as show in follow Figure 3-2. Each polymer monomer unit of poly (isobutylene-alt-maleic anhydride) has an anhydride ring, and we will let 75% anhydride rings coupled with dodecylamine by react with the NH_2 group of dodecylamine, and 25% anhydride rings will keep intact without reaction.

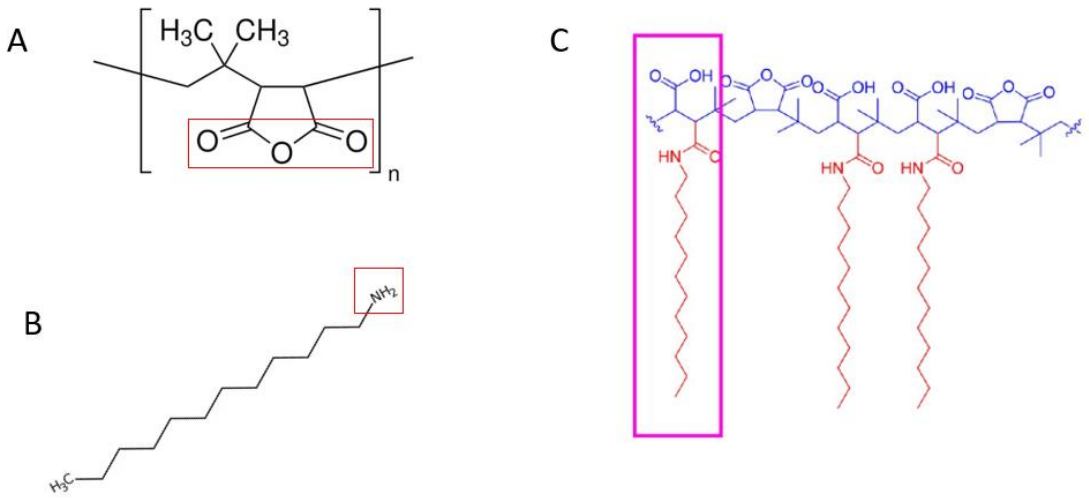

Figure 3-2: (A) Chemical Structure of poly (isobutylene-alt-maleic anhydride). (B) Chemical Structure of Dodecylamine. The red box in A and B show the reaction group by integrate together. (C) Chemical Structure of poly (isobutylene-alt-maleic anhydride)-graft-dodecyl. The purple box in C shows the monomer unit of intact PMA with connect with side chain, and the bule part is shows the hydrophilic backbone and the red part shows the hydrophobic side chains. The figure (C) is extracted from reference [121].

3.084g poly (isobutylene-alt-maleic anhydride) (PMA, Sigma, CAS Number 531278) dispersed in 100mL anhydrous tetrahydrofuran (THF, CAS Number 186562) in a 250mL round bottom flask by sonication. And molecular weight of one PMA monomer unit is about 154g/mol, and molecular weight of one dodecylamine is about 185.35g/mol. According to *eq 3.2* and *eq 3.3*, calculated the 2.78g dodecylamine (DDA, CAS Number 44170) was added into the aforementioned PMA solution, and the mixture was sonicated for about 20 seconds, then under stirring heated to 60℃ for overnight. The next day, the solution was dried by an evaporator to remove THF, then redissolved in 40mL chloroform (CAS Number 372978) and dried by evaporator, this step was repeated twice to remove the residual THF. Finally, PMA was stored in 40mL chloroform, according to the *eq 3.4*, the final PMA monomer concentration is 0.5M.

$n_{PMA\text{-}m}=m_{PMA}/M_{PMA\text{-}m}=3.084g/(154g/mol)=20\ mmol$ *eq 3.2*

$m_{DDA}=n_{DDA}\times M_{DDA}=0.75\ n_{PMA}\times M_{DDA}=0.75\times 20\ mmol\times (185.35g/mol)=2.78g$ *eq 3.3*

$c_P = n_{PMA\text{-}m}/V=20\ mmol/0.04L=0.5M$ *eq 3.4*

$n_{PMA\text{-}m}$: amount of PMA monomer unit

n_{DDA}: amount of DDA

m_{PMA}: mass of PMA

m_{DDA}: mass of DDA

$M_{PMA\text{-}m}$: Molar mass of PMA monomer unit

M_{DDA}: Molar mass of DDA

c_P : Molar concentration of intact PMA monomer unit

3.5.5. Transfer AuNPs from water to chloroform

Citrate is a weak ligand by physically absorbed on the surface of Au nanoparticles through central carboxylate groups of citrate anions[122], and citrate ligand tend to desorb from the surface of Cit-Au, leading Au-cit nanoparticles irreversible aggregation in subsequent centrifugation, dialysis or other operation, so we use Polyethylene glycol (PEG) as a stronger ligand to replace citrate by Au-S bond forming with the Au atom of the surface of Au-cit NPs . PEG's unique solubility in both aqueous and organic media provides excellent colloidal stability for nanoparticles in both media. In addition, PEGylation enhance nanoparticles' biocompatibility and reduces the absorption of non-specific proteins with nanoparticles, and prolong nanoparticles' circulation time in vivo[123].

Herein, Thiolated polyethylene glycol (SH-PEG-CH_3O, 2kDa, CAS Number 12750-40) was dissolved in Milli-Q water to obtain 100mg/mL PEG solution, the calculation amount of PEG added according to $c_{PEG}/c_{NP} = 50\times10^4$, to ensure that the surface of AuNPs is capped with enough PEG molecule, and ca. 5-15 PEG per nm^2 of AuNP[121]. After stirring 2 min, adjust pH value of the mixture solution of PEG and Au NPs to 8-9 with 2 M NaOH, this step is for deprotonate thiol groups of SH-PEG-CH_3O and increase their reactivity, and stirred for at least 3 hours or overnight at room temperature, after this step, Au-cit nanoparticles will completely be coating with PEG and changed to Au-PEG NPs.

Dodecylamine (DDA, CAS number 124-22-1) is a hydrophobic chain, and can dissolve in organic solvent, and transfer Au-PEG NPs from aqueous phase to organic phases by coating DDA. Herein, DDA was dissolved in chloroform to obtain 0.2M DDA solution, then mixed with Au-PEG NPs with a volume ratio of 1:1, and calculation amount of DDA added according to

c_{DDA}/c_{NP} = 40×10^6, which ensure partial/full exchange of PEG by DDA. Aqueous phase containing Au-PEG NPs on the top and organic phase with the DDA at the bottom, these two phases were mixed by magnetic stirring at about 800 rpm for about 4 hours, this step ensure PEG and DDA firmly attached. After this step, nanoparticles were intently transfer to the chloroform phase, then cleaned twice to remove free PEG and DDA molecules by centrifugation at 540 rcf for 30 min, discard the supernatant and redispersed in chloroform, finally collect the Au-DDA NPs dissolved in chloroform.

3.5.6. PMA coating of Au NPs

In the above steps, we have obtained 0.5M PMA in 40 mL chloroform and diameter about 100nm Au-DDA NPs in chloroform, now coating PMA on the surface of Au NPs, the principle is attached 4000 monomer units of PMA-g-dodecyl per nm^2 of effective surface area of 100nm Au NPs. According to *eq 3.5*, calculate the amount of polymer monomer unit added to the NPs.

$$V_{P\_sol} = (R_{P/Area} \times A_{eff} \times c_{NP} \times V_{NP\_sol}) / c_P \qquad \textit{eq 3.5}$$

V_{P_sol}: Volume of polymer solution

$R_{P/Area}$: The number of monomer units per nm^2 effective surface of NPs

A_{eff}: The effective surface area of one NPs

c_{NP}: Molar concentration of NPs

V_{NP_sol}: Volume of nanoparticles

c_P: Molar concentration of polymer monomer unit

Mixed the PMA and Au-DDA NPs together in one neck round glass flask, then shaken and sonicated for about 1 min, then used a rotary evaporator to evaporate chloroform under reduced pressure at 40℃ until the bottom no flowing liquid, then add chloroform again and do this rotary evaporator for more two times, this process forced the PMA coat on the surface of Au-DDA NPs, at the last time rotary, the mixture was completely dry until there was a film on the glass flask bottom. Then added 0.1M NaOH into the flask to disperse the PMA coated Au NPs, if necessary, using sociation to accelerate dissolution. The NaOH solution make PMA hydrolyzed forming carboxylate groups and allow Au-PMA NPs with good colloidal stability in water solution. After dissolution for a while, centrifugation at 536

rcf for 25min to discarded the supernatant with polymer, then added milli-Q water in the bottom pellet.

3.5.8. PMA coating of $NaYF_4$ NPs

This nanoparticle is synthesized by Miao Feng[124], the synthesis was under nitrogen atmosphere, and surface is linked by oleic acid, and store in chloroform solution, then coating with PMA. Take out 200μL NaYF4 NPs in 20mL chloroform, put in 100mL round bottom flask, then added 100 μL 0.5M PMA, gently shaken then sonicated for 1 min, then place the flask on a rotary evaporator, set the water bath is 40℃, and rotating speed is 80 rpm, and atmospheric pressure is 300 bar, reduce pressure to dry the solvent, repeat rotary evaporator for another two times. The last time evaporator, must be sure there is no solution in the flask, absolutely dry, then added 10mL 0.1M NaOH solution in the flask, until the film at the bottom of glass bottle is completely dissolved. then use an ultrafiltration tube (Ultra-4 centrifugal filter unit 100 kDa, Sigma Aldrich) to remove the excess PMA and NaOH, 3000rpm 5min for 5 times, washed with Milli Q water. Then keep these nanoparticles in MilliQ water for subsequent experiments.

3.5.8. cell culture

The five different cell lines: Hela, MCF-7, NRK, MDA-MB-231, and 3T3, were obtain from our cell lab, these all are adherent cells. Dulbecco's modified eagle's medium-high glucose (DMEM, Sigma-Aldrich) store in 4℃, with 10% fetal calf serum (FBS), as culture medium; 0.05% Trypsin-EDTA (gibco) as agent to detach cell from culture flask; Phosphate Buffered Saline Tablets (Fisher BioReagents), one tablet dissolved in 200mL Milli-Q water, then sterile by autoclave, was as cells buffer (PBS). The added amount of these agents was according to the *table 3-1*. Cells are incubated in 37℃, 5% CO_2, humid air atmosphere incubator. When cells growth reach above 90% of flak bottom area, usually every two days, cells passaged, washed cells with PBS, then added trypsin. Different cells have different detach time: when added 800uL 0.05% Trypsin in T25 flask, waited for 1min for MDA-MB-231, 1-2min for MCF-7, 2min for Hela, 2-3 min for NRK, and less than 1 min for 3T3 under in 37℃ incubators. Then

immediately added complete cell culture medium to stop digestion, collected the cells and centrifuge at 300g for 5min, dispersed in complete medium again for continue culture. The cells (the five types of cells mentioned above) seeding number in different 96, 24, 12, 6-well plate and T25, T75 flask are shows on *Table 3-1*. And from ATCC website (American type culture collection) obtain the cells centrifuge situation is 130 rcf 5min for Hela and NRK, 150 rcf 5-8 mins for 3T3, 125 rcf 5min for MDA-MB-231 and MCF-7.

Table 3-1. the added amount of medium, pbs, trypsin and cells seeding number under different culture flask or plate.

Culture flask or plate	96-well	24-well	12-well	6-well	T 25	T 75
Bottom area / cm^2	0.32	2	4.5	9.6	25	75
Medium / mL	0.1	0.625	1.4	2	5	15
PBS / mL	0.1	0.5	1	2	5	15
0.05% Trypsin / mL	-	0.02	0.05	0.4	0.8	2
Seed Cells number	1 0000	6 2500	14 0000	30 0000	78 0000	234 0000

3.5.9. cell viability assay

Cell viability assay has may methods: MTT by spectrophotometer (living cells reduce a yellow tetrazole to purple formazan)[125], LIVE/DEAD assays by flow cytometer or confocal (calcein-AM label live cells, propidium iodide or Ethidium homo dimer 1 label dead cells), and so on. We chose resazurin (sigma Aldrich, CAS number: 62758-13-8) to measure cell viability[126]. The detection principle is that during the cell proliferation process, the ratios of NADPH/NADP, FADH/FAD, FMNH/FMN and NADH/NAD in the cells increase and they are in a reducing environment. The resazurin taken into the cells is reduced to resorufin, as show in Figure 3-3, then released outside the cells and dissolved in the culture medium, causing the culture medium to change from non-fluorescent indigo blue to fluorescent pink. Finally, a spectrophotometer or fluorescence photometer is used for detection, its maximum absorbance is 573nm, and its fluorescence is excitation light 579nm/emission light 584nm. The absorbance and fluorescence intensity are proportional to the number of active cells.

When nanoparticles incubate with cell for a period, then use resazurin to detect the cell viability to determine the cytotoxicity of nanoparticles[127].

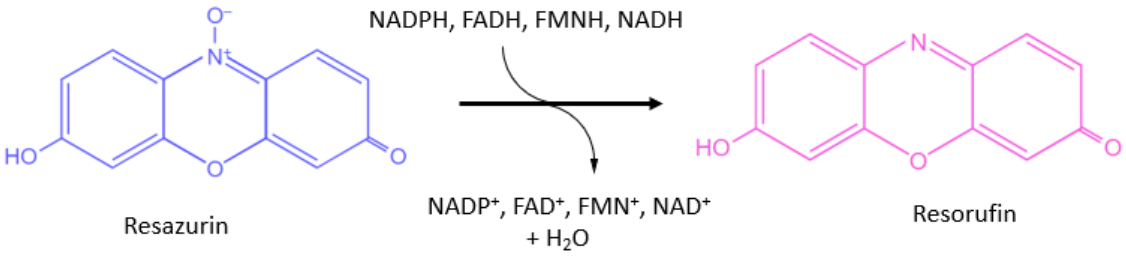

Figure 3-3: Changes of the structure of resazurin in detecting cell viability. Active cells can produce NADPH, FADH, FMNH, NADH.

Cells were seeded in 96-well plate in the first day, left the cells overnight for attach to the bottom of well; In the second day, washing with 100 µL PBS, then 100uL medium containing different concentration nanoparticles in each well to culture cells, the specific steps of which are: firstly added 100 µL medium in each well, then added 40 µL medium and 60 µL nanoparticles solution in one well and set this well as highest concentrated well with total volume of 200 µL, then a dilution series was done by taking out 100 µL, transfer and mixing with the following well to obtain1/2 dilution, so get a series concentration with ½ dilution. Each concentration was done for three times, and keep some cells were only incubate with complete medium not added NPs, as negative control sample in the later test. And incubated these cells for overnight; In the third day, prepared 0.2mg/mL resazurin in PBS as stock solution, washed cells with 100 µL PBS, repeat three times, to remove the remaining nanoparticles, then incubated with complete medium within 10% resazurin stock solution (v/v), which also added in empty well for blank. Kept in incubator for 4 hours, then test by fluorescence meter with excitation at 560nm and emission from 570nm to 620nm. And the fluoresce intensity at 585nm used for calculation of cell viability, according to the *eq 3.6*.

$V\% = (I_{sample} - I_{blank}) / (I_{control} - I_{blank})$ *eq 3.6.*

V%: Active cell ratio

I_{sample}: Fluorescence intensity at 585nm of sample well (NPs +cells+ 0.025mg/mL resazurin in medium)

I_{blank}: Fluorescence intensity at 585nm of only 0.025mg/mL resazurin in medium

$I_{control}$: Fluorescence intensity at 585nm of only cells with 0.025mg/mL resazurin in medium

3.5.10. cellular uptake assay

Study cell uptake is important for the interaction between nanoparticles with cell[112, 128-129].As previously reported[130-131], uptake study of Au NPs exposed to Hela-PMA cells, Ag-PMA NPs exposed to MCF-7, FeOx -PMA NPs exposed to NRK cells, Pd-PMA NPs exposed to 3T3, and CdSe-PMA QDs exposed to MDA-MB-231 cells were performed by ICP-MS. For that, 140 000 Hela cells, MCF-7 cells, NRK cells, MCF-7 cells, and MDA-MB-231 cells were seeded per 12-well plate 4.5cm^2 surface area per well respectively, 1.4 mL medium added, according to *Table 3-1*, and put in incubator for overnight. The next day, these cells were exposed to the different nanoparticles at different concentration, see Table 3-2, in complete cell medium for 6 hours and 24 hours. After the desired incubation time, removed the supernatant, and washed the cells with 1mL PBS per well for three times, then added 50 µL 0.05% trypsin, still the cells can detach the bottom as soon as possible added the complete 1mL medium, collected the cells for centrifugation at 300g for 5min, discarded the supernatant, and added 1mL PBS in the pellet, pipetting the cells and counted, then centrifugation again and kept the pellet cells, then added 200 µL aqua regia (HNO_3:HCl=1:3) for overnight to destroys cells and degrades nanoparticles into metal ions. The mental content in cells was measured by ICP-MS, then the mass of mental per cell could be obtained. Each sample were performed in independent three times, so each experiment was with different generations of cells, and incubated at different days.

Table 3-2. different nanoparticles added in different cells at different concentrations range.

cells	samples	Concentration (µg/mL)
Hela	Au-PMA NPs	0.25 - 7.6
MCF-7	Ag-PMA NPs	0.062 - 2
NRK	FeOx-PMA NPs	1.2 - 40
3T3	Pd-PMA NPs	1.2 - 39
MCF-7	TiO_2-PMA NPs	
3T3	$NaYF_4$-PMA NPs	0 - 100

3.5.11. cell exocytosis assay

As previous reported[130-131], to study the long-term labeling efficiency of Hela with Au-PMA NPs, MCF-7 with Ag-PMA NPs, NRK with FeOx-PMA NPs, 3T3 with Pd-PMA NPs, and MDA-MB-231 with CdSe-PMA QDs in the fresh medium after exposure to nanoparticles. The 14 0000 cells in 1.4mL medium were seeded in 12-well plate overnight in incubator, then replaced the medium by 1.4mL medium with different concentration nanoparticles to expose 24 hours. Then, removed the medium and washed by 1 mL PBS for three times to remove the non-internalization nanoparticles, then added fresh medium, and incubated for 0, 6, 24 hours. After desired time, washed cells with PBS, and collected cells by centrifugation and counted the cells, and obtain the cells pellet, then added 200 µL aqua regia for overnight, and measured by ICP-MS.

3.5.12. seed cell of uptake mental nanoparticles on silicon nitride membranes

1. Prepare silicon nitride membranes for seeding cells

As shown in Figure 3-4, silicon nitride (Si_3N_4) membranes membranes: frame size = 5 x 5 mm, frame thickness = 200 µm, membrane size 1.5 x 1.5 mm, membrane thickness 500 nm; According to the literature[132], the flat side of the membrane should face up for cell seeding, and the other side of the membrane is a cavity, which should face the bottom of the dish; It is fragile and should be handled with care;

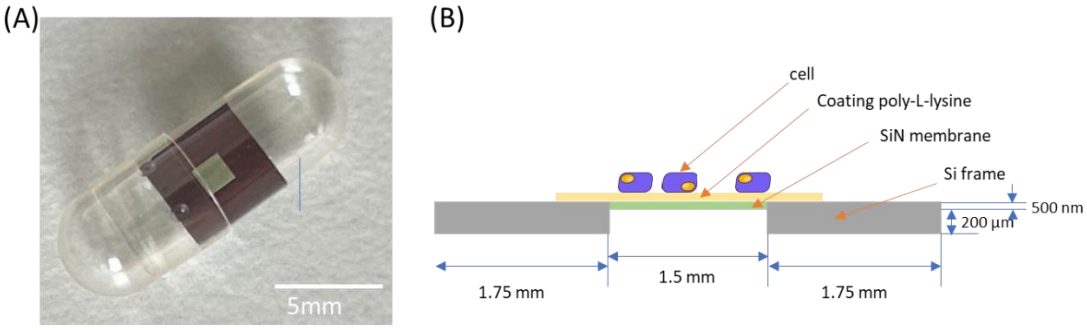

Figure 3-3. (A) A Si_3N_4 membrane in its protective capsule, from (B) the thickness of membrane window is 500nm, which is fragile. (B) the silicon nitride windows after cell seeding, the cells are cultured onto the flat surface of SiN membrane and poly-L-lysine

coated before seeding cell for promote cell adhesion.

Hold a corner of the membrane with tweezers, gently take out the membrane, and place it in a six-well plate (stick a small section of double-sided adhesive tape on the bottom of the six-well plate in advance, and gently stick to the corner of the Si_3N_4 membrane to fix the membrane); Use a 200 mL pipette gun to take 70% ethanol, drop the liquid to cover the membrane, and open the cover of the six-well plate in the ultra-clean hood for five minutes, then use 200 microliter pipettes to gently suck out the residual liquid on the membrane; take 100% ethanol cover the membrane, repeat the above operation; (This step is to sterilize the surface of the membrane. The method mentioned in the literature[132] is to expose the membrane to UV.) The ethanol was removed by suction and the membrane left to air dry at room temperature in a sterile environment. Then, 2-3 drops of 0.01 % poly - L - lysine was added directly to each membrane for 20 min. (poly-L-lysine is a nonspecific attachment factor for cell to increasing the number of positively charged sites available for cell binding, used in promoting cell adhesion to solid substrates, by enhancing electrostatic interaction between the culture surface and negatively charged ions of the cell membrane[133]) The grids were washed with PBS (2 x 3 mL), the PBS was removed and left to air - dry at room temperature.

2. seed cell of uptake mental NPs on Si_3N_4 membranes

Two days before this, seed 200 000 cells in 2mL DMEM (+ 5%FBS and + 0.5%PS) per well of 6-well-plate, and overnight, the second day removed the medium, added the medium contain different concentration of NPs, after incubate 24 h in incubator, removed the medium, and added 2mL PBS per well and shanked it a few times to wash cell, and repeat three to six times to remove the NPs that not entered the cell as many as possible, but still has some nanoparticles still adhere to the cell surface. Then added 100 μL 0.05% Trypsin to detach the cells from dish bottom, then added 1900 μL medium containing FBS to stop digestion, collected the cells.

Count the cells that have uptake the nanoparticles, and set the cell concentration to 50000 cells/mL; Then drop about 50 μL of 50 000 cells / mL suspension of cancer cells was added directly to each membrane and left to incubate for 2 h (37°C, 5 % CO_2). 2 mL of the same 50000 cells / mL cell suspension was added to each well and incubated for about 16 h (37°C,

5 % CO_2).

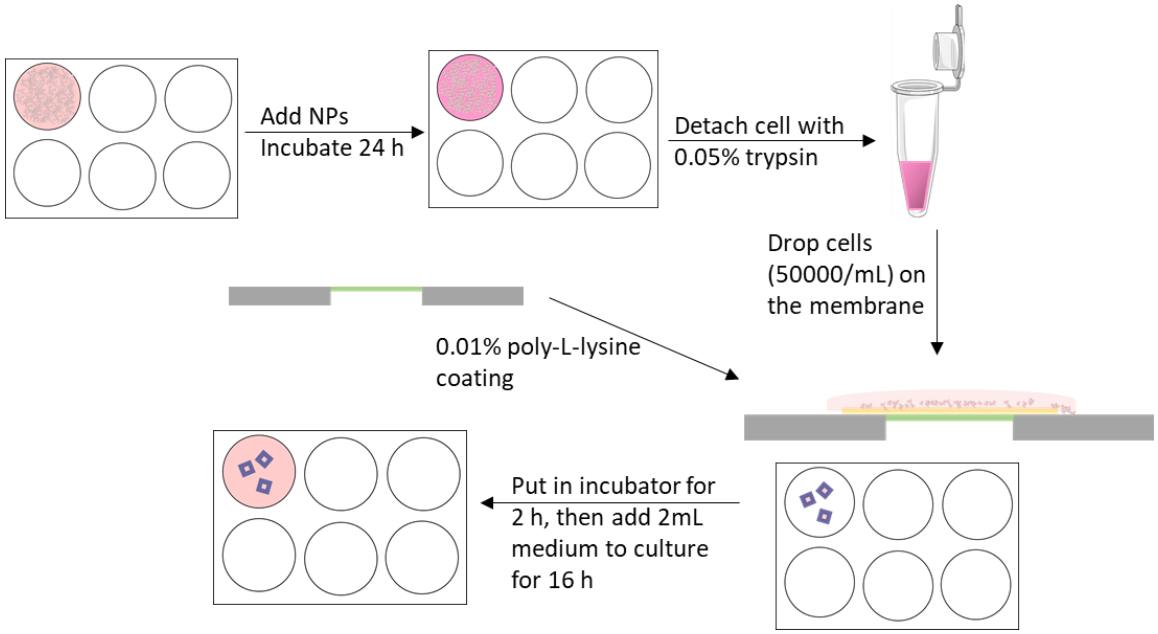

Figure 3-4. Scheme of procedures for seed of uptake NPs on SiN membranes.

3. Fixed cells by 4% paraformaldehyde

After 16h incubate, the medium was removed and the membrane were washed with PBS buffer before fixing cells with 4 % paraformaldehyde (PFA) for 10 min; Then PFA was removed and the grids were washed with 2 mL tris-glucose buffer (containing 261 mM glucose, 9mM acetic acid and 10mM tris buffer, pH 7.4) for three times, then blotted and let it to dry in air[134].

3.5.13. P06 beamline at the PETRA III synchrotron

In this project, we use hard X-ray Micro-probe beamline P06 at PETRA Ⅲ providing microscopic resolution X-ray fluorescence imaging, located in experimental hutches EH1 microprobe[135], and at 38.5m from the undulator the optical element generate a fixed vertical offset ranging from 2.4 to 100 keV, then to generate the energy from 4 to 30 keV by three different material(Si, Cr, Pt), at 43.3m X-ray pre-focusing by a refractive lenses. The detect setup as shown in the Figure 3-5, located at the end of the beamline at 92m. The Beam energy is range 5-23 keV (KB Mirrors), and we use the energy is 18 keV, and the focus size

(beam spot) is 300nm and 1.5µm, and containing 10^{10} photon per second, working distance is larger 150mm. and the detector is Fluorescence detector, Vortex ME4 Si drift detector and pco.edge (2048x2048 pixels, 6.5x6.5µm²). According to the Planck's constant, and eq. 3.7, calculating the wavelength of X-ray is 0.0689-0.059 nm. And atom diameter is 0.05-0.5nm. Therefore, these photons can hit metal atoms without diffraction, exciting electrons to undergo energy level transitions and thereby releasing energy.

$E=h\,c/\lambda$ eq. 3.7

E: energy.

h: Planck's constant, 4.1356676969×10-15 eV·s

c: lightspeed, 299792458m/s

Finding cells in the brightfield, then choose area of scanning, for signal cell scanning, set the scan area usually 0.1-0.2 mm^2, and move 50-100 steps horizontally or vertically, and the beamline stays for 0.1s at each step. For mix cell sample, need to scan a large area, set the scan area 0.5-1mm^2, and move 400-800 steps horizontally or vertically, and the beamline stays for 0.1s at each step. Then use ImageJ to preliminary analysis the image, including: added the color to grayscale value in mage, in here, blue to Zn channel, grays to K channel, red for Au channel, Green to Fe channel, Yellow to Y channel, purple for Ti. Then adjust the brightness and contrast, then add scale bar.

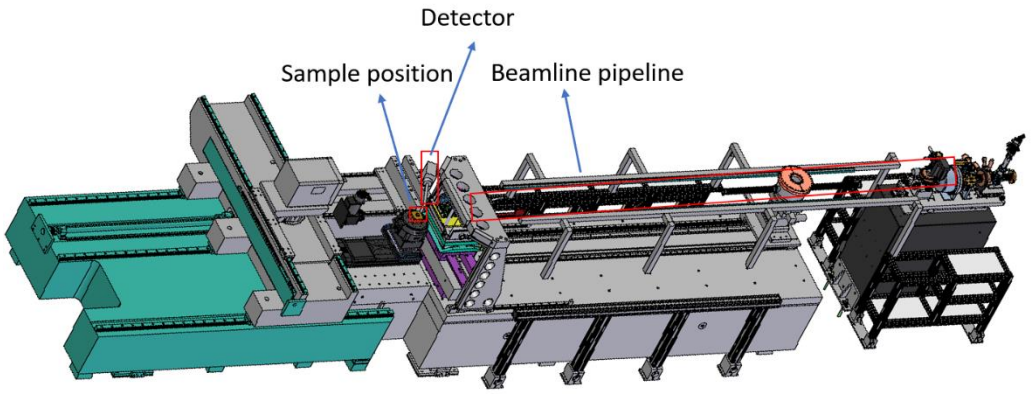

Figure 3-5: Device layout of hard X-ray Micro Probe Beamline P06. Picture is from https://photon-science.desy.de/facilities/petra_iii/beamlines/p06_hard_x_ray_micro_nano_probe.

3.6. results and discussions

3.6.1. nanoparticles synthesis and characterization

Transmission electron microscopy (TEM) uses electron beams instead of light for imaging. The energy of these electrons is usually 100keV to 300keV. According to the de Broglie formula, the wavelength of these electrons can reach 0.0025nm. When passing through the sample, they interact with the atoms in the sample and scatter, recording the transmitted electron information of the electrons, which is then converted into the morphology and structure of the sample. Therefore, the sample is required to be relatively thin, usually less than 100nm, so that the electron beam can pass through more easily. According to the Abbe formula, the resolution of the transmission electron microscope is sub-nanometer. It is used for a direct measure of the size and shape of nanoparticles. From these TEM image, observed the NPs shapes, obtained the frequency distribution of nanoparticles core diameter (d_c) using ImageJ, measured at least 100 NPs for each size distribution histogram, then calculated the NPs' mean diameter and its standard deviation.

Dynamic Light Scatting (DLS) was used to measure the hydrodynamic diameter (d_h) of NPs dispersed in water solvent, including number hydrodynamic diameter distributions ($d_{h,N}$) and intensity hydrodynamic diameter distributions ($d_{h,I}$) (the intensity of scattered light). The detection principle is based on Brownian motion and light scattering, analyzing the change of scattered light intensity over time to infer the size of particles. At the same temperature and solution, the smaller the particle, the faster the Brownian motion and the faster the change in scattered light intensity. DLS will generate an autocorrelation function based on the actual measured light scattering change speed, and then calculate the particle size based on the Stokes-Einstein equation.

Laser Doppler anemometry (LDA) was used to measure zeta-potentials (ζ), this characterizes the charge carried on the surface of nanoparticles. Nanoparticles coated with PMA and dissolved in water, inducing to ζ is in negative region. Its detection principle: apply an electric field to the sample, the charged particles will move in this electric field, irradiate these particles with laser, scatter will occur, detect the Doppler shift of the scattered light, to calculate the moving speed of the particles, and then calculate the zeta potential of the particles according to the Helmholtz-Smoluchowski equation.

UV-Vis Spectroscopy is based on the principle that when light (UV wavelength range is 200-400nm, visible wavelength range is 400-700nm) passes through the sample, the molecules or atoms in the sample will absorb light of a specific wavelength. The absorbed light energy causes the electrons in the molecules to undergo energy level transitions. Here, only the intensity and wavelength of the absorbed light are detected. The Beer-Lambert law describes the relationship between solution concentration and absorbed light intensity, and can thus quantify the concentration of the sample. The shape and characteristic peaks of the absorption spectrum can reflect the molecular structure information of the sample for qualitative analysis.

The characterization of Au-PMA NPs shows in Figure 3-6-1, TEM images determined the Au-PMA NPs shape were spherical or oval shape, and measured mor than 100 particles to obtain the d_c distribution, d_c was 103.41 ± 2.91 nm, $d_{h,N}$ was 115.4 ± 7.8 nm, $d_{h,I}$ was 151.6 ± 4.5 nm, ζ was -36.4 ± 4.68 mV. The characterization of FeOx-PMA NPs shows in Figure 3-6-2, TEM images determined the FeOx-PMA NPs were mainly cube shape, and measured the short distances (length of sides of a square), not the distance between its opposite corners, measured more than 100 particles to obtain the core diameter d_c was 26.87 ± 3.83 nm, $d_{h,N}$ was 137.03 ± 2.17 nm, $d_{h,I}$ was 181.23 ± 1.36 nm, ζ was -16.67 ± 0.75 mV, . The characterization of $NaYF_4$-PMA NPs shows in Figure 3-6-3, TEM images determined the NaYF4 NPs shape were spherical, this picture was done by Miao Feng, measured more than 100 particles to get the d_c was 37.76 ± 1.05 nm, $d_{h,N}$ was 37.08 ± 2.47 nm, $d_{h,I}$ was 74.29 ± 1.35 nm, ζ was -26.47 ± 5.38 mV. The characterization of TiO_2-PMA NPs shows in Figure 3-6-4, TEM images determined the TiO_2-PMA NPs were mainly spherical, measured more than 100 particles to obtain the core diameter d_c was 6.99 ± 0.29 nm, $d_{h,N}$ was 115.13 ± 8.28 nm, $d_{h,I}$ was 203.97 ± 2.57 nm, ζ was -41.46 ± 1.04 Mv, there shows these particles are easy agglomeration, so the hydrated particle size will be larger, and the particle surface potential is negative, indicating that it is modified with PMA. The characterization of Pd-PMA NPs shows in Figure 3-6-5, TEM images determined the Pd-PMA NPs shape were mainly spherical, Pd-PMA NPs d_c was 5.08 ± 0.29 nm, $d_{h,N}$ was 14.52 ± 0.53 nm, the distribution of $d_{h,I}$ has two peaks since the intensity distribution can provide overestimated values of hydrodynamic diameter for a very small agglomerates, ζ was -33.27 ± 3.10 mV. The characterization of Ag-PMA NPs shows in Figure 3-6-6, TEM images determined the Ag-PMA NPs shape were mainly

spherical, dc was 101.75 ± 1.97 nm, $d_{h,N}$ was 70.02 ± 5.48 nm, $d_{h,I}$ was 129.87 ± 3.16 nm, ζ was -14.40 ± 0.1 mV. The characterization of CdSe-PMA QDs and Pd-PMA NPs shows in Figure 3-6-7, TEM images determined CdSe-PMA QDs were mainly spherical and very small in a 50nm scale, CdSe-PMA QDs d_c was 4.65 ± 0.18 nm, $d_{h,N}$ was 8.74 ± 0.92 nm, the distribution of dh,I has two peaks since the intensity distribution can provide overestimated values of hydrodynamic diameter for a very small agglomerates, ζ was -30.97 ± 4.02.

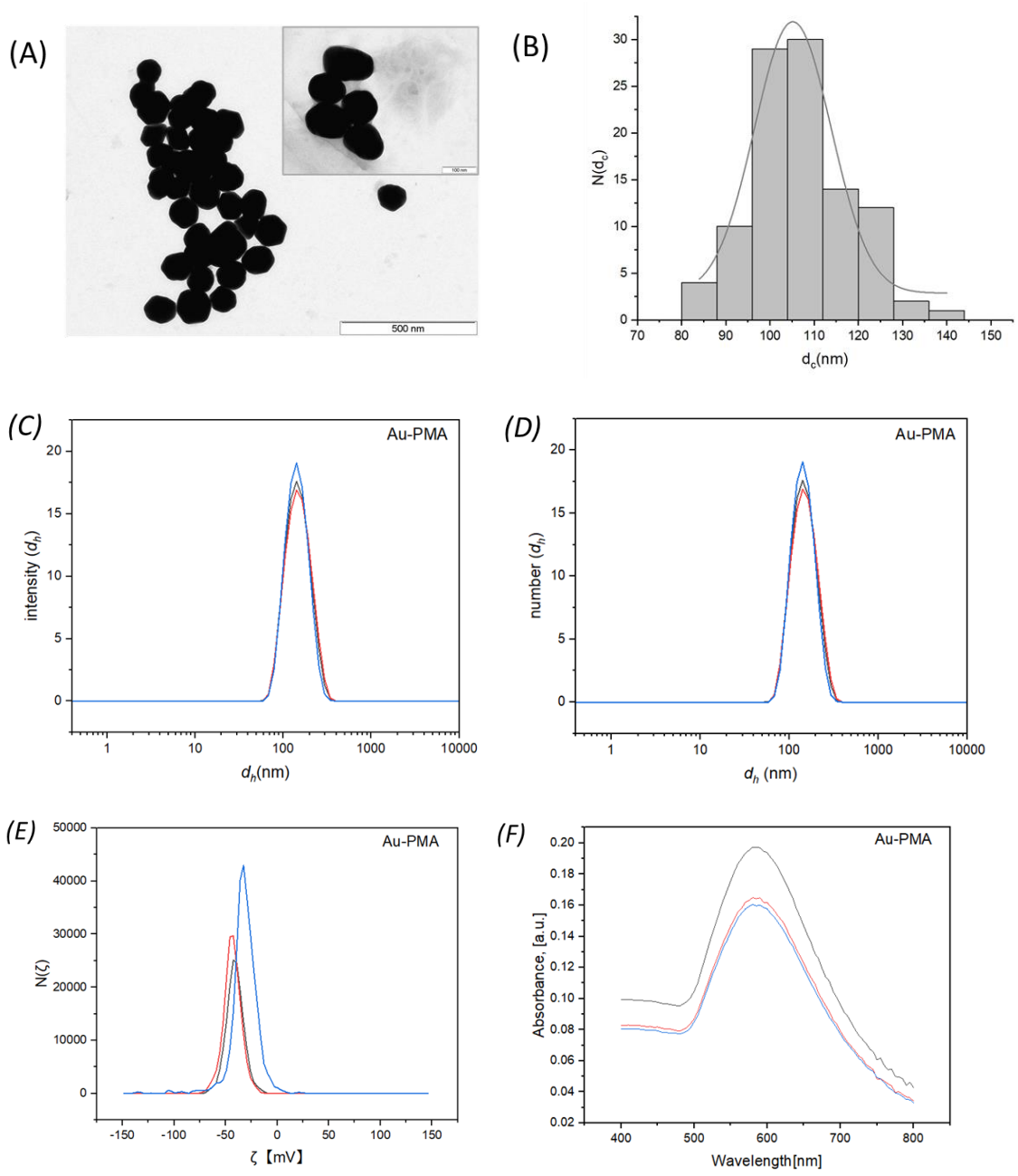

Figure 3-6-1: (A) The TEM of Au-PMA NPs with PMA coating in water. (B) The respective

size distribution histogram N (dc) of the Au-PMA NPs core diameter dc. The mean values ± standard deviation (SD) is dc = 105.18 ± 2.49 nm. (C) Number hydrodynamic distribution N (dh) of the hydrodynamic diameter d_h in water. (D) Intensity distribution I(d_h) of the hybrodynamic diameter dh in water. (E) ζ-potential distribution N (ζ) of the Au-PMA NPs in water. (F) Absorbance spectra of Au-PMA NPs.

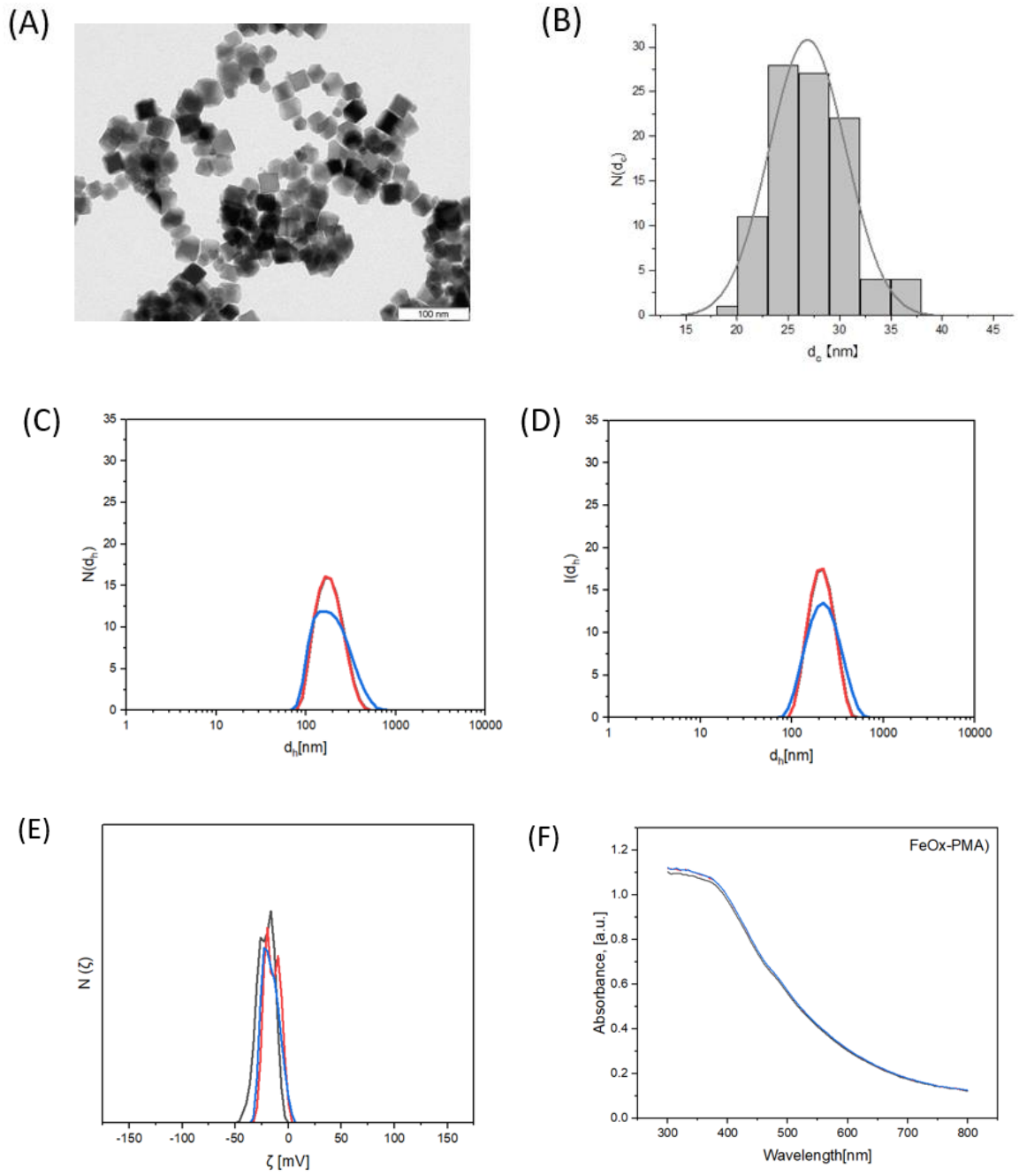

Figure 3-6-2: (A) The TEM of FeOx-PMA NPs with PMA coating in water. (B) The respective size distribution histogram N (dc) of the FeOx-PMA NPs core diameter dc. The

mean values ± standard deviation (SD) is dc = 26.87 ± 3.83 nm. (C) Number hydrodynamic distribution N (dh) of the hydrodynamic diameter dh in water. (D) Intensity distribution I(dh) of the hybrodynamic diameter dh in water. (E) ζ-potential distribution N (ζ) of the FeOx-PMA NPs in water. (F) Absorbance spectra of FeOx-PMA NPs.

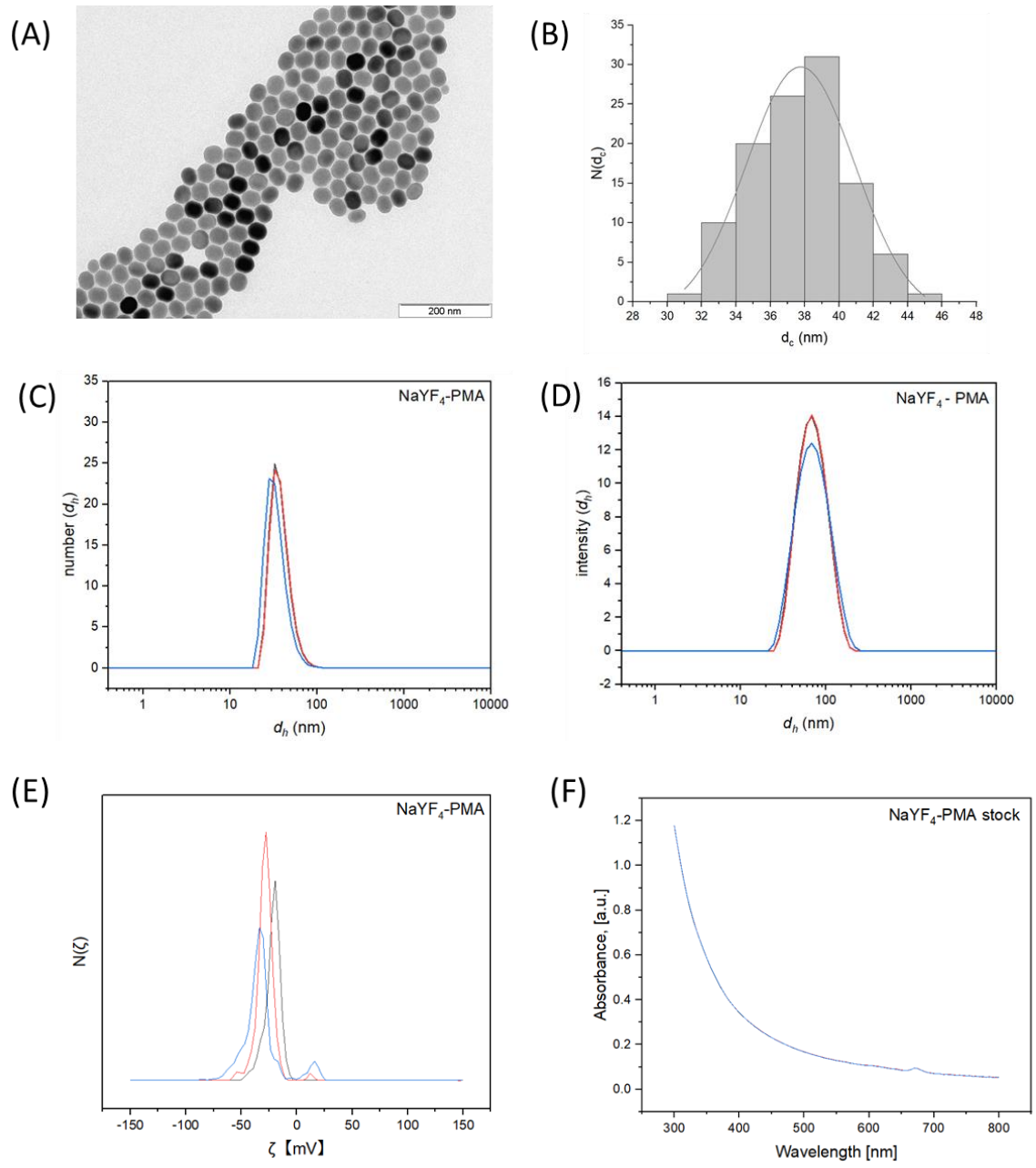

Figure 3-6-3: (A) The TEM of NaYF4 NPs in chloroform, this picture is made by Miao Feng; (B) The respective size distribution histogram N (dc) of the NaYF4 NPs core diameter dc.

The mean values ± standard deviation (SD) is dc = 37.76 ± 1.05 nm. (C) Number hydrodynamic distribution N (dh) of the hydrodynamic diameter dh of the NaYF4 -PMA NPs in water. (D) Intensity distribution I(dh) of the hybrodynamic diameter of the NaYF4 -PMA NPs dh in water. (E) ζ-potential distribution N (ζ) of the of the NaYF4 –PMA NPs in water. (F) Absorbance spectra of NaYF4-PMA NPs in water.

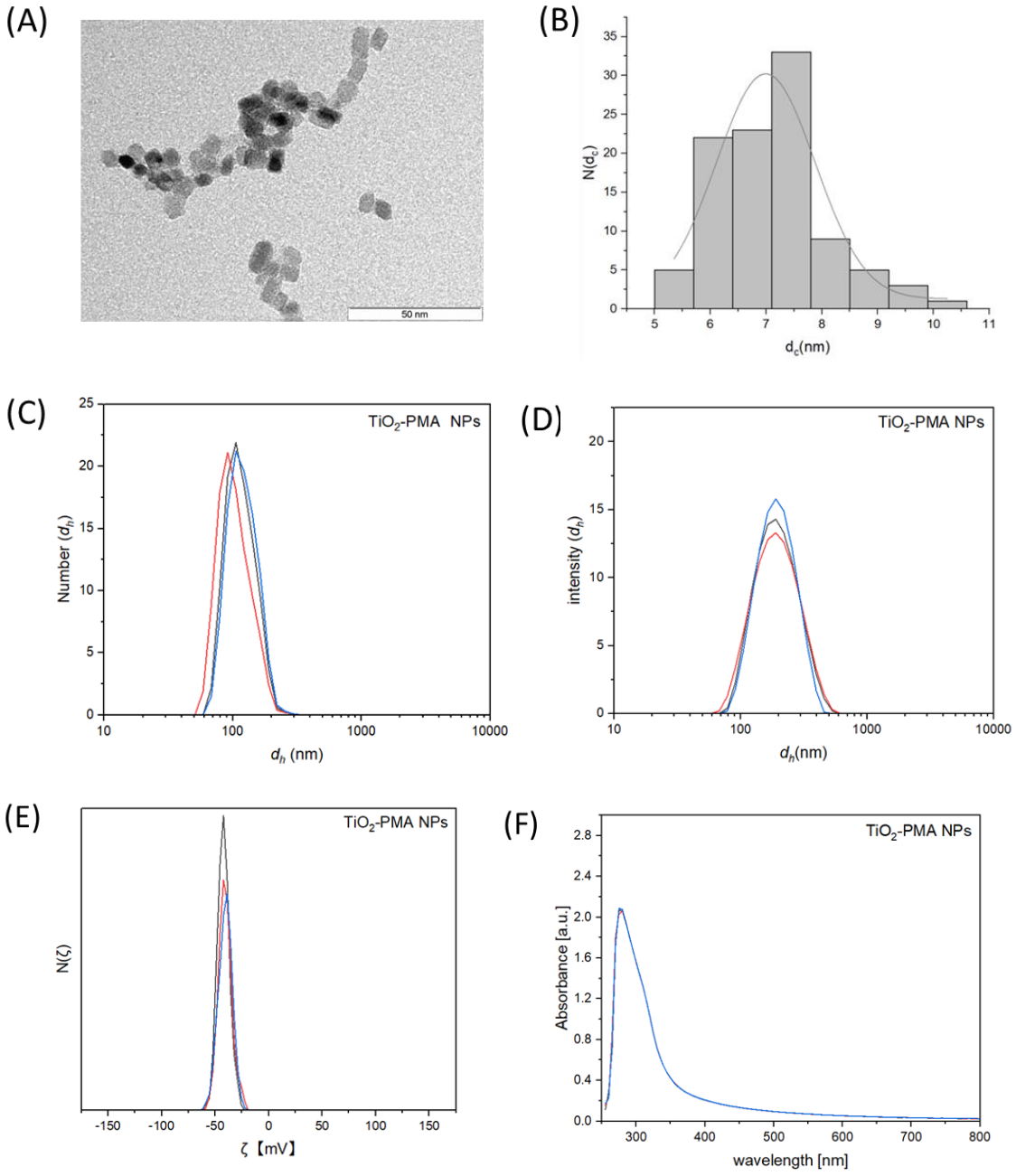

Figure 3-6-4: (A) The TEM of TiO_2-PMA NPs with PMA coating in water. (B) The

respective size distribution histogram N (d_c) of the TiO_2-PMA NPs core diameter dc. The mean values ± standard deviation (SD) is dc = 6.99 ± 0.29 nm. (C) Number hydrodynamic distribution N (dh) of the hydrodynamic diameter dh of the TiO_2-PMA NPs in water. (D) Intensity distribution I(d_h) of the hybrodynamic diameter of the TiO_2-PMA NPs dh in water. (E) ζ-potential distribution N (ζ) of the of the TiO_2-PMA NPs in water. (F) UV-vis Absorbance spectra of TiO_2-PMA NPs.

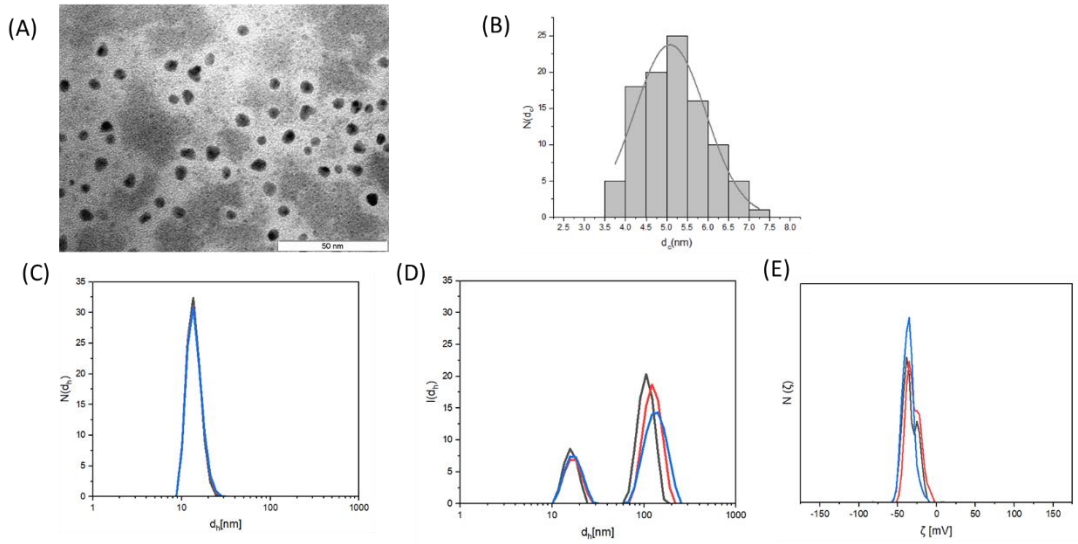

Figure 3-6-5. (A) The TEM of Pd-PMA NPs with PMA coating in water. (B) The respective size distribution histogram N (dc) of the Pd-PMA NPs core diameter dc. The mean values ± standard deviation (SD) is dc = 5.08 ± 0.29 nm.(C) Number hydrodynamic distribution N (dh) of the hydrodynamic diameter dh in water. (D) Intensity distribution I(dh) of the hybrodynamic diameter dh in water. (E) ζ-potential distribution N (ζ) of the Pd-PMA NPs in water.

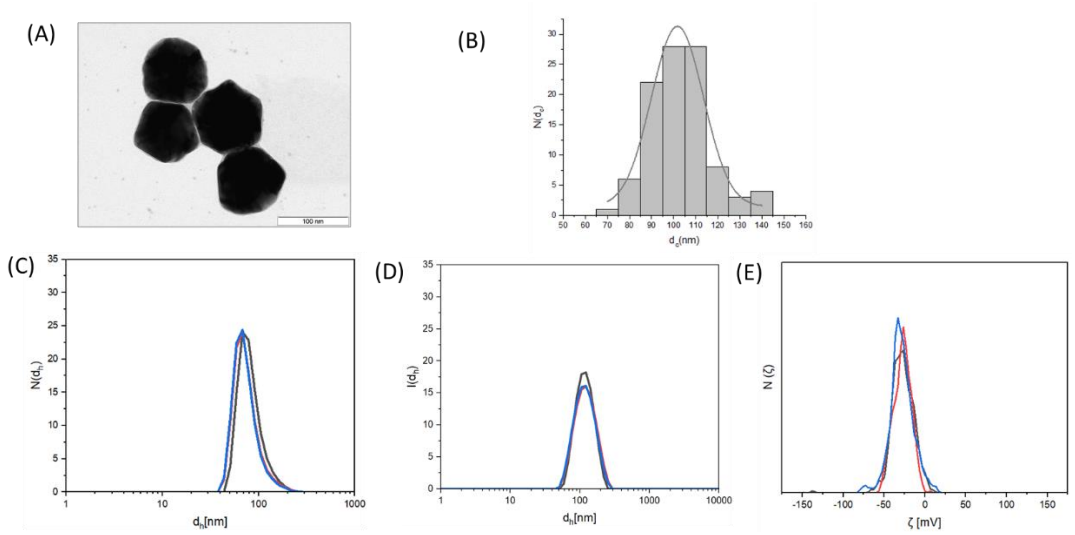

Figure 3-6-6. (A) The TEM of Ag-PMA QDs in water. (B) The respective size distribution histogram N (dc) of the Ag-PMA QDs core diameter dc. The mean values ± standard deviation (SD) is dc = 101.75 ± 1.97 nm. (C) Number hydrodynamic distribution N (dh) of the hydrodynamic diameter dh in water. (D) Intensity distribution I(dh) of the hydrodynamic diameter dh in water. (E) ζ-potential distribution N (ζ) of the Ag-PMA QDs in water.

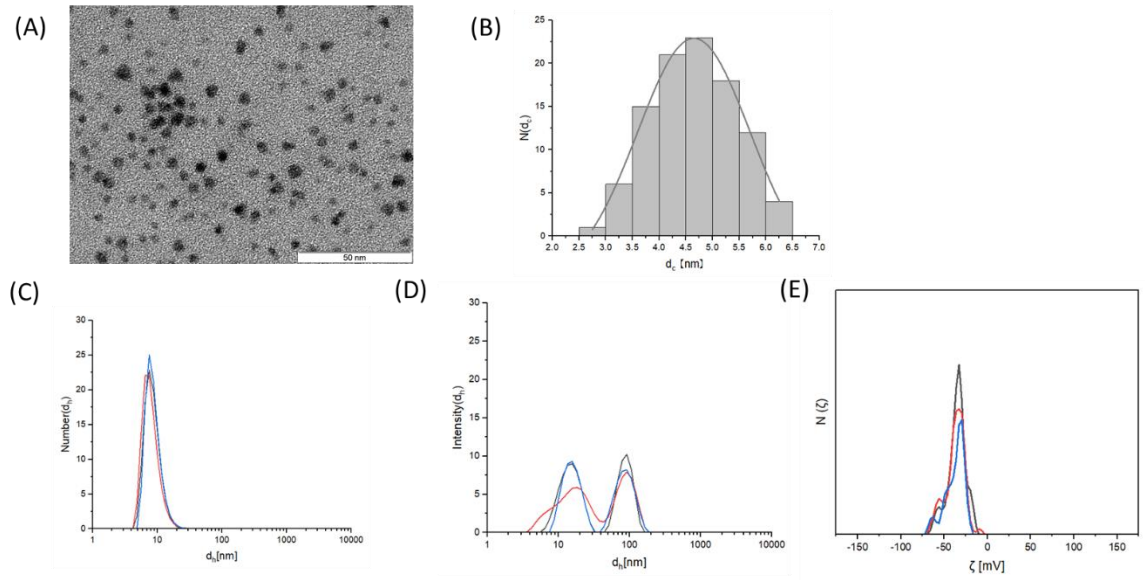

Figure 3-3-7. (A) The TEM of CdSe-PMA QDs in water. (B) The respective size distribution histogram N (dc) of the CdSe-PMA QDs core diameter dc. The mean values ± standard deviation (SD) is dc = 4.65 ± 0.18 nm. (C) Number hydrodynamic distribution N (dh) of the hydrodynamic diameter dh in water. (D) Intensity distribution I(dh) of the hydrodynamic diameter dh in water. (E) ζ-potential distribution N (ζ) of the CdSe-PMA QDs in water.

3.6.2. cell osmotic pressure

For NPs coating PMA in aqueous solution, we research the maximum addition volume per well in 96-well-plate, at the same time, we also consider the cell osmotic pressure, make sure the maximum NPs solution volume per well should in safe range of cell osmotic pressure. So here we use MilliQ water to study the cells osmotic pressure, the designed water ratio is 100%, 80%, 70%, 60%, 50%, 40%, 30%, 20%, 15%, 10%, 7.5%, 3.75%, 1.875%, 0.938% and 0.469% per well (100µL medium solution to culture cell). Three times repeat experiments get the results in Figure 3-6-2, shows when cell viability is about 90%, for Hela, 3T3 and MDA-MB-231 cells, the maximum addition volume percent per well is 30%, and for NRK and MCF-7 cells, maximum addition volume percent per well is 15%, as the increasing of water ratio, the cell viability will become down, this is mean cell will die by the low environmental osmotic pressure. So, add no more than 30% volume ratio for Hela, MDA-MB-231 and 3T3 cell, and 15% volume ratio for MCF-7 and NRK cell make sure cell is in a safe osmotic pressure.

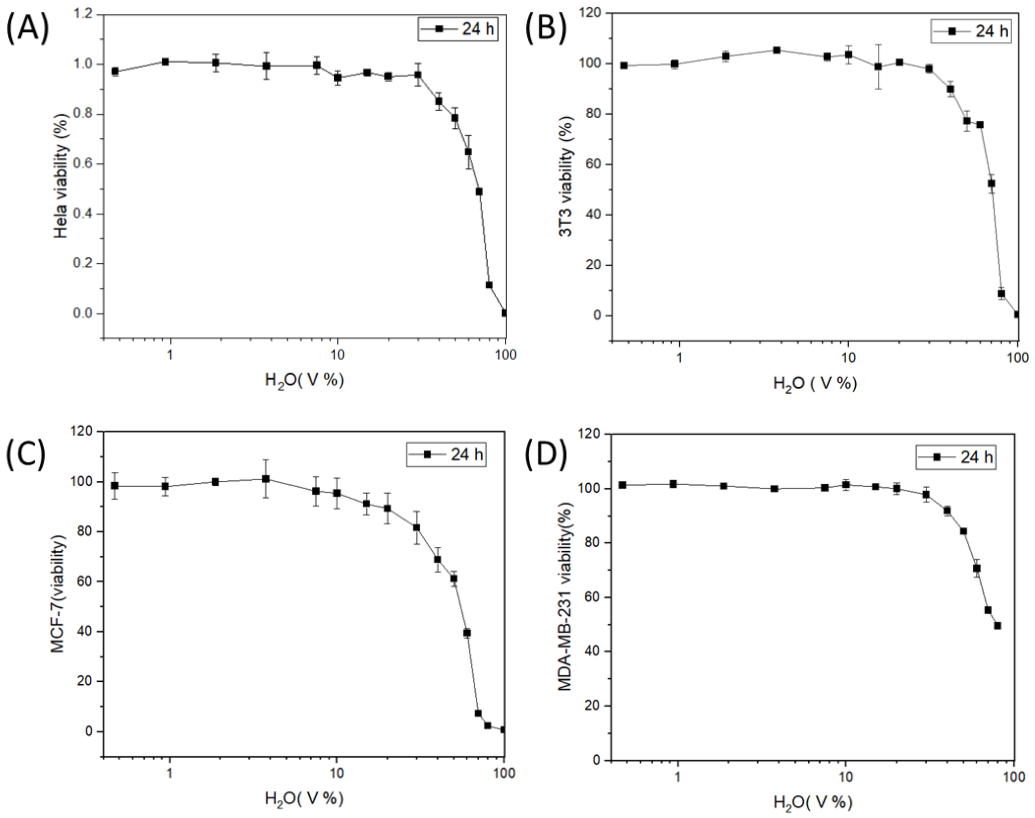

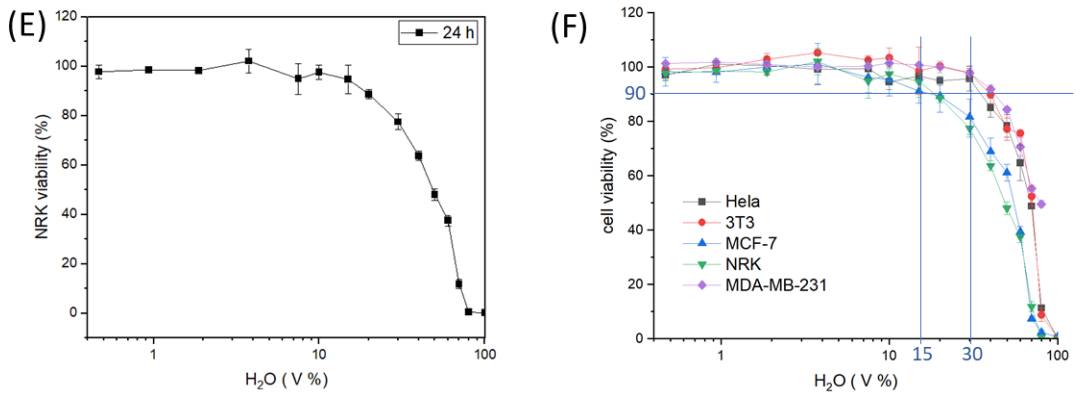

Figure 3-6-8: (A)Hela cell, (B) 3T3 cell, (C) MCF-7 cell, (D) MDA-MB-231 cell and (E) NRK cell viability under different osmotic pressures. Resazurin assay with a dilution series using milliQ water. Results are presented from three individual experiment.

3.6.3. cell viability study

Cell viability assay is to study the biocompatibility, gives some guides in how amount nanoparticles can be used in cells when apply in treatment, diagnosis and biomedical application. Usually, the activity cells viability is above 90%, are considered to normal and unaffected by culture environment. Here, we evaluated the toxicity of Hela cells with Au-PMA NPs, NRK cells with FeOx-PMA NPs, 3T3 cells with NaYF4-PMA NPs, MCF-7 cells with TiO_2-PMA NPs, 3T3 cells with Pd-PMA NPs, MCF-7 cells with Ag-PMA NPs, and MDA-MB-231 with CdSe-PMA QDs, they are all operate under safe osmotic pressure condition. Different nanoparticles incubated with different cells for 24, then resazurin reagent to test the cells viability. As shown in Figure 3-6-4, for Hela cells with Au-PMA NPs (diameter about 100nm), there is no cytotoxicity at low Au mental NPs concentrations, the non-cytotoxic concentration up to 105 µg/mL, until concentration increase to 210.75 µg/mL, the Hela viability decrease to 89.69%. For 3T3 cells with $NaYF_4$-PMA NPs, there is no cytotoxicity at low Y metal concentrations, the non-cytotoxic concentration up to 20.25 µg/mL, until concentration increase to 40.5 µg/mL, the 3T3 cells viability decreases to 81.07%. For NRK cells with IONP-PMA, there is no cytotoxicity at low Fe mental concentrations, the non-cytotoxic concentration up to 22.79 µg/mL, until concentration increase to 45.58 µg/mL, the NRK cells viability decrease to 87.38%. For MCF-7 cells with TiO_2-PMA NPs, there is no cytotoxicity at low Ti metal concentrations, and the cell viability are between 90% and 110%,

the non-cytotoxic concentration up to 51.22 µg/mL, until concentration increase to 102.45 µg/mL, the max addition, the MCF-7 cells viability decreases to 67.88%. For MCF-7 cells with Ag-PMA NPs (diameter about 100nm), there is no cytotoxicity at low Ag mental concentrations, the non-cytotoxic concentration up to 14.05 µg/mL, until concentration increase to 28.1 µg/mL, the MCF-7 cells viability decreases to 84.03%. For 3T3 cells with Pd-PMA NPs, there is no cytotoxicity at whole Pd mental concentrations, the cell viability is between 94% to 104% when concentration up to 32.94 µg/mL, which is the maxed added concentration. For MDA-MB-231 cells with CdSe-PMA QDs, the maxed added concentration Se is 0.4758 µg/mL, in this concentration cells viability is 108.8%.

Although we did not find the toxic concentration for MDA-MB-231 cells with CdSe-PMA QDs and 3T3 cells with Pd-PMA NPs, the stock concentration is too low to get the positive results, or because this two kind cells have a better performance in biocompatibility, but these results already guide the next experiments, just need to control the added Pd mental concentration be lower than 32.94 µg/mL of using Pd-PMA NPs in 3T3 cells, and Se mental concentration be lower than 0.4758 µg/mL of using CdSe-PMA QDs in MDA-MB-231 cells.

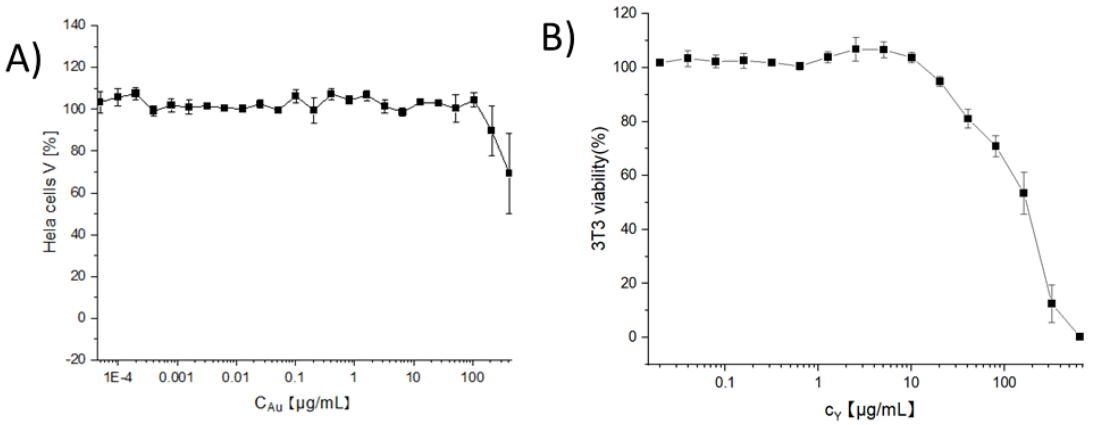

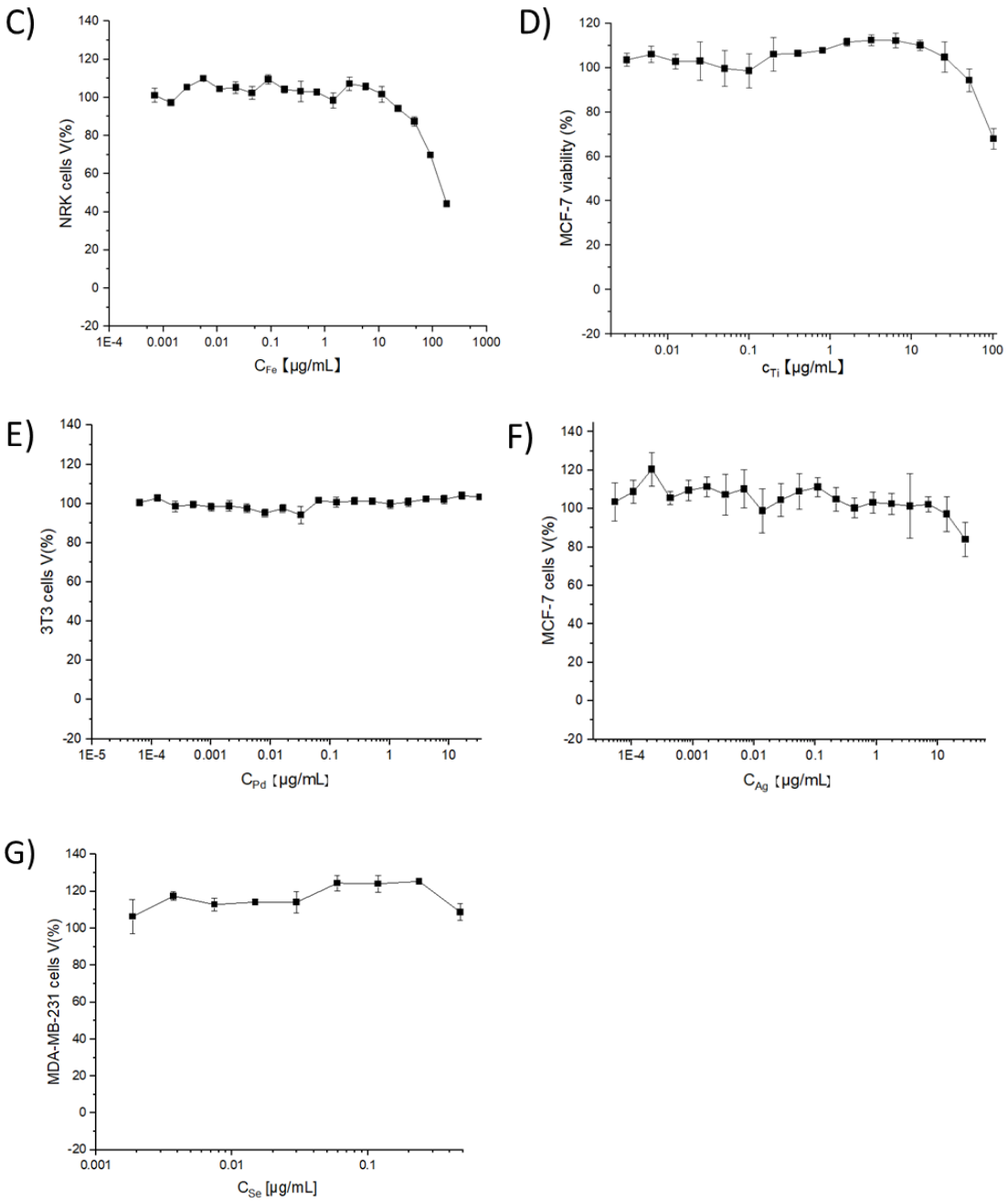

Figure 3-6-9: Cell viability of Hela exposed to Au-PMA NPs (A), 3T3 exposed to $NaYF_4$-PMA NPs (B), NRK exposed to FeOx-PMA NPs (C), MCF-7 exposed to TiO_2-PMA NPs (D), 3T3 exposed to Pd-PMA NPs (E), MCF-7 exposed to Ag-PMA NPs (F), and MDA-MB-231 exposed to CdSe-PMA QDs (G) at different Au, Y, Fe, Ti, Pd, Ag and Se element concentrations after 24h incubate by resazurin assay. Results are presented from three individual experiment.

3.6.4. cell uptake study

Although there has a lot of discuss about entry mechanisms for nanoparticles in cell, such as phagocytosis and micropinocytosis for large NPs (> 500 nm) and aggregates, pinocytosis by different protein inducing enter mechanism, via direct penetration and pore formation for smaller NPs (< 10 nm) [128, 136]. Here, endocytosis assay about cells and nanoparticles is to study the labeling mental elemental content of nanoparticles in cell. Though these research, we want to clear whether these nanoparticles can enter cells? And how many elemental contents of NPs will in cells? To address these two questions, we culture cells, according to section 3.5.8, added NPs of different mental concentration in cells, according to section 3.5.10, for incubating 6 and 24 hours, then used ICP-MS to get the mental amount and calculated the amount of elemental found per cell.

As show in Figure 3-6-10 (A), for Hela cells exposed to Au-PMA NPs (diameter is about 100nm), as the mental concentration of added Au-PMA NPs increase in medium, doesn't matter incubate for 6 hours or 24 hours, the amount of Au per Hela cells after incubating also increase, the highest amount of Au per cell is 19.05 pg/cell when added 7.6 μg Au-PMA NPs per mL medium after 6 hours incubate, and 18.9 pg Au per cell can be tested after 24 hours incubate when added 7.6 μg Au-PMA NPs per mL medium. After different incubate times, the elemental amounts per cells are similar, maybe because the cell's number increased bigger in incubating 24 hours than 6 hours, leading to the amount of endocytosis NPs become less. (How to address this question? The number of cells seeded on the first day can be increased so that the cells have grown to fill the bottom of the dish on the second day, and the cells will contact to inhibit growth, then the number of cells will not change significantly after 6 hours and 24 hours of incubation.)

As show in Figure 3-6-10 (B), for NRK cells exposed to FeOx-PMA NPs (diameter is about 27nm), as the Fe mental concentration of added FeOx-PMA NPs increase in medium, doesn't matter incubate for 6 hours or 24 hours, the amount of Fe per NRK cells after incubating also increase, the highest amount of Fe per cell is 180.98 pg/cell when added 40 μg Fe of FeOx-PMA NPs per mL medium after 6 hours incubate, and 173.16 pg Fe per cell can be tested after 24 hours incubate when added 40 μg FeOx-PMA NPs per mL medium. After different incubate times, the elemental amounts per cells are similar, maybe because the cell's

number increased bigger in incubating 24 hours than 6 hours, leading to metal concentration become less, but here need take attention, Iron oxide nanoparticles easy to agglomeration in cell salt medium, some particles are gathered around the cell membrane, so here uptake data used for a reference.

In Figure 3-6-10 (C), the uptake results of Y metal concentration per cell for 3T3 cells exposed to $NaFY_4$-PMA NPs (diameter is about 40nm), as the Y mental concentration of added $NaFY_4$-PMA NPs increase in medium, incubate for 24 hours, the amount of Y per 3T3 cells increase, the highest amount of Y per cell is 0.79 pg/cell when added 100 μg Y of $NaFY_4$-PMA NPs per mL medium after 24 hours incubate. At same time, the 3T3 cell number decrease, which is consistent with the 3T3 cell viability of $NaFY_4$-PMA NPs, from Figure 3-6-6, the cell viability is between 70%-53% in this exposed concentration.

As show in Figure 3-6-10 (D), for MCF-7 cells exposed to TiO_2-PMA NPs, as the Ti mental concentration of added TiO_2-PMA NPs increase in medium from 0μg/mL to 5.04μg/mL, incubate for 24 hours, the amount of Ti per MCF-7 cells increase to 0.35pg/cell, However, as the amount of Ti added continued to increase to 25.184ug/mL, the Ti content in each cell was detected to be maintained at around 0.36pg/cell after 24 hours incubate.

As show in Figure 3-6-10 (E), for MCF-7 cells exposed to Ag-PMA NPs (diameter is about 100nm), as the Ag mental concentration of added Ag-PMA NPs increase in medium, doesn't matter incubate for 6 hours or 24 hours, the amount of Ag per Hela cells after incubating also increase, the highest amount of Ag per cell is 0.912 pg/cell when added 2 μg Ag-PMA NPs per mL medium after 24 hours incubate. And the Ag elemental amount per cell after incubating 24 hours is bigger than incubating 6 hours, and the cells amount after incubating 24 hours is close to incubating 6 hours, so incubating time is longer, the endocytosis NPs is increase.

As show in Figure 3-6-10 (F) (G), for MDA-MB-231 cells exposed to CdSe-PMA QDs (diameter is about 5nm). Added different concentration of CdSe-PMA QDs in medium, after 6 and 24 hours, then using ICP-MS measured the Cd element and Se element content in cell at same time. For Cd elemental content in cell, which is trend of increasing as the added amount of CdSe-PMA QDs increasing, and the highest amount of Cd per cell is 0.05418 pg/cell when added 196 μg CdSe-PMA QDs per mL medium after 24 hours incubate. And the Cd elemental amount per cell after incubating 24 hours is bigger than incubating 6 hours, incubating time

is longer, the endocytosis NPs is increase. For Se elemental content in cell, which is no trend, and the tested Se content per cell is between 0.002388692 pg/cell and 0.054184773 pg/cell, and this content is too low to measure correctly by ICP-MS. But from the results of Cd content in cell, CdSe-PMA-QDs can enter MDA-MB-231 cell, and the content will increase as the incubate time longer.

As show in Figure 3-6-10 (H), for 3T3 cells exposed to Pd-PMA NPs (diameter is about 5nm), as the Pd mental concentration of added Pd-PMA NPs increase in medium, doesn't matter incubate for 6 hours or 24 hours, the amount of Pd per 3T3 cells after incubating also increase, the highest amount of Pd per cell is 1.70 pg/cell when added 39 μg Pd-PMA NPs per mL medium after 24 hours incubate. And the Pd elemental amount per cell after incubating 24 hours is bigger than incubating 6 hours, and the cells amount after incubating 24 hours is close to incubating 6 hours, so incubating time is longer, the endocytosis NPs is increase.

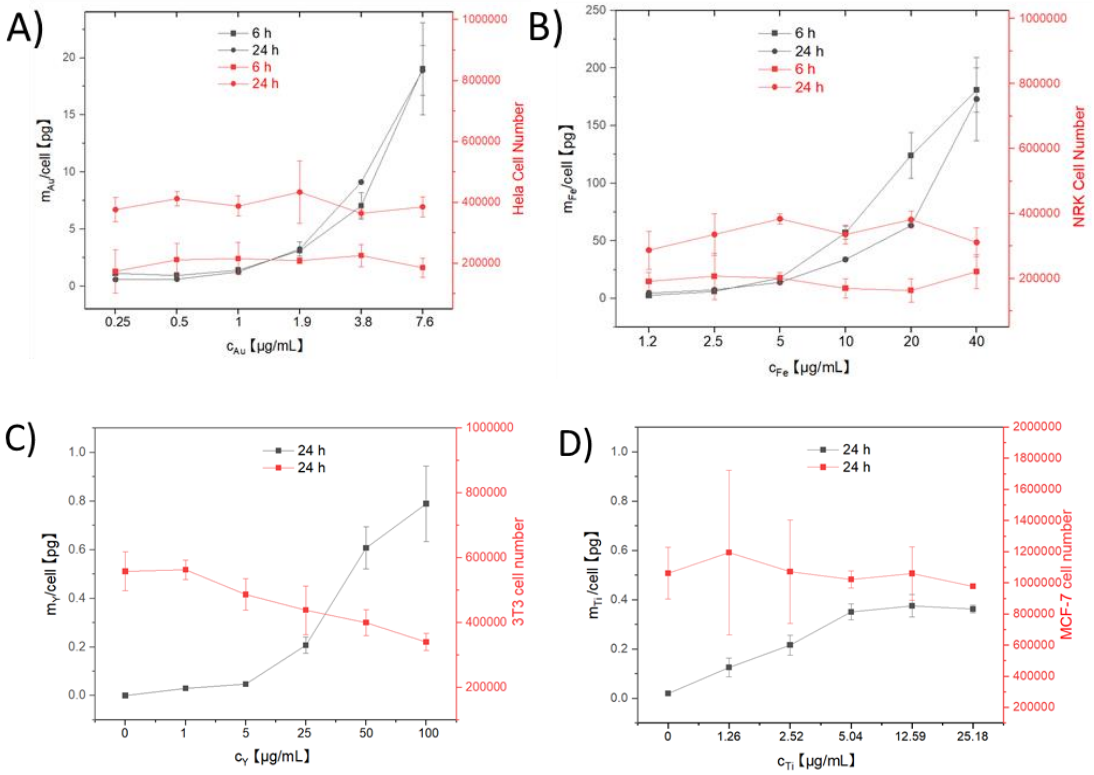

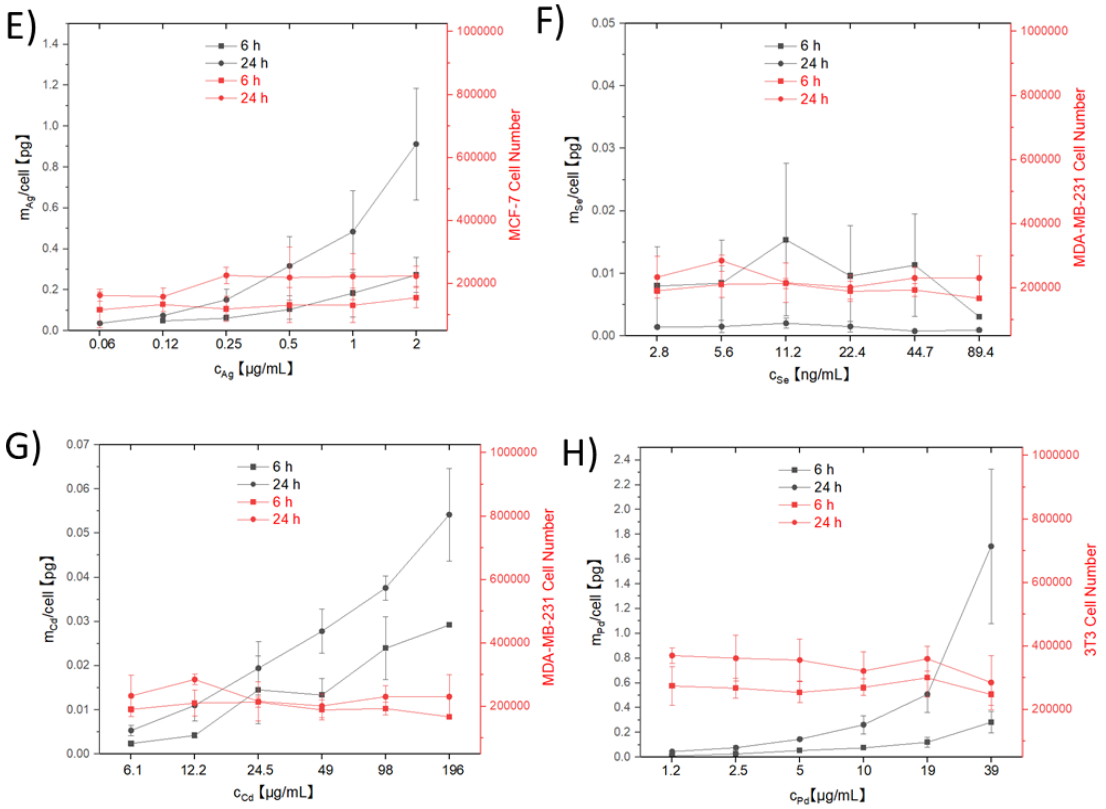

Figure 3-6-10： Amount of elemental (black line) found per cell and cell number (red line) in Hela exposed to Au-PMA NPs (A), NRK exposed to FeOx-PMA NPs (B), 3T3 exposed to $NaYF_4$ -PMA NPs(C), MCF-7 exposed to TiO_2-PMA NPs (D), MCF-7 exposed to Ag-PMA NPs (E), MDA-MB-231 exposed to CdSe-PMA QDs (F) (G), and 3T3 exposed to Pd-PMA NPs (H) at different Au(A), Fe(B), Y(C), Ti(D), Ag(E), Se(F), Cd(G) and Pd(H) element concentrations after 6 and 24 h by ICP-MS. Results are presented from three individual experiment.

3.6.5. cell exocytosis study

The metal content in cells is governed by endocytosis, also influenced by exocytosis, so cell exocytosis study is an important factor to be evaluated[137]. The mental content in cells by endocytosis will dilution in a cell population[138], surface chemistry of nanoparticles also will affect the exocytosis process and its relatively long time for cationic gold NP retained in cell[139]. Here, exocytosis study about cells and nanoparticles is to study the retained mental

elemental content in cell after removed the medium with nanoparticles and added fresh medium without nanoparticles for incubating 6 and 24 hours. Through this research, we want to know whether these mental elementals will retain in cell? And how many elemental contents will in cell? To address these questions, we added fresh medium in cells after incubating 24 hours with different NPs concentration in medium, then incubated 6 and 24 hours again, then using ICP-MS to get the metal content and calculated the metal content per cell.

As show in Figure 3-6-11, Au content in Hela cell, Fe content in NRK cell, Y content in 3T3 cell, Ti content in MCF-7 cell, Ag content in MCF-7 cell, Pd content in 3T3 cell and Cd content in MDA-MB-231 cell, these seven metal contents all has a trend of decrease after added fresh medium for 6 hours, and there continue have a trend of decrease after 24 hours, it may be that cell division dilutes the metal content in cells, or it may be caused by cell exocytosis, but no matter which one, there is still metal content in the cells. After 24 hours fresh medium, about metal highest content in cell: There still have 6.86 pg/cell Au content in Hela cell after incubate 24 hours in fresh medium when added 7.6 μg Au-PMA NPs per mL medium for 24 hours; there have 0.73 pg/cell Ag content in MCF-7 cell after incubate 24 hours in fresh medium when added 2 μg Ag-PMA NPs per mL medium for 24 hours; There have 74.79 pg/cell Fe content in NRK cell after incubate 24 hours in fresh medium when added 40 μg FeOx-PMA NPs per mL medium for 24 hours; There have 1.03 pg/cell Pd content in 3T3 cell after incubate 24 hours in fresh medium when added 39 μg Pd-PMA NPs per mL medium for 24 hours; There have 0.034 pg/cell Cd content in MDA-MB-231 cell after incubate 24 hours in fresh medium when added 196 μg Cd in CdSe-PMA QDs per mL medium for 24 hours, in here we not show Se metal amount per cell, because its concentration is too low to give a reality value; There have 0.85 pg/cell Y content in 3T3 cell after incubate 24 hours in fresh medium when added 23.77 μg Y in $NaYF_4$-PMA NPs per mL medium for 24 hours; There have 0.054 pg/cell Ti content in MCF-7 cell after incubate 24 hours in fresh medium when added 5.04 μg Ti in TiO_2-PMA NPs per mL medium for 24 hours.

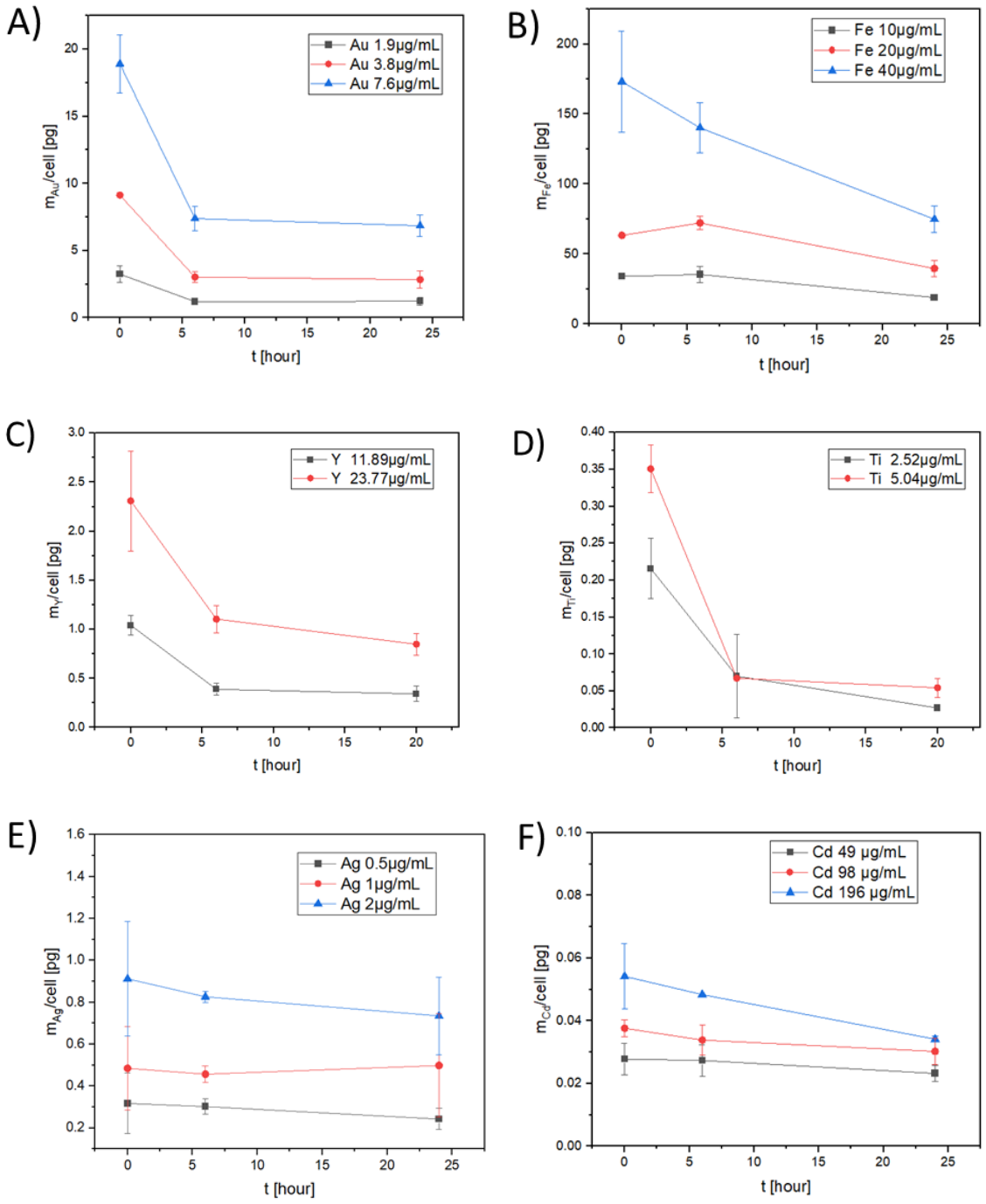
A)
Au 1.9µg/mL
Au 3.8µg/mL
Au 7.6µg/mL
m_Au/cell [pg]
t [hour]
B)
Fe 10µg/mL
Fe 20µg/mL
Fe 40µg/mL
m_Fe/cell [pg]
t [hour]
C)
Y 11.89µg/mL
Y 23.77µg/mL
m_Y/cell [pg]
t [hour]
D)
Ti 2.52µg/mL
Ti 5.04µg/mL
m_Ti/cell [pg]
t [hour]
E)
Ag 0.5µg/mL
Ag 1µg/mL
Ag 2µg/mL
m_Ag/cell [pg]
t [hour]
F)
Cd 49 µg/mL
Cd 98 µg/mL
Cd 196 µg/mL
m_Cd/cell [pg]
t [hour]

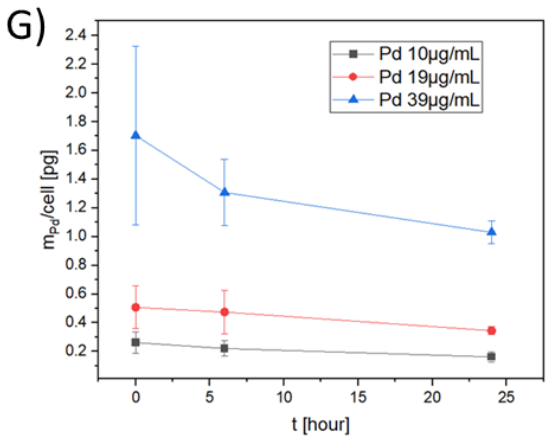

Figure 3-6-11: (A) Amount of Au per Hela cell mAu/cell of labeled by Au-PMA NPs after incubation in cell medium for another 0, 6 and 24 h. (B) Amount of Fe per NRK cell mFe/cell of labeled by FeOx-PMA NPs after incubation another 0, 6 and 24 h.(C) Amount of Y per 3T3 cell mY/cell of labeled by NaYF4-PMA NPs after incubation another 0, 6 and 24 h. (D) Amount of SeTi per MCF-7 cell mTi/cell of labeled by TiO2-PMA NPs after incubation another 0, 6 and 24 h. (E) Amount of Ag per MCF-7cell mAg/cell of labeled by Ag-PMA NPs after incubation another 0, 6 and 24 h. (F) Amount of Cd per MDA-MB-231 cell mCd/cell of labeled by CdSe-PMA QDs after incubation another 0, 6 and 24 h. (G) Amount of Pd per 3T3 cell mPd/cell of labeled by Pd-PMA NPs after incubation another 0, 6 and 24 h. The data was from three repeat experiments.

3.6.6. cell co-culture viability

In order to research the co-culture viability of these five different cells (Hela, 3T3, MDA-MB-231, MCF-7 and NRK cell), we seed 10000 cell of each kind in 96-well-plate per well, at same time seed 10000 mix cell of containing 2000 Hela cell, 2000 3T3 cell, 2000 MDA-MB-231 cell, 2000 MCF-7 cell and 2000 NRK cell, and medium (+5% FBS and +0.5% P/S) is 0.1mL, put in incubator for 24 hour, then changed with fresh medium containing 0.025mg/mL resazurin, then put in incubator 4 hour, then use microplate reader to test the fluoresce intensity, use excitation filter is Ex544, and the Emission filter is 590-10. Get the emission fluorescence intensity per well, use the *eq 3.6 to calculate the cells viability of each well of containing Hela, 3T3, MDA-MB-231, MCF-7, NRK or 5 Mix.*

Cell viability= $\frac{I_{Cell}-I_{blank}}{I_{average}-I_{blank}}$ *eq 3.6*

$I_{average}$: the average of Fluoresce intensity at 590nm of 10000 Hela, 10000 3T3, 10000 MDA-MB-231, 10000 MCF-7 and 10000 NRK

I_{blank}: the fluoresce intensity at 590nm of only 0.025mg/mL resazurin in medium

I_{cell}: the fluoresce intensity at 590nm of cell sample

As show in Figure 3-6-12 (A), the five different cells can co-culture, and the cell viability is larger than 0.8, and round 1. (B) shows the bright field of different cell and 5 Mix cell in 96-well-plate.

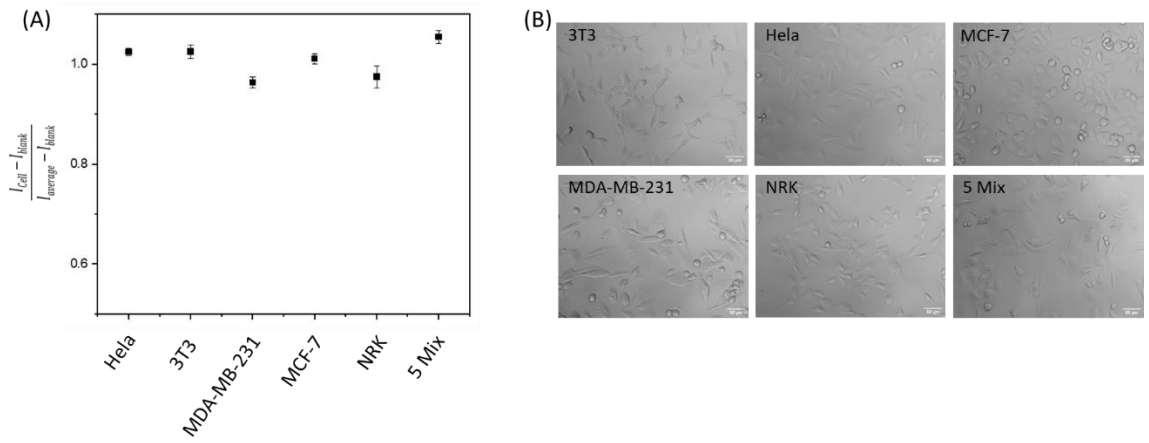

Figure 3-6-12. (A) Determination of cell co-culture. Each cell is 10000 in 0.1 mL medium (+5% FBS and +0.05%P/S), in incubator 24 h, then added 0.1mL medium contain 0.025mg/mL Resazurin, in incubator 4h, then test the solution's emission light intensity. 5 Mix: 2000 Hela + 2000 3T3 + 2000 MDA-MB-231 + 2000 MCF-7 + 2000 NRK. (B) the bright images of the five different cell and 5 kinds cells co-culture. The scar bar is 50μm.

3.6.7. analysis by synchrotron-based x-ray

Four different cells exposed to four different nanoparticles in complete medium: Hela cell exposed to Au-PMA NPs, 100μg Au/mL; NRK cell exposed to FeOx-PMA NPs, 75 μg Fe/mL; 3T3 cell exposed to $NaYF_4$-PMA NPs, 75 μg Y/mL; MCF-7 cell exposed to TiO2-PMA NPs, 13 μg Ti/mL. Expose for 24 hours, then detach cell by 0.05% trypsin, and seeded on the Si_3N_4

membrane, after 16 hours, the cells adhered to the membrane, then wash with PBS and ammonium acetate buffer (100mM in H2O) by tweezer take the membrane to soak in, blotted away the excess liquid, then rapid freezing by immediately plunged into liquid ethane, then stored in liquid nitrogen, then freeze dried in a programmed temperature rise. At same time also do some sample of only cell as control, not treat by nanoparticles.

XFI results of Hela treat with Au-PMA NPs and Hela show in Figure 3-6-13, Zn signal shows cell nucleus, and K signal shows cell cytoplasm, in Figure 3-6-13 (A) these has four Hela cell, and detected signal in Au, Fe, Ti channel, it is that the fluorescence emission of Au is complex and can be detected by other element channels, some interfering emission light can be removed by post-processing so that only the Au channel detect the signal. and from the merge image of Zn, K and Au channel, the red signal of Au and the blue signal of nucleus are overlap, shows purple color, although the cell morphology here is not obvious, we selected cells with normal cell morphology for scanning in bright field, so here we can get the location of Au in the cell is more inclined to be in the nucleus. in Figure 3-6-13 (B) these has many Hela cell, and there not detected signal in Au, Fe, Y and Ti channel, these negative results to proves that the signal detected in the metal detection channel in the treated Hela cells is from Au-PMA NPs.

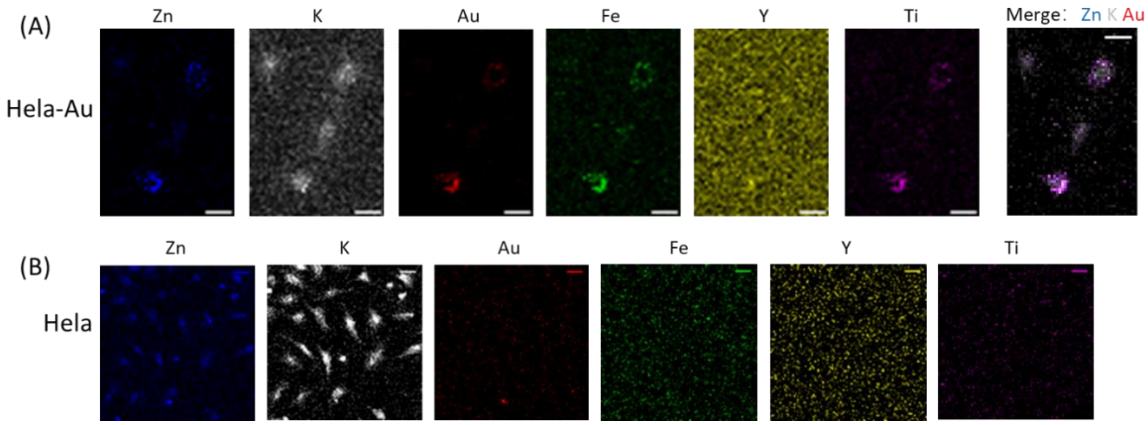

Figure 3-6-13. XFI of Hela in different detect elemental channel, (A) Hela exposed to Au-PMA NPs, (B) Hela as control. Scale bar is 30µm. the XFI operate is take by Marvin Skiba.

XFI results of NRK treat with FeOx-PMA NPs and NRK show in Figure 3-6-14, Zn signal shows cell nucleus, and K signal shows cell cytoplasm, in Figure 3-6-14 (A) these has one NRK cell, and detected signal in Fe, Ti channel, it is that the fluorescence emission of Fe can be

detected by Ti element channels, this interfering emission light can be removed by post-processing so that only the Fe channel detect the signal. although the cell morphology here is not obvious in cytoplasm of K channel, we selected cells with normal cell morphology for scanning in bright field, and nucleus of Zn signal is full in all cell, which is mean Zn enters the cytoplasm, and Fe signal has a circular blank in the middle, which is the location of the cell nucleus, so we can get that the location of Fe in the cell is the cytoplasm. in Figure 3-6-14 (B) these has two NRK cell, and there not detected signal in Au and Y channel, and a weak signal in Fe channel, which is by the cells themselves contain iron, Ti channel signal maybe made by Fe emission light. These results prove that the strong signal detected in the metal detection channel in the treated NRK cells is from FeOx-PMA NPs.

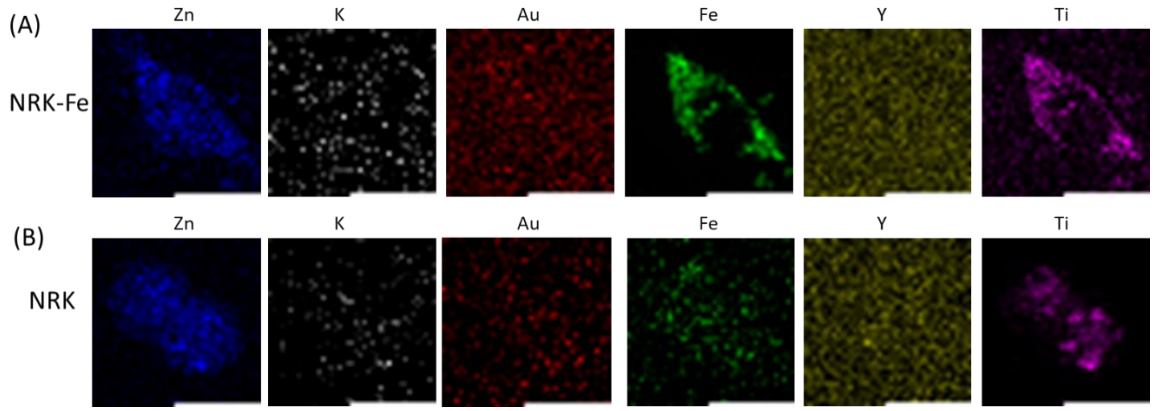

Figure 3-6-14. XFI of NRK in different detect elemental channel, (A) NRK exposed to FeOx-PMA NPs, (B) NRK as control. Scale bar is 20µm. the XFI operate is take by Marvin Skiba.

XFI results of 3T3 treat with NaYF4-PMA NPs and 3T3 show in Figure 3-6-15, Zn signal shows cell nucleus, and K signal shows cell cytoplasm, in Figure 3-6-15 (A) these has about three 3T3 cell, and detected signal in Y channel, there is no fluorescence emission of Y to interfere the other detected element channels. and from the merge image of Zn, K and Y channel, the yellow signal of Y and the blue signal of nucleus are not overlap, and the yellow takes the place of with, although the cell morphology here is not obvious in nucleus of Zn channel, we selected cells with normal cell morphology for scanning in bright field, so here we can get the location of Y in the cell is in the cytoplasm. in Figure 3-6-15 (B) these has two 3T3 cell, and there not detected signal in Au, Fe, Y and Ti channel, these negative results to prove that the signal detected in the metal detection channel in the treated 3T3 cells is from

NaYF4-PMA NPs.

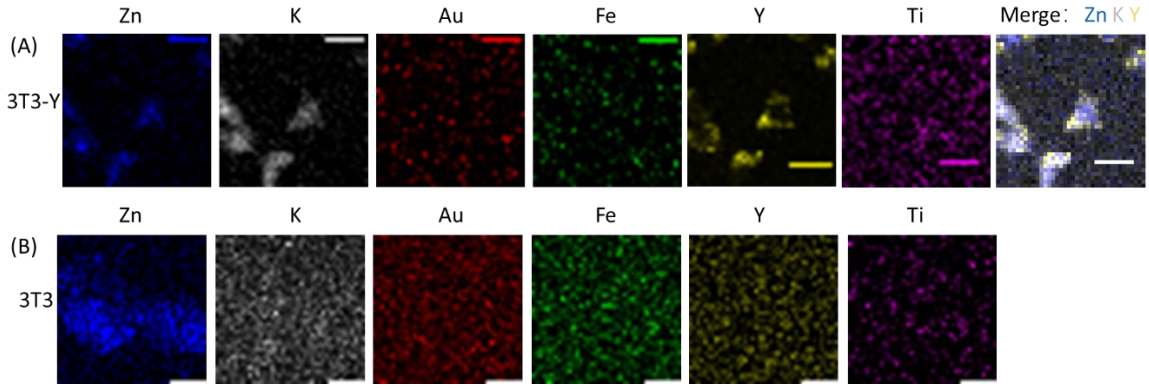

Figure 3-6-15. XFI of 3T3 in different detect elemental channel, (A) 3T3 exposed to NaYF4-PMA NPs, Scale bar is 30μm; (B) 3T3 as control, Scale bar is 10μm. the XFI operate is take by Marvin Skiba.

XFI results of MCF-7 treat with TiO2-PMA NPs and MCF-7 show in Figure 3-6-16, Zn signal shows cell nucleus, and K signal shows cell cytoplasm, in Figure 3-6-16 (A) these has about five MCF-7 cell, in Figure 3-6-16 (B) these has about two MCF-7 cell, these two group images show there cannot detected any signal in all elemental channel, the reason maybe TiO2-PMA NPs cannot enter the cell, or the treat concentration is too low to detect.

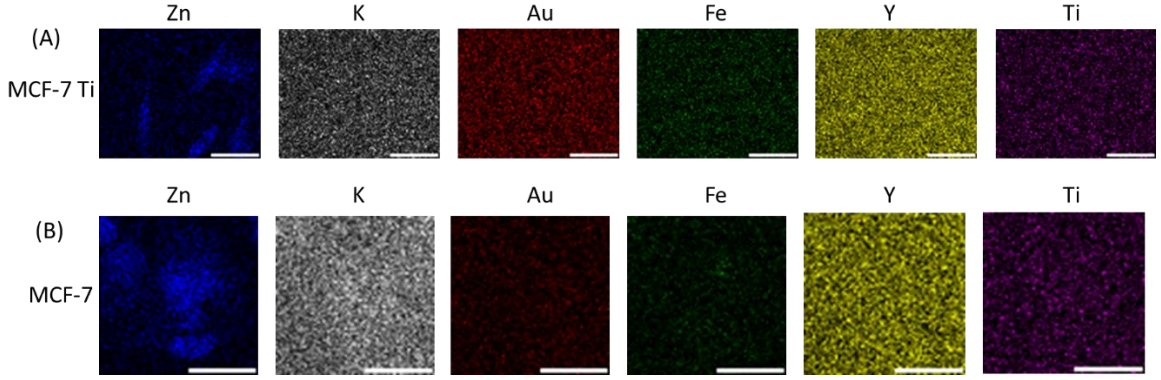

Figure 3-6-16. XFI of MCF-7 in different detect elemental channel, (A) MCF-7 exposed to TiO2-PMA NPs; (B) MCF-7 as control, Scale bar is 30μm. the XFI results operate is take by Marvin Skiba.

XFI results of mix four different cells: Hela, NRK, 3T3 and MCF-7, and these cells are not

treated with nanoparticles, as shows in Figure 3-6-17, Zn signal shows cell nucleus, and K signal shows cell cytoplasm, here, we can see obvious cell morphology, but no any metal signal can be detected in any metal channel. This is a negative result for mix treat cells.

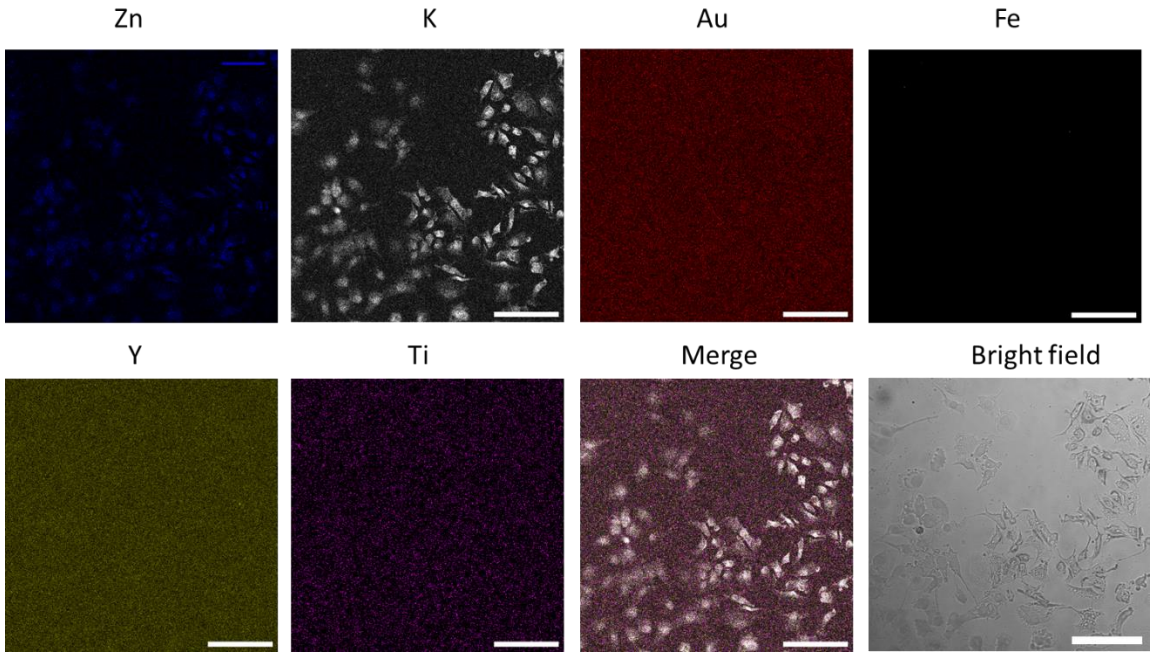

Figure 3-6-17. XFI of Mix five different cells in different detect elemental channel, the four different cells are: Hela, NRK, 3T3, MDA-MB-231 and MCF-7 separately culture for 24 hours, then mix together and culture in one SiN membrane. Scale bar is 100μm. the XFI operate is take by Marvin Skiba.

XFI of Mix four different cells shows in Figure 3-6-18, and four different cells are treated with four different nanoparticles: Hela exposed in Au-PMA NPs, NRK exposed in FeOx-PMA NPs, 3T3 exposed in NaYF4-PMA NPs, and MCF-7 exposed in TiO2-PMA NPs. The results a large amount of iron signal and strong, very little gold signal and weak, and almost no titanium signal can be detected. Which are consistent with the above results. And from the merge image of Au, Fe, Y and Ti, the four colors position are basically separated, but there are also some locations that contain multiple metal signals, and there are many messy point signals in the locations where there are no cells. This may be because during the sample preparation process, the cells ruptured and released nanoparticles, which stuck to the membrane.

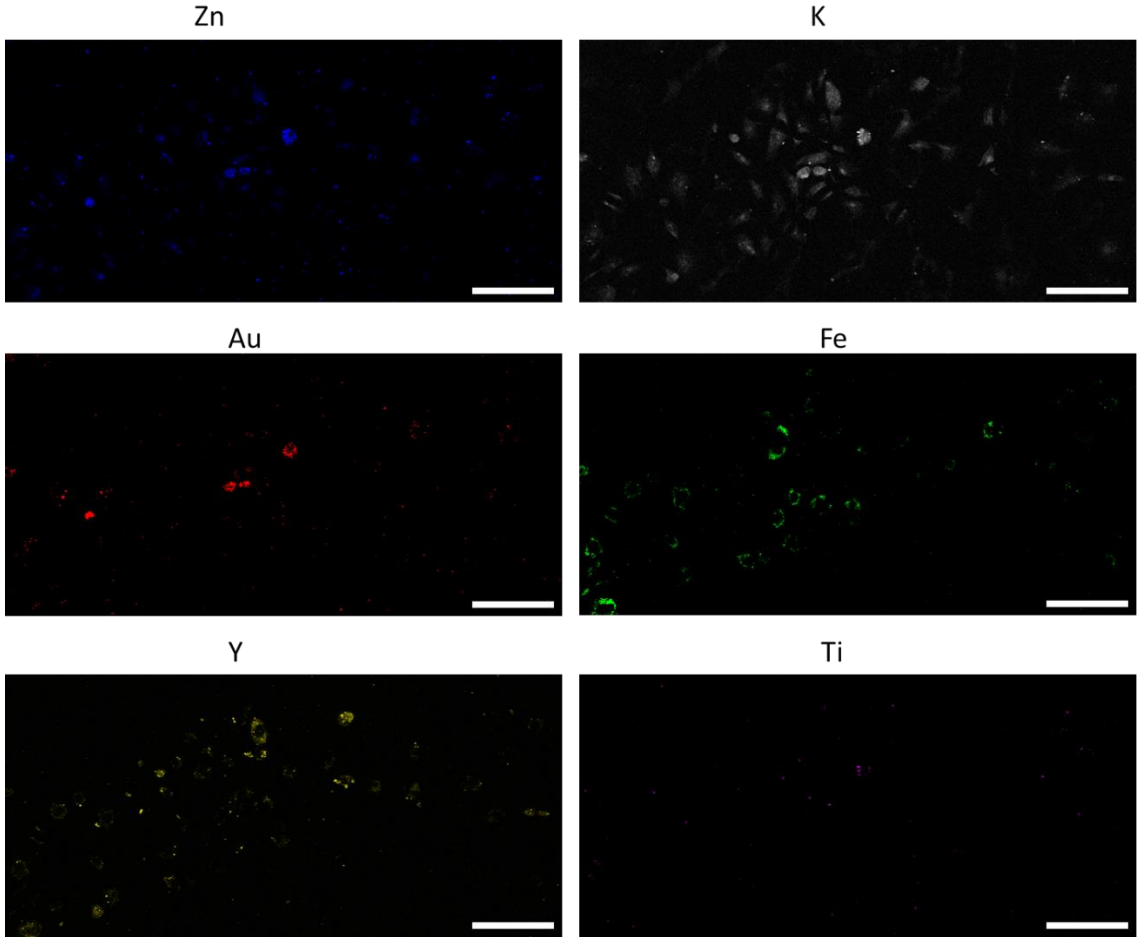
Zn
K
Au
Fe
Y
Ti

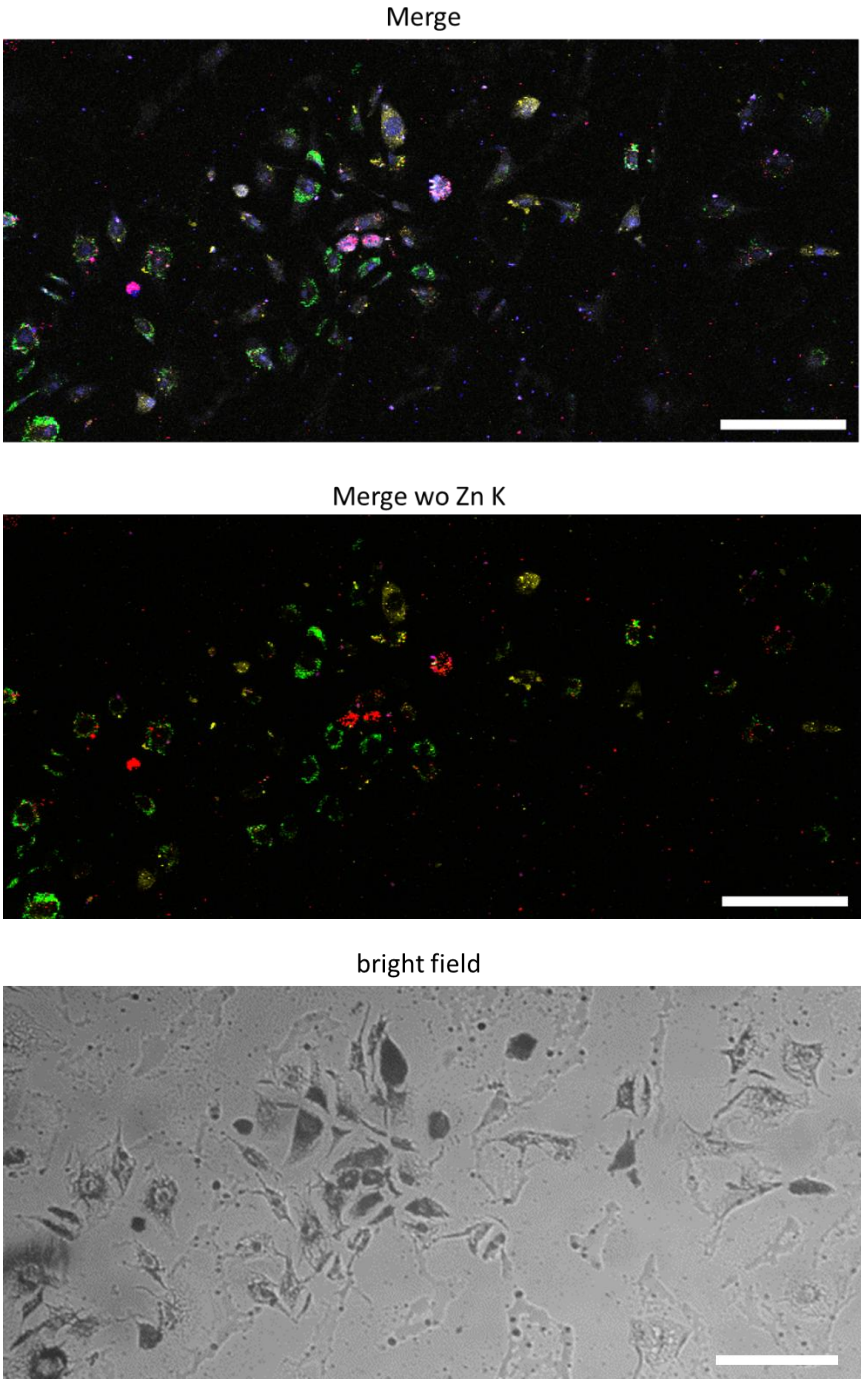

Figure 3-6-18. XFI of Mix four different cells in different detect elemental channel, the four different cells exposed in four different nanoparticles: Hela exposed in Au-PMA NPs, NRK exposed in FeOx-PMA NPs, 3T3 exposed in NaYF4-PMA NPs, and MCF-7 exposed in TiO2-PMA NPs for 24 hours, then mix together and culture in one SiN membrane. Scale bar is 100μm. the XFI operate is take by Marvin Skiba.

3.7. Conclusion

X-ray is a very nice and sensitive method to detect metal signal, in vivo and in situ, no extra modification, by XFI to research the metal nanoparticle's location in cell is hopeful and meaningful[69, 140-142].

From my results, we can preliminarily get the conclusion that iron oxide nanoparticles are located in the cytoplasm, sodium yttrium tetrafluoride nanoparticles are located in the cytoplasm, and gold nanoparticles are more likely to be located in the nucleus. For titanium dioxide nanoparticles, I am more inclined to believe that it is located on the cell membrane. And further XFI is necessary to prove the above point. And there still has more work to analysis the spectra to get the unique each peak be described to an element[143].

From the report of Reagan McRae et al[144], Au Lα and Zn Kβ emission bands are proximity, this consistent with our results, Zn signal is highly overlapped with Au signal, and in this report, nanogold are non-specific binding with the nuclear region, Au fluorescence remaining within nuclear region, this is also consistent with our results. Larabell' group used primary antibodies to label the microtube in cell, then incubated with gold nanoparticles conjugated secondary antibodies, then reduction to form aggregates, 50nm, using transmission X-ray microscopy image, this method detects that immunogold labeling can locate proteins in the cell nucleus and cytoplasm, the control group only has gold from the secondary antibody but no cellular localization information[145].

From the report of Paunesku et al[146-147], they design a composite of connect TiO2 nanoparticles and oligonucleotide, and oligonucleotide extend the retention of nanoparticles in cell/ nucleus. From the report of Koshonna Brown et al[148], they seed MCF-7 cells for 1 hour, then added titanium dioxide nanoparticles and cultured them overnight, then used flow cytometry to sort and collect cells marked with fluorescent signals. Then they inoculated the cells again and after 3 hours fixed the cells, then they observed the cell with fluorescence microscopy and X-ray fluorescence microscopy. They observed that the fluorescence microscopy signal of fluorescently labeled titanium dioxide and the x-ray fluorescence microscopy signal of titanium element could be co-localized and existed in the cytoplasm. In our experiment, titanium dioxide was labeled with PMA, and attach with

membrane for 16 hours. There was no flow cytometry to enrich the labeled cells. This may be the reason why no signal can be detected: The cells carrying titanium dioxide stay in the new culture medium for too long, resulting in an increase in the excretion of nanoparticles, and the cells carrying nanoparticles are difficult to find. From the report of Jichao Zhang et al[149], they incubated titanium dioxide nanoparticles with Hela cells, then fix the cells, dehydrate them, and drop them onto a silicon nitride membrane, performed XFI 3D imaging of the cells, observing titanium signals on the cell membrane. In our experiment, the cells were digested and centrifuged to remove excess nanoparticles, and then re-inoculated into fresh culture medium for 16 hours. So, it is very likely that the nanoparticles fell off the cell membrane, so no Ti signals were detected in XFI.

From the report of Yi et al[150], they use core-shell Fe_3O_4 @SiO_2 nanoparticle to label hMSCs, then use scanning transmission X-ray microscopy to observed the Fe location, which is mainly in cytoplasm without in nucleus. From the report of Fei et al[151], they analysis the stability of Fe_3O_4 and Fe_3O_4 @ SiO_2 nanoparticle in lysosomal model, then label them in hMSC cell, use X-ray fluorescence to observe the Fe position is evenly located in the cytoplasm. These reports are consistent with our results, so these has a clearly conclusion that the iron oxide nanoparticles are located in cell plasma.

From the report of Yanchun et al[152], they medicated the up-conversion nanoparticles (NaYF4: Yb3+, Er3+) with folic acid molecule (tumor-specific targeting) and microtubule inhibitor CA4P (depolymerization microtubule, stop cell division and induce cell apoptosis), and here NaYF4 nanoparticles are excite in near-infrared, and these nanoparticles can be detected in cells. And from the report of Mengxiao et al[153], they research the photobleaching and background fluorescence of NaYF4 nanoparticles labeling cell, these shows these nanoparticles are located in the cell plasma. These results are consistent with our results, so we have a clearly conclusion that the sodium yttrium tetrafluoride nanoparticles are located in cell plasma.

And there still has some difficult to do this imaging, firstly, nanoparticles are easy agglomeration in cell salt medium environment, e.g. In our experiments, it can be clearly observed that iron oxide nanoparticles and titanium dioxide nanoparticles aggregate into large particles visible to the naked eye after 24 hours in the cell culture medium. It is may form a protein corona and adhere to the outside of the cell membrane, which maybe fall off

and adhere to other cells and affect the detect results when prepare mix cell samples; Second, the sample prepare method is difficult for signal detection of the nanoparticles not enter cells, and like to adhere the outside membrane, sample prepare process is cell exposed with nanoparticles, then detach and seed on Si_3N_4 membrane, here use trypsin will destroy the protein on the membrane, this meaning the nanoparticle also will fall off from cell, leading to there is no detected signal; Third, fix cell process will affect the cell metal signal detection, Fixing cells allows cells go from alive to dead, but maintains the morphology of the cells. This process does not guarantee that dead cells remain exactly the same as living cells. (In my previous flow cytometry experiments, cells fixed with 4% PFA increased cell heterogeneity and reduced size.); Fourth, X-ray scanning is very time-consuming, for a large number of cells it will conduct in a about $0.5*0.5mm^2$ area , and for single cell scanning it is necessary to scanning in high resolution and using nanoprobes to detect signals; Fifth, technical and operational complication of X-ray fluorescence microscopy, and the data of x-ray emission spectrum is need to analysis and get the unique peak position to described each element, and which is not easy for such a complex cell samples. Sixth, it should prepare different concentration treatment of nanoparticles, and scan more single cells in high resolution, one cell is not representative, especially for metal signals within the cell itself, because cells are in the cell cycle and cells in different states may show different gene expression, and environment pressure trigger signaling cascade of cell induce protein network expression, which may affect the localization of nanoparticles, so more cells should be scanned to obtain more stable and reliable conclusions. Seventh, the metal elements in cells are to complex, because they contain potassium, magnesium, calcium, and zinc, these elements will interfere the detection signals of our target elements, making the final X-ray fluorescence spectrum very complex and difficult to determine the accurate element signals. In summary, XFI is a good technique for observing metal nanoparticles in cells, but the operation of XFI equipment and the subsequent data analysis are still challenging.

4. X-ray fluorescence imaging for metal-based drugs and contrast agents

4.1. Introduction

One of the most dreaded diseases is cancer in the recently century, which is caused by abnormal cell proliferation, when cancer is detected early, and the cell has not metastasized, it can be treated with surgery, radiation therapy, chemotherapy, or by regulating the immune system to fight the cancer. Once cancer cell metastasizes and invades other tissues, it is difficult to cure[93, 154-155]. And why do cells proliferate abnormally and uncontrollably? It is mainly due to abnormal gene expression or abnormal gene translation into protein. Chemotherapy for cancer is focus on interfere the synthesis of DNA, RNA or protein in cell to affect the cancer cell division[155].

Over the past decade, there has been considerable interest in identifying compounds with potential anticancer activity, and a lot of researchers are working in developing anticancer drugs, and elucidating the mechanisms of these compound[156], and developing better ways to diagnosis lesions. And metal-based compound also has highly effective in clinic, and many different metals, such as Seleno-L-cystine, Auranofin, cis-platin and so on, some of which mechanisms of action are unclear. In the lab, the researcher mainly researches the biomolecular expression to elucidate the drug working mechanisms[157]. And develop contrast agents for disease, such as Gadovist and Iohexol.

In here, based on the different metal has different X-ray attenuation, so we want use X-ray imaging method to study the position of metal-based drugs in cancer cell, to providing some information on the mechanism of action of metal-based drugs.

4.2. Major regents

Name	Purity	Company
Seleno-L-cystine	95%	Sigma Aldrich

Gadobutrol monohydrate	-	Sigma Aldrich
Auranofin	≥ 98 %	Sigma Aldrich
Cis-platin	-	-
Iohexol	-	Accupaque
Penicillin/streptomycin	NA	Sigma Aldrich
Resazurin	~80%	Sigma Aldrich
Phosphate buffered saline	-	Invitrogen
Dulbecco's modified eagle medium	-	Thermofisher
0.05% Trypsin	-	Thermofisher
Fetal bovine serum	-	Biochrom

4.3. Key instruments

Name	Model	Company	Function
X-ray micro-probe beamline	P06 hutch	Desy	For cell imaging
microplate reader	Omega S/N 415-4273	BMG LABTECH GmbH	For cell viability

Indcuctively coupled plasma mass spectrometry (ICP-MS)	7700 Series studies	Agilent	get Mental content per cell

4.4. Experiments and methods

This part in similar to the section 3, only change the nanoparticle to metal-based compounds.

4.5. results and discussions

4.5.1. cell viability for different metal drugs and contrast agents

From the results Figure 4-1, the Gadovist in high concentration there still has no cell cytotoxic; for cis platin, when added concentration become 3μM, there shows cell viability is about 90 %; and for Seleno-L-Cystine, when the concentration become about 20 μM, there shows cell viability is about 80%, and Seleno-L-Cystine is dissolved in 0.5M NaOH, consider cytotoxicity of NaOH, Figure 4-1 (E) shows the cell viability is all around 100% at different NaOH concentration, so the cytotoxicity in high addition is from Seleno-L-Cystine not NaOH; for Auranofin, when concentration become about 0.6 μM, the cell viability is about 100%, and then the value become down by add more Auranofin; Figure 4-1 (F) shows Hela viability with treated with Iohexol, in high concentration there still has no cell cytotoxic. So, this Figure gives a guide for treatment concentration.

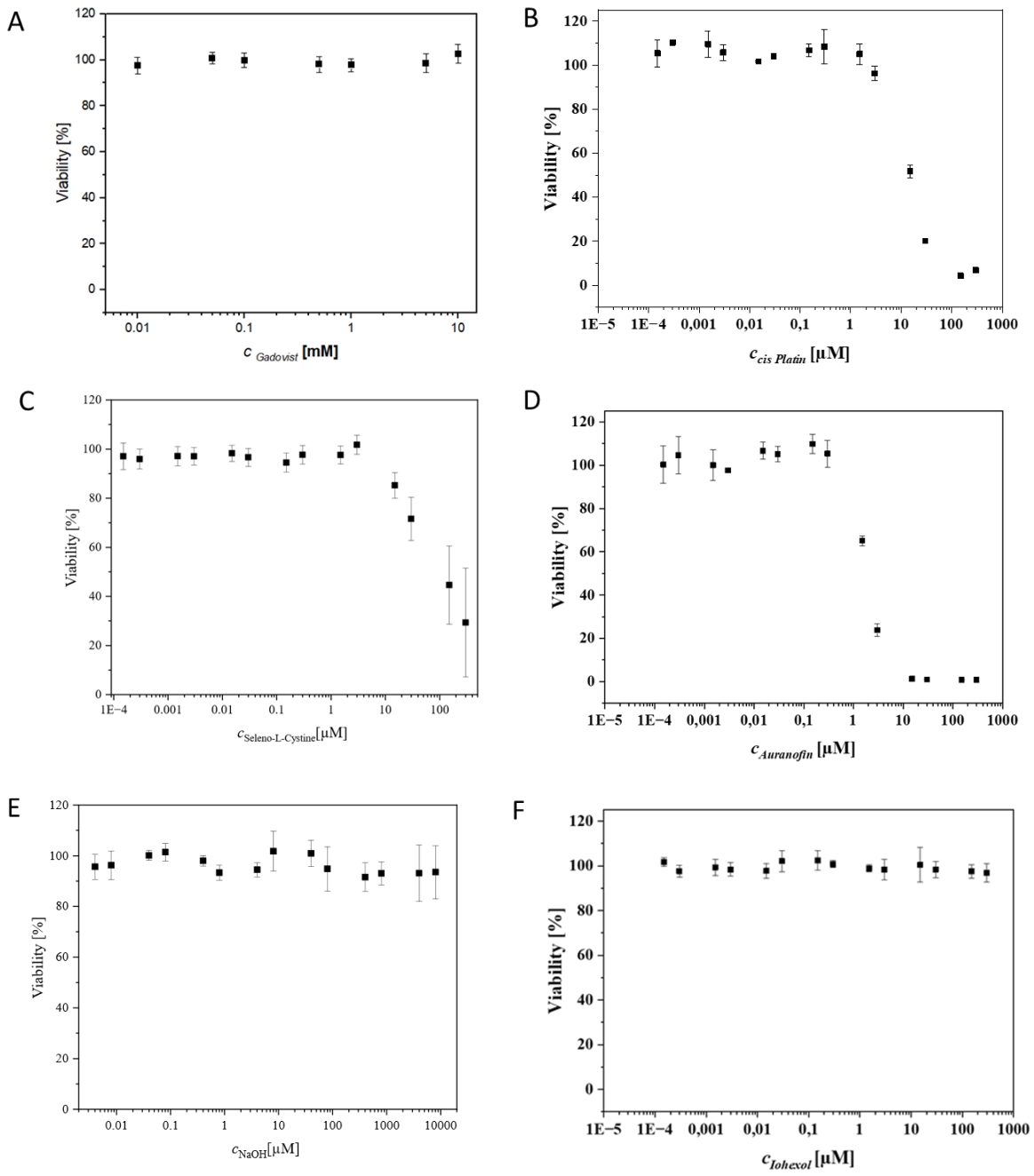

Figure 4-1: Cell viability of Hela exposed to Gadovist (A), cis platin (B), Seleno-L-Cystine (C), Auranofin (D), NaOH (E) and Iohexol (F) at different compound concentrations after 24h incubate by resazurin assay. Results are presented from three individual experiment. (B) and (D) are made by Marvin skiba.

4.5.2. cell uptake for different metal drugs and contrast agents

From the Figure 4-2, there shows the elemental concentration per cell after the compound

incubate with Hela for 24h, then wash with PBS for three times, then detach with 0.05% Trypsin, and collected cells to count cell by counting plate, then centrifuge to collected the cell pellets, digested by 200μL aqua regie at least overnight, the add 1800 μL 2% HNO3 dilute and detected by ICP-MS. For Hela uptake Gadovist, as the add concentration increase, the Gd concentration per cell is increase, and the Gd amount per cell up to 0.0069±0.0015pg when added Gadvovist is 100μM; For Hela uptake cis platin, as the add concentration increase, the Pt concentration per cell is increase, and the Pt amount per cell up to 0.046±0.012pg when added cis platin is 15μM; For Hela uptake Seleno-L-Cystine, as the add concentration increase, the Se concentration per cell is increase, and the Se amount per cell up to 0.090±0.016pg when added Seleno-L-Cystine is 15μM; For Hela uptake Auranofin, as the add concentration increase, the Au concentration per cell is increase, and the Au amount per cell up to 0.24 ±0.068 pg when added Auranofin is 2μM; For Hela uptake Iohexol, as the add concentration increase, the Iodine concentration per cell is increase, and the I amount per cell up to 10.75 ± 3.02 pg when added Iodine is 80 mM.

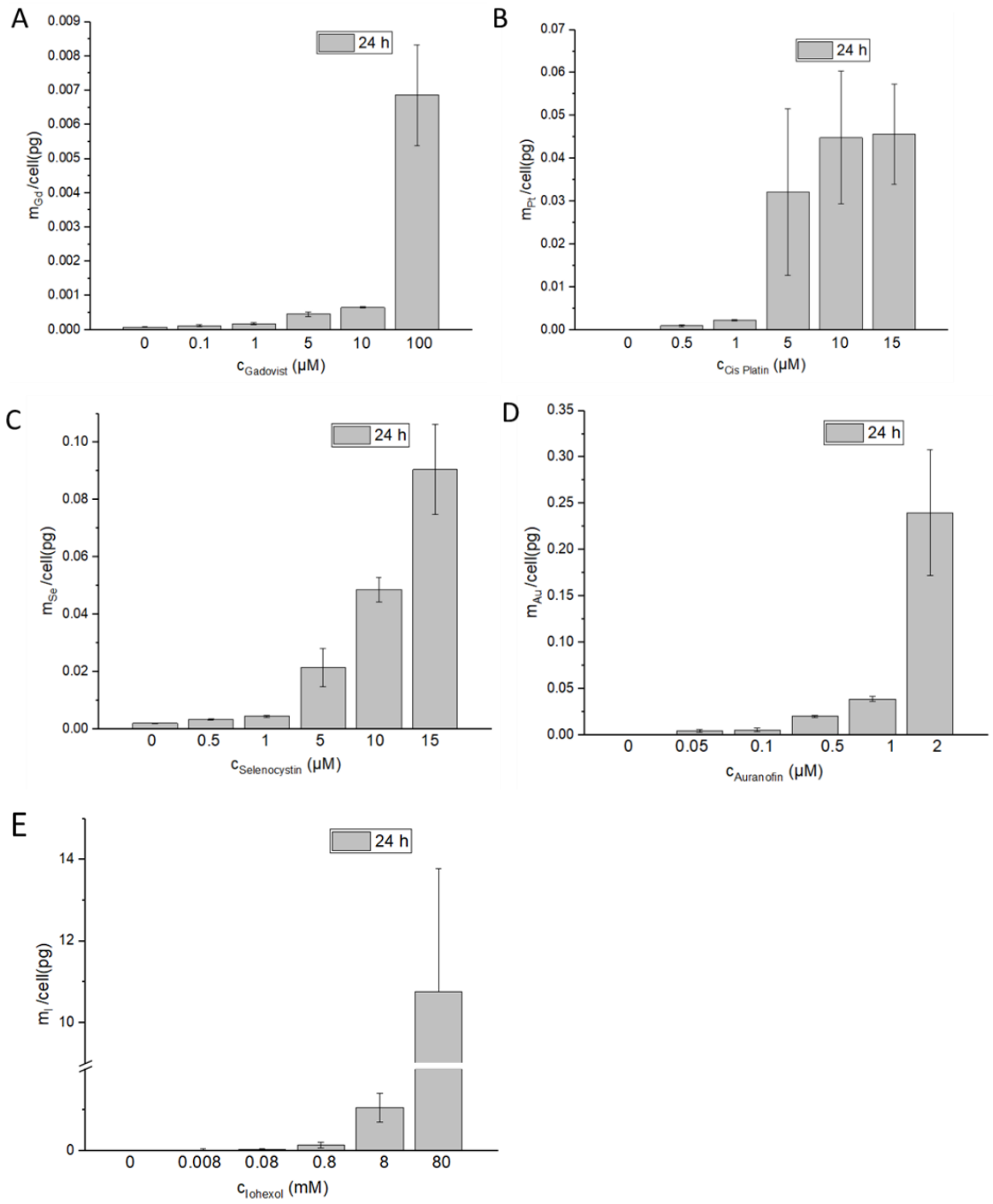

Figure 4-2: Amount of elemental found per cell in Hela exposed to Gadovist (A), Cis platin (B), Selen-L-cystin (C), Auranofin (D), Iohexol (E) at different compounds concentrations after 6 and 24 h by ICP-MS. Results are presented from three individual experiment.

At same time, the cell number under different treat concentration after 24 hours also show here, Figure 4-3 (A) For Gadovist treatment Hela cell number is not decrease, which is

constant with Hela viability results of Gadovist; For cis platin, cell number is become around half of not treat cell, when add 15μM cis platin, and from the Figure 4-3 (B) the cell viability is around 50%, they are consistent, this also shows that half of the decrease in cell viability is due to the halving of the cell number; For Selen-L-cystin, cell number is become around 80% of not treat cell, when add 15μM Selen-L-cystin, and from the Figure 4-3 (C) the cell viability is around 85%, they are consistent, this also shows that the decrease in cell viability is mainly due to the decrease of the cell number; For Auranofin, cell number is become around 53.4% of not treat cell, when add 2 μM Auranofin, and from the Figure 4-3 (D) the cell viability is around 65%, they are consistent, this also shows that the decrease in cell viability is due to the decrease of the cell number; In Figure 4-3 (E), for Iohexol treatment Hela cell number is not significance decrease, which is constant with Hela viability results of Iodine.

these mental concentration per cell can provide some information for the later detect by X-ray.

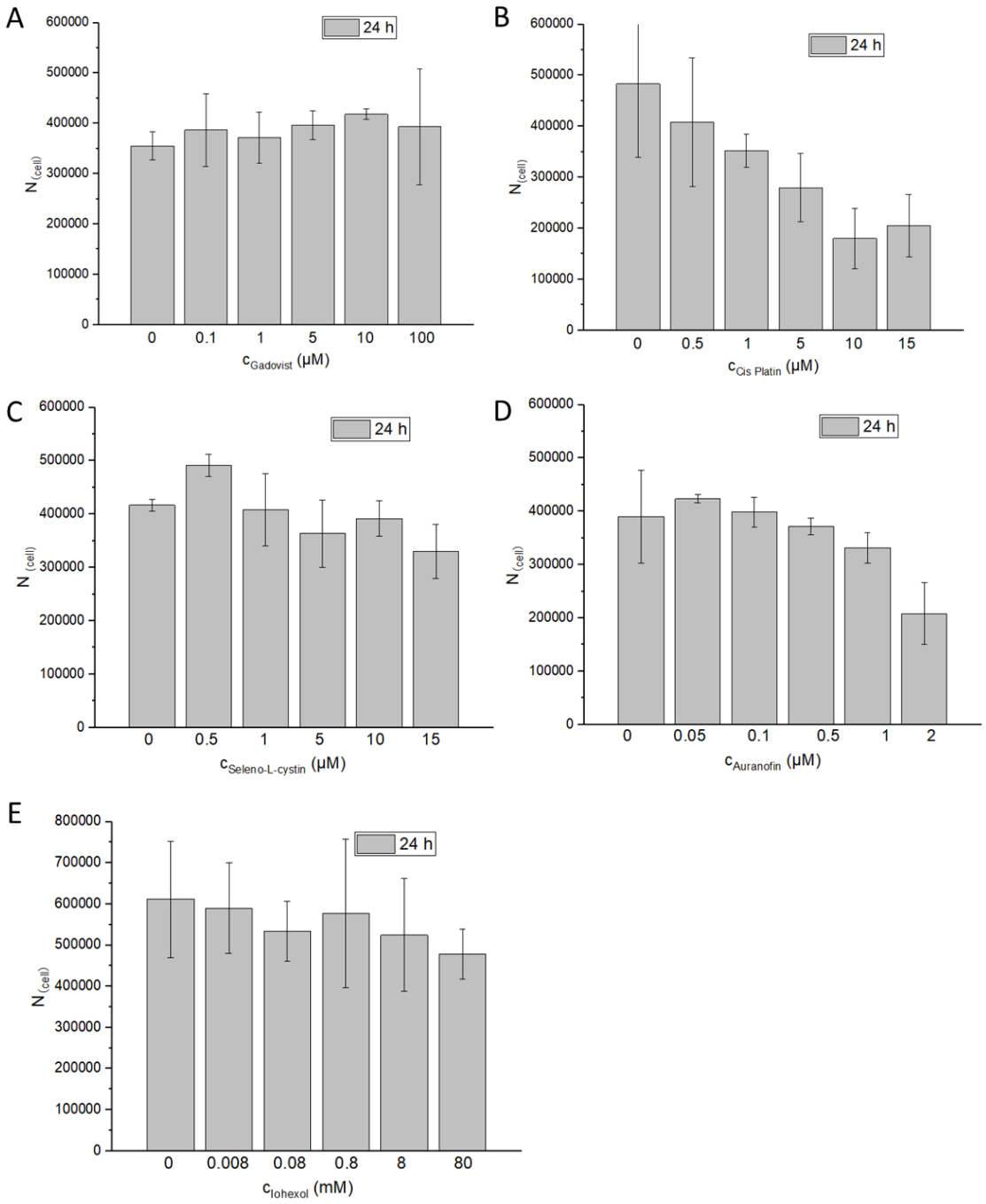

Figure 4-3: Cell number in Hela exposed to Gadovist (A), Cis platin (B), Selen-L-cystin (C), Auranofin (D) and iohexol (E) at different compounds concentrations after 24 h. Results are presented from three individual experiment.

4.6. conclusion and perspective

From above results, we can know metal-based drugs and Iodine are can uptake by Hela cell. And for Cis platin, Selen-L-cystin, and Auranofin in high concentration will lead to cytotoxicity, for Gadovist and Iohexol, there shows no cytotoxicity. For cell samples used for XFI, for cell safety considerations, the maximum amount of Gadovist added can be 10mM, the maximum amount of cisplatin added can be 3μM, the maximum amount of Auranofin added can be 0.3μM, and the maximum amount of Iohexol added can be 300 μM.

The above conclusions reveal the treatment concentrations of metal drugs on Hela cancer cells and no conclusions about the location of metal drugs in cells, but we make some perspective on these metal-drugs respectively:

Cisplatin is a platinum-containing anticancer drug, its structure is that the platinum atom is coordinated with two amino ligands and two chloride ions, and the same ligands are adjacent to each other, to form a planar four-coordinate construction. In the cell, the two chloride ions in cisplatin can be replaced by water molecules to form hydrated cisplatin, and this coordination is unstable, exposing the platinum center and making it easy to react. The platinum ion has two vacancies, which can form covalent bonds with the nitrogen of the bases of nucleotides in DNA, thereby causing abnormal DNA molecular construction and causing cell apoptosis[158-159], so it is located in the cell nucleus, it can be predicted that the location of cisplatin in cell nucleus observed by XFI.

Selenium is an important trace element in organisms and has strong antioxidant capacity. The structure of seleno-L-cystine is similar to L-cystine, but the sulfur atom is replaced by a selenium atom, which affects the redox balance in cells, leading to DNA damage and mitochondrial dysfunction in cells, and ultimately inducing cell apoptosis[160-161], seleno-L-cystine affects hydrogen peroxide production, antioxidant enzymes, and protein expression in MCF-7 cancer cells to affect the redox state reducing cell dead, and these processes are carried out in the cytoplasm, so it can be predicted that the location of seleno-L-cystine in cell membrane observed by XFI.

Auranofin is a gold-containing drug, its mechanism of action as an anticancer drug is still no clear, but basic research many focused on inhibiting thioredoxin reductase activiey[162], as an

inhibitor of thioredoxin reductase, it inhibit the reduction of disulfide bonds on the cell surface of HeLa cells from this article[163] . If the mechanism of action of Auranofin is related to this enzyme, perhaps we can determine whether they are related by co-localizing signals. The labeling of proteases is more of an immunofluorescence labeling, so the resolution of the detection technology and the off-target signal will affect the accuracy of the results, so, XFI is a good technology to analyze the location of Auranofin in cells in situ, and developing XFI-based immunostaining to determine whether it interacts with thioredoxin reductase.

Iohexol is an iodine-containing compound used as a contrast agent in medical imaging. iodine is a high atomic sequence element with a high electron density, and can effectively absorb X-rays compare to the surrounding tissue, therefore, iohexol is often used in X-ray imaging of CT scans and angiography[164]. Tumors and other lesion areas have more abundant blood supply and increased permeability of the blood vessel walls, so these areas will accumulate more iohexol, making the lesions visible. Here we expect to use XFI to observe the distribution of iohexol in Hela cancer cell.

Gadovist is a Gadolinium-containing compound used as a contrast agent in medical imaging, its ingredient is Gadobutrol monohydrate, and Gadolinium is a magnetic element that can be detected by magnetic resonance imaging (MRI). and it also has a high atomic sequence and high electron density, and can be detected by X-ray imaging. Here we expect to use XFI to observe the distribution of Gadovist in Hela cancer cell.

References

1. PARAK, N. F. A. W. J., Developing future nanomedicines. *SCIENCE* **2024,** *384* (6694).
2. Dlouhy, A. C.; Outten, C. E., The iron metallome in eukaryotic organisms. *Met Ions Life Sci* **2013,** *12*, 241-78.
3. Morales, M.; Xue, X., Targeting iron metabolism in cancer therapy. *Theranostics* **2021,** *11* (17), 8412-8429.
4. E., P., The iron oxides: structure, properties, reactions, occurrences and uses. *John Wiley & Sons* **1999**.
5. El-Hammadi, M. M.; Arias, J. L., Iron oxide-based multifunctional nanoparticulate systems for biomedical applications: a patent review (2008-present). *Expert Opin. Ther. Patents* **2015,** *25* (6), 691-709.
6. Wu, W.; Wu, Z.; Yu, T.; Jiang, C.; Kim, W. S., Recent progress on magnetic iron oxide nanoparticles: synthesis, surface functional strategies and biomedical applications. *Sci Technol Adv Mater* **2015,** *16* (2), 023501.
7. Ali, A.; Shah, T.; Ullah, R.; Zhou, P.; Guo, M.; Ovais, M.; Tan, Z.; Rui, Y., Review on Recent Progress in Magnetic Nanoparticles: Synthesis, Characterization, and Diverse Applications. *Front Chem* **2021,** *9*, 629054.
8. Komeili, A., Molecular mechanisms of compartmentalization and biomineralization in magnetotactic bacteria. *FEMS Microbiol Rev* **2012,** *36* (1), 232-55.
9. Dadfar, S. M.; Roemhild, K.; Drude, N. I.; von Stillfried, S.; Knuchel, R.; Kiessling, F.; Lammers, T., Iron oxide nanoparticles: Diagnostic, therapeutic and theranostic applications. *Adv Drug Deliv Rev* **2019,** *138*, 302-325.
10. Elahi, N.; Rizwan, M., Progress and prospects of magnetic iron oxide nanoparticles in biomedical applications: A review. *Artif Organs* **2021,** *45* (11), 1272-1299.
11. Hu, X.; Yu, J. C.; Gong, J.; Li, Q.; Li, G., α-Fe2O3 Nanorings Prepared by a Microwave-Assisted Hydrothermal Process and Their Sensing Properties. *Advanced Materials* **2007,** *19* (17), 2324-2329.
12. Q A Pankhurst, J. C., S K Jones and J Dobson, Applications of magnetic nanoparticles in biomedicine. *Journal of physics D: Applied physics* **2003,** *36*, R167.
13. Trpkov, D.; Panjan, M.; Kopanja, L.; Tadić, M., Hydrothermal synthesis, morphology, magnetic properties and self-assembly of hierarchical α-Fe2O3 (hematite) mushroom-, cube- and sphere-like superstructures. *Applied Surface Science* **2018,** *457*, 427-438.
14. Gavilán, H.; Kowalski, A.; Heinke, D.; Sugunan, A.; Sommertune, J.; Varón, M.; Bogart, L. K.; Posth, O.; Zeng, L.; González-Alonso, D.; Balceris, C.; Fock, J.; Wetterskog, E.; Frandsen, C.; Gehrke, N.; Grüttner, C.; Fornara, A.; Ludwig, F.; Veintemillas-Verdaguer, S.; Johansson, C.; Morales, M. P., Colloidal Flower-Shaped Iron Oxide Nanoparticles: Synthesis Strategies and Coatings. *Particle & Particle Systems Characterization* **2017,** *34* (7).
15. Sayed, F. N.; Polshettiwar, V., Facile and sustainable synthesis of shaped iron oxide nanoparticles: effect of iron precursor salts on the shapes of iron oxides. *Sci Rep* **2015,** *5*, 9733.
16. Wang, X.; Zhao, Z.; Qu, J.; Wang, Z.; Qiu, J., Shape-Control and Characterization of Magnetite Prepared via a One-Step Solvothermal Route. *Crystal Growth & Design* **2010,** *10* (7), 2863-2869.
17. Wu, W.; Xiao, X. H.; Ren, F.; Zhang, S. F.; Jiang, C. Z., A Comparative Study of the Magnetic Behavior of Single and Tubular Clustered Magnetite Nanoparticles. *Journal of Low Temperature Physics* **2012,** *168* (5-6), 306-313.
18. Muller*, S. L. D. F. M. P. A. R. C. R. L. V. E. R. N., Magnetic Iron Oxide Nanoparticles: Synthesis, Stabilization, Vectorization, Physicochemical Characterizations, and Biological

Applications. *Chemical Reviews* **2008,** *108* (6).
19. Bobo, D.; Robinson, K. J.; Islam, J.; Thurecht, K. J.; Corrie, S. R., Nanoparticle-Based Medicines: A Review of FDA-Approved Materials and Clinical Trials to Date. *Pharm Res* **2016,** *33* (10), 2373-87.
20. Arias, L. S.; Pessan, J. P.; Vieira, A. P. M.; Lima, T. M. T.; Delbem, A. C. B.; Monteiro, D. R., Iron Oxide Nanoparticles for Biomedical Applications: A Perspective on Synthesis, Drugs, Antimicrobial Activity, and Toxicity. *Antibiotics (Basel)* **2018,** *7* (2).
21. Noh, S.-h.; Moon, S. H.; Shin, T.-H.; Lim, Y.; Cheon, J., Recent advances of magneto-thermal capabilities of nanoparticles: From design principles to biomedical applications. *Nano Today* **2017,** *13*, 61-76.
22. Mahmoudi, M.; Sant, S.; Wang, B.; Laurent, S.; Sen, T., Superparamagnetic iron oxide nanoparticles (SPIONs): development, surface modification and applications in chemotherapy. *Adv Drug Deliv Rev* **2011,** *63* (1-2), 24-46.
23. Haun, J. B.; Yoon, T. J.; Lee, H.; Weissleder, R., Magnetic nanoparticle biosensors. *Wiley Interdiscip Rev Nanomed Nanobiotechnol* **2010,** *2* (3), 291-304.
24. Castro-Giner, F.; Aceto, N., Tracking cancer progression: from circulating tumor cells to metastasis. *Genome Med* **2020,** *12* (1), 31.
25. Chen, Y.; Wu, Z.; Sutlive, J.; Wu, K.; Mao, L.; Nie, J.; Zhao, X. Z.; Guo, F.; Chen, Z.; Huang, Q., Noninvasive prenatal diagnosis targeting fetal nucleated red blood cells. *J Nanobiotechnology* **2022,** *20* (1), 546.
26. Plouffe, B. D.; Murthy, S. K.; Lewis, L. H., Fundamentals and application of magnetic particles in cell isolation and enrichment: a review. *Rep Prog Phys* **2015,** *78* (1), 016601.
27. Tang, W.; Jiang, D.; Li, Z.; Zhu, L.; Shi, J.; Yang, J.; Xiang, N., Recent advances in microfluidic cell sorting techniques based on both physical and biochemical principles. *Electrophoresis* **2019,** *40* (6), 930-954.
28. Leary, J. F., Ultra high-speed sorting. *Cytometry A* **2005,** *67* (2), 76-85.
29. Wang, Z.; Wang, H.; Lin, S.; Ahmed, S.; Angers, S.; Sargent, E. H.; Kelley, S. O., Nanoparticle Amplification Labeling for High-Performance Magnetic Cell Sorting. *Nano Lett* **2022,** *22* (12), 4774-4783.
30. Yun, H.; Kim, K.; Lee, W. G., Cell manipulation in microfluidics. *Biofabrication* **2013,** *5* (2), 022001.
31. Robert, D.; Pamme, N.; Conjeaud, H.; Gazeau, F.; Iles, A.; Wilhelm, C., Cell sorting by endocytotic capacity in a microfluidic magnetophoresis device. *Lab Chip* **2011,** *11* (11), 1902-10.
32. Iler, R. K., Multilayers of colloidal particles. *Journal of Colloid and Interface Science* **1966,** *21* (6), 569-594.
33. FRANK CARUSO, R. A. C., AND HELMUTH MÖHWALD, Nanoengineering of Inorganic and Hybrid Hollow Spheres by Colloidal Templating. *SCIENCE* **6 Nov 1998,** *282* (5391), 1111-1114.
34. Decher, G., Fuzzy Nanoassemblies: Toward Layered Polymeric Multicomposites. *SCIENCE* **29 Aug 1997,** *277* (5330), 1232-1237.
35. Parakhonskiy, B.; Zyuzin, M. V.; Yashchenok, A.; Carregal-Romero, S.; Rejman, J.; Mohwald, H.; Parak, W. J.; Skirtach, A. G., The influence of the size and aspect ratio of anisotropic, porous CaCO3 particles on their uptake by cells. *J Nanobiotechnology* **2015,** *13*, 53.
36. Becker, A. L.; Johnston, A. P.; Caruso, F., Layer-by-layer-assembled capsules and films for therapeutic delivery. *Small* **2010,** *6* (17), 1836-52.
37. Johnston, A. P. R.; Cortez, C.; Angelatos, A. S.; Caruso, F., Layer-by-layer engineered capsules and their applications. *Current Opinion in Colloid & Interface Science* **2006,** *11* (4), 203-209.
38. Yan, Y.; Björnmalm, M.; Caruso, F., Assembly of Layer-by-Layer Particles and Their Interactions with Biological Systems. *Chemistry of Materials* **2013,** *26* (1), 452-460.

39. Zhao, S.; Caruso, F.; Dahne, L.; Decher, G.; De Geest, B. G.; Fan, J.; Feliu, N.; Gogotsi, Y.; Hammond, P. T.; Hersam, M. C.; Khademhosseini, A.; Kotov, N.; Leporatti, S.; Li, Y.; Lisdat, F.; Liz-Marzan, L. M.; Moya, S.; Mulvaney, P.; Rogach, A. L.; Roy, S.; Shchukin, D. G.; Skirtach, A. G.; Stevens, M. M.; Sukhorukov, G. B.; Weiss, P. S.; Yue, Z.; Zhu, D.; Parak, W. J., The Future of Layer-by-Layer Assembly: A Tribute to ACS Nano Associate Editor Helmuth Mohwald. *ACS Nano* **2019,** *13* (6), 6151-6169.
40. Zyuzin, M. V.; Diez, P.; Goldsmith, M.; Carregal-Romero, S.; Teodosio, C.; Rejman, J.; Feliu, N.; Escudero, A.; Almendral, M. J.; Linne, U.; Peer, D.; Fuentes, M.; Parak, W. J., Comprehensive and Systematic Analysis of the Immunocompatibility of Polyelectrolyte Capsules. *Bioconjug Chem* **2017,** *28* (2), 556-564.
41. Lena Kastl†, D. S., Verena Wulf†, Raimo Hartmann†, Josif Mircheski‡, Christiane Ranke†, Susana Carregal-Romero†§, José Antonio Martínez-López‡, Rafael Fernández-Chacón‡, Wolfgang J. Parak†, Hans-Peter Elsasser⊥, and Pilar Rivera_Gil†*, Multiple Internalization Pathways of Polyelectrolyte Multilayer Capsules into Mammalian Cells. *ACS Nano* **2013,** *7* (8), 6605–6618.
42. Ochs, M.; Carregal-Romero, S.; Rejman, J.; Braeckmans, K.; De Smedt, S. C.; Parak, W. J., Light-addressable capsules as caged compound matrix for controlled triggering of cytosolic reactions. *Angew Chem Int Ed Engl* **2013,** *52* (2), 695-9.
43. A. Muñoz Javier†‡∇, P. d. P., M. F. Bedard§, D. Ho∥, A. G. Skirtach§, G. B. Sukhorukov⊥, C. Plank‡, and W. J. Parak*†∥#, Photoactivated Release of Cargo from the Cavity of Polyelectrolyte Capsules to the Cytosol of Cells. *Langmuir* **2008,** *24* (21), 12517–12520.
44. Zhu, D.; Feng, L.; Feliu, N.; Guse, A. H.; Parak, W. J., Stimulation of Local Cytosolic Calcium Release by Photothermal Heating for Studying Intra- and Intercellular Calcium Waves. *Adv Mater* **2021,** *33* (24), e2008261.
45. Roy, S.; Zhu, D.; Parak, W. J.; Feliu, N., Lysosomal Proton Buffering of Poly(ethylenimine) Measured In Situ by Fluorescent pH-Sensor Microcapsules. *ACS Nano* **2020,** *14* (7), 8012-8023.
46. Kantner, K.; Rejman, J.; Kraft, K. V. L.; Soliman, M. G.; Zyuzin, M. V.; Escudero, A.; Del Pino, P.; Parak, W. J., Laterally and Temporally Controlled Intracellular Staining by Light-Triggered Release of Encapsulated Fluorescent Markers. *Chemistry* **2018,** *24* (9), 2098-2102.
47. Valdeperez, D.; Del Pino, P.; Sanchez, L.; Parak, W. J.; Pelaz, B., Highly active antibody-modified magnetic polyelectrolyte capsules. *J Colloid Interface Sci* **2016,** *474*, 1-8.
48. Möhwald, A. A. A. G. B. S. S. L. I. L. R. E. D. a. H., Polyelectrolyte multilayer capsule permeability control. *Colloids and Surfaces A: Physicochemical and Engineering Aspects* **18 February 2002,** *198–200*
, , 535-541.
49. Gao, H.; Goriacheva, O. A.; Tarakina, N. V.; Sukhorukov, G. B., Intracellularly Biodegradable Polyelectrolyte/Silica Composite Microcapsules as Carriers for Small Molecules. *ACS Appl Mater Interfaces* **2016,** *8* (15), 9651-61.
50. El-Hajjar, L.; Ali Ahmad, F.; Nasr, R., A Guide to Flow Cytometry: Components, Basic Principles, Experimental Design, and Cancer Research Applications. *Curr Protoc* **2023,** *3* (3), e721.
51. Manohar, S. M.; Shah, P.; Nair, A., Flow cytometry: principles, applications and recent advances. *Bioanalysis* **2021,** *13* (3), 181-198.
52. Maciorowski, Z.; Chattopadhyay, P. K.; Jain, P., Basic Multicolor Flow Cytometry. *Curr Protoc Immunol* **2017,** *117*, 5 4 1-5 4 38.
53. Wu, L.; Zhang, Y.; Hong, X.; Wu, M.; Wang, L.; Yan, X., Deciphering the Relationship between Cell Growth and Cell Cycle in Individual Escherichia coli Cells by Flow Cytometry. *Anal Chem* **2024**.
54. Ionescu, L. I.; Blydt-Hansen, T.; Foster, B. J.; Allen, U.; Birk, P. E.; Hamiwka, L.; Phan, V.; Min, S.; Ivison, S.; Levings, M.; West, L. J.; Mital, S.; Urschel, S., Immune phenotyping in a pediatric multicenter transplant study: Suitability of a preformulated dry-antibody panel system. *Hum*

Immunol **2024,** *85* (5), 110837.
55. Vanzo-Sparks, H. K.; Webster, S. E.; Webster, M. K.; Linn, C. L., Quantification of Proliferating and Mitotically Active Retinal Cells in Mice by Flow Cytometry. *Bio Protoc* **2024,** *14* (13), e5024.
56. Ammann, A. A., Inductively coupled plasma mass spectrometry (ICP MS): a versatile tool. *J Mass Spectrom* **2007,** *42* (4), 419-27.
57. Nageswara Rao, R.; Talluri, M. V., An overview of recent applications of inductively coupled plasma-mass spectrometry (ICP-MS) in determination of inorganic impurities in drugs and pharmaceuticals. *J Pharm Biomed Anal* **2007,** *43* (1), 1-13.
58. McNulty, The future of X-ray holography. *Nuclear Instruments and Methods in Physics Research* **1994,** *347*, 170-176.
59. Atsushi Momose, T. T., Yuji Itai & Keiichi Hirano Phase–contrast X–ray computed tomography for observing biological soft tissues. *Nature Medicine* **01 April 1996,** *2*, 473–475
60. Fahrni, C. J., Biological applications of X-ray fluorescence microscopy: exploring the subcellular topography and speciation of transition metals. *Curr Opin Chem Biol* **2007,** *11* (2), 121-7.
61. Decelle, J.; Veronesi, G.; Gallet, B.; Stryhanyuk, H.; Benettoni, P.; Schmidt, M.; Tucoulou, R.; Passarelli, M.; Bohic, S.; Clode, P.; Musat, N., Subcellular Chemical Imaging: New Avenues in Cell Biology. *Trends Cell Biol* **2020,** *30* (3), 173-188.
62. Otto, F.; Sun, X.; Schulz, F.; Sanchez-Cano, C.; Feliu, N.; Westermeier, F.; Parak, W. J., X-Ray Photon Correlation Spectroscopy Towards Measuring Nanoparticle Diameters in Biological Environments Allowing for the In Situ Analysis of their Bio-Nano Interface. *Small* **2022,** *18* (37), e2201324.
63. Liming Wang 1, T. Z., Panyun Li 2, Wanxia Huang 2, Jinglong Tang 1, Pengyang Wang 1, Jing Liu 1, Qingxi Yuan 2, Ru Bai 1, Bai Li 1, Kai Zhang 2, Yuliang Zhao 1, Chunying Chen, Use of Synchrotron Radiation-Analytical Techniques To Reveal Chemical Origin of Silver-Nanoparticle Cytotoxicity. *ACS Nano* **2015,** *9(6):6532-47*.
64. Skiba, M.; Guedes, G.; Karpov, D.; Feliu, N.; A, L. C.; Parak, W. J.; Sanchez-Cano, C., Probing the Cellular Fate of the Protein Corona around Nanoparticles with Nanofocused X-ray Fluorescence Imaging. *Int J Mol Sci* **2023,** *25* (1).
65. Gruner, F.; Blumendorf, F.; Schmutzler, O.; Staufer, T.; Bradbury, M.; Wiesner, U.; Rosentreter, T.; Loers, G.; Lutz, D.; Richter, B.; Fischer, M.; Schulz, F.; Steiner, S.; Warmer, M.; Burkhardt, A.; Meents, A.; Kupinski, M.; Hoeschen, C., Localising functionalised gold-nanoparticles in murine spinal cords by X-ray fluorescence imaging and background-reduction through spatial filtering for human-sized objects. *Sci Rep* **2018,** *8* (1), 16561.
66. Liu, Y.; Kornig, C.; Qi, B.; Schmutzler, O.; Staufer, T.; Sanchez-Cano, C.; Magel, E.; White, J. C.; Feliu, N.; Gruner, F.; Parak, W. J., Size- and Ligand-Dependent Transport of Nanoparticles in Matricaria chamomilla as Demonstrated by Mass Spectroscopy and X-ray Fluorescence Imaging. *ACS Nano* **2022,** *16* (8), 12941-12951.
67. Staufer, T.; Kornig, C.; Liu, B.; Liu, Y.; Lanzloth, C.; Schmutzler, O.; Bedke, T.; Machicote, A.; Parak, W. J.; Feliu, N.; Bosurgi, L.; Huber, S.; Gruner, F., Enabling X-ray fluorescence imaging for in vivo immune cell tracking. *Sci Rep* **2023,** *13* (1), 11505.
68. Kornig, C.; Staufer, T.; Schmutzler, O.; Bedke, T.; Machicote, A.; Liu, B.; Liu, Y.; Gargioni, E.; Feliu, N.; Parak, W. J.; Huber, S.; Gruner, F., In-situ x-ray fluorescence imaging of the endogenous iodine distribution in murine thyroids. *Sci Rep* **2022,** *12* (1), 2903.
69. Sanchez-Cano, C.; Alvarez-Puebla, R. A.; Abendroth, J. M.; Beck, T.; Blick, R.; Cao, Y.; Caruso, F.; Chakraborty, I.; Chapman, H. N.; Chen, C.; Cohen, B. E.; Conceicao, A. L. C.; Cormode, D. P.; Cui, D.; Dawson, K. A.; Falkenberg, G.; Fan, C.; Feliu, N.; Gao, M.; Gargioni, E.; Gluer, C. C.; Gruner, F.; Hassan, M.; Hu, Y.; Huang, Y.; Huber, S.; Huse, N.; Kang, Y.; Khademhosseini, A.; Keller,

T. F.; Kornig, C.; Kotov, N. A.; Koziej, D.; Liang, X. J.; Liu, B.; Liu, S.; Liu, Y.; Liu, Z.; Liz-Marzan, L. M.; Ma, X.; Machicote, A.; Maison, W.; Mancuso, A. P.; Megahed, S.; Nickel, B.; Otto, F.; Palencia, C.; Pascarelli, S.; Pearson, A.; Penate-Medina, O.; Qi, B.; Radler, J.; Richardson, J. J.; Rosenhahn, A.; Rothkamm, K.; Rubhausen, M.; Sanyal, M. K.; Schaak, R. E.; Schlemmer, H. P.; Schmidt, M.; Schmutzler, O.; Schotten, T.; Schulz, F.; Sood, A. K.; Spiers, K. M.; Staufer, T.; Stemer, D. M.; Stierle, A.; Sun, X.; Tsakanova, G.; Weiss, P. S.; Weller, H.; Westermeier, F.; Xu, M.; Yan, H.; Zeng, Y.; Zhao, Y.; Zhao, Y.; Zhu, D.; Zhu, Y.; Parak, W. J., X-ray-Based Techniques to Study the Nano-Bio Interface. *ACS Nano* **2021,** *15* (3), 3754-3807.

70. Carlton, J. G.; Jones, H.; Eggert, U. S., Membrane and organelle dynamics during cell division. *Nat Rev Mol Cell Biol* **2020,** *21* (3), 151-166.

71. Lydia A Finney 1, T. V. O. H., Transition metal speciation in the cell: insights from the chemistry of metal ion receptors. *Science* **2003,** *300* (5621), 931-6.

72. F Y Wu, C. W. W., Zinc in DNA replication and transcription. *Annu Rev Nutr* **1987,** *7*, 251-72.

73. Wu, F. Y.; Huang, W. J.; Sinclair, R. B.; Powers, L., The structure of the zinc sites of Escherichia coli DNA-dependent RNA polymerase. *Journal of Biological Chemistry* **1992,** *267* (35), 25560-25567.

74. MacDonald, R. S., The Role of Zinc in Growth and Cell Proliferation. *J Nutr* **2000,** *130* ((5S Suppl):1500S-8S).

75. Chesters, J. K., Trace element-gene interactions with particular reference to zinc. *Proc Nutr Soc* **1991,** *50* (2), 123-9.

76. McRae, R.; Lai, B.; Fahrni, C. J., Subcellular redistribution and mitotic inheritance of transition metals in proliferating mouse fibroblast cells. *Metallomics* **2013,** *5* (1), 52-61.

77. P.H. Näslund, T. H., Structural and functional defects in mammalian ribosomes after potassium deficiency. *Biochimica et Biophysica Acta (BBA)-Nucleic Acids and Protein Synthesis* **1971,** *254* (1), 104-116.

78. LUBIN, M., A priming reaction in protein synthesis. *Biochim Biophys Acta* **1963,** *25* (72), 348-8.

79. Civan, M. M., Intracellular activities of sodium and potassium. *American Journal of Physiology-Renal Physiology* **1978,** *234* (4), F261-F355.

80. Andersson, B.; Janson, V.; Behnam-Motlagh, P.; Henriksson, R.; Grankvist, K., Induction of apoptosis by intracellular potassium ion depletion: using the fluorescent dye PBFI in a 96-well plate method in cultured lung cancer cells. *Toxicol In Vitro* **2006,** *20* (6), 986-94.

81. Lang, F.; Foller, M.; Lang, K.; Lang, P.; Ritter, M.; Vereninov, A.; Szabo, I.; Huber, S. M.; Gulbins, E., Cell volume regulatory ion channels in cell proliferation and cell death. *Methods Enzymol* **2007,** *428*, 209-25.

82. Cameron, I. L.; Pool, T. B.; Smith, N. K., An X-ray microanalysis survey of the concentration of elements in the cytoplasm of different mammalian cell types. *J Cell Physiol* **1979,** *101* (3), 493-501.

83. Nguyen, L. H.; Tran, T. T.; Truong, L. T. N.; Mai, H. H.; Nguyen, T. T., Overcharging of the Zinc Ion in the Structure of the Zinc-Finger Protein Is Needed for DNA Binding Stability. *Biochemistry* **2020,** *59* (13), 1378-1390.

84. Rozov, A.; Khusainov, I.; El Omari, K.; Duman, R.; Mykhaylyk, V.; Yusupov, M.; Westhof, E.; Wagner, A.; Yusupova, G., Importance of potassium ions for ribosome structure and function revealed by long-wavelength X-ray diffraction. *Nat Commun* **2019,** *10* (1), 2519.

85. Lisong Xiao 1, J. L., Dermot F Brougham, Eoin K Fox, Neus Feliu, Alexey Bushmelev, Annette Schmidt, Natascha Mertens, Fabian Kiessling, Martin Valldor, Bengt Fadeel, Sanjay Mathur, Water-soluble superparamagnetic magnetite nanoparticles with biocompatible coating

for enhanced magnetic resonance imaging. *ACS Nano* **2011,** *23* (5（8）), 6315-24.
86. Kunzmann, A.; Andersson, B.; Vogt, C.; Feliu, N.; Ye, F.; Gabrielsson, S.; Toprak, M. S.; Buerki-Thurnherr, T.; Laurent, S.; Vahter, M.; Krug, H.; Muhammed, M.; Scheynius, A.; Fadeel, B., Efficient internalization of silica-coated iron oxide nanoparticles of different sizes by primary human macrophages and dendritic cells. *Toxicol Appl Pharmacol* **2011,** *253* (2), 81-93.
87. Gonçalves, A. I.; Miranda, M. S.; Rodrigues, M. T.; Reis, R. L.; Gomes, M. E., Magnetic responsive cell-based strategies for diagnostics and therapeutics. *Biomedical Materials* **2018,** *13* (5).
88. Parak, B. Z. S. S. B. S. L. R. J., Magnetic Targeting and Cellular Uptake of Polymer Microcapsules Simultaneously Functionalized with Magnetic and Luminescent Nanocrystals. *Langmuir* **2005,** *21* (10), 4262-4265.
89. Verkhovskii, R.; Ermakov, A.; Grishin, O.; Makarkin, M. A.; Kozhevnikov, I.; Makhortov, M.; Kozlova, A.; Salem, S.; Tuchin, V.; Bratashov, D., The Influence of Magnetic Composite Capsule Structure and Size on Their Trapping Efficiency in the Flow. *Molecules* **2022,** *27* (18).
90. Verkhovskii, R.; Ermakov, A.; Sindeeva, O.; Prikhozhdenko, E.; Kozlova, A.; Grishin, O.; Makarkin, M.; Gorin, D.; Bratashov, D., Effect of Size on Magnetic Polyelectrolyte Microcapsules Behavior: Biodistribution, Circulation Time, Interactions with Blood Cells and Immune System. *Pharmaceutics* **2021,** *13* (12).
91. Semmling, M.; Kreft, O.; Munoz Javier, A.; Sukhorukov, G. B.; Kas, J.; Parak, W. J., A novel flow-cytometry-based assay for cellular uptake studies of polyelectrolyte microcapsules. *Small* **2008,** *4* (10), 1763-8.
92. Feliu, N.; Sun, X.; Alvarez Puebla, R. A.; Parak, W. J., Quantitative Particle-Cell Interaction: Some Basic Physicochemical Pitfalls. *Langmuir* **2017,** *33* (27), 6639-6646.
93. Society., A. C., Cancer facts & figures *(ACS, 2024).* **2024**.
94. Drezek, C. L. L. H. W., Immunotargeted Nanoshells for Integrated Cancer Imaging and Therapy. *Nano Letters* **2005,** *5* (4), 709-711.
95. Chen, J. X. J. Z. J. Y. T. K. T. X. W. R. X. W. J., Gold-based nanoparticles for breast cancer diagnosis and treatment. *Proceedings - IEEE International Symposium on Circuits and Systems* **2007**, 2882-2885.
96. Dalby, M., Cree, I. A., Challoner, B. R., Ghosh, S. & Thurston, D. E., The precision medicine approach to cancer therapy: part 1 — solid tumours. *Pharmaceutical Journal* **2019**.
97. Hua, S.; de Matos, M. B. C.; Metselaar, J. M.; Storm, G., Current Trends and Challenges in the Clinical Translation of Nanoparticulate Nanomedicines: Pathways for Translational Development and Commercialization. *Front Pharmacol* **2018,** *9*, 790.
98. Ou, W.; Thapa, R. K.; Jiang, L.; Soe, Z. C.; Gautam, M.; Chang, J. H.; Jeong, J. H.; Ku, S. K.; Choi, H. G.; Yong, C. S.; Kim, J. O., Regulatory T cell-targeted hybrid nanoparticles combined with immuno-checkpoint blockage for cancer immunotherapy. *J Control Release* **2018,** *281*, 84-96.
99. Chan, W. C. W., Principles of Nanoparticle Delivery to Solid Tumors. *BME Front* **2023,** *4*, 0016.
100. Xu, L.; Xu, M.; Sun, X.; Feliu, N.; Feng, L.; Parak, W. J.; Liu, S., Quantitative Comparison of Gold Nanoparticle Delivery via the Enhanced Permeation and Retention (EPR) Effect and Mesenchymal Stem Cell (MSC)-Based Targeting. *ACS Nano* **2023,** *17* (3), 2039-2052.
101. Francia, V.; Yang, K.; Deville, S.; Reker-Smit, C.; Nelissen, I.; Salvati, A., Corona Composition Can Affect the Mechanisms Cells Use to Internalize Nanoparticles. *ACS Nano* **2019,** *13* (10), 11107-11121.
102. Wechsler, M. E.; Ramirez, J. E. V.; Peppas, N. A., 110(th) Anniversary: Nanoparticle mediated drug delivery for the treatment of Alzheimer's disease: Crossing the blood-brain barrier. *Ind Eng Chem Res* **2019,** *58* (33), 15079-15087.

103. Salvati, A.; Pitek, A. S.; Monopoli, M. P.; Prapainop, K.; Bombelli, F. B.; Hristov, D. R.; Kelly, P. M.; Aberg, C.; Mahon, E.; Dawson, K. A., Transferrin-functionalized nanoparticles lose their targeting capabilities when a biomolecule corona adsorbs on the surface. *Nat Nanotechnol* **2013,** *8* (2), 137-43.
104. Blanco, E.; Shen, H.; Ferrari, M., Principles of nanoparticle design for overcoming biological barriers to drug delivery. *Nat Biotechnol* **2015,** *33* (9), 941-51.
105. Chan, B. D. C. A. G. C. W., Determining the Size and Shape Dependence of Gold Nanoparticle Uptake into Mammalian Cells. *Nano Letters* **2006,** *6* (4).
106. Yue, J.; Feliciano, T. J.; Li, W.; Lee, A.; Odom, T. W., Gold Nanoparticle Size and Shape Effects on Cellular Uptake and Intracellular Distribution of siRNA Nanoconstructs. *Bioconjug Chem* **2017,** *28* (6), 1791-1800.
107. Behzadi, S.; Serpooshan, V.; Tao, W.; Hamaly, M. A.; Alkawareek, M. Y.; Dreaden, E. C.; Brown, D.; Alkilany, A. M.; Farokhzad, O. C.; Mahmoudi, M., Cellular uptake of nanoparticles: journey inside the cell. *Chem Soc Rev* **2017,** *46* (14), 4218-4244.
108. Lu, H.; Su, J.; Mamdooh, R.; Li, Y.; Stenzel, M. H., Cellular Uptake of Gold Nanoparticles and Their Movement in 3D Multicellular Tumor Spheroids: Effect of Molecular Weight and Grafting Density of Poly(2-hydroxyl ethyl acrylate). *Macromol Biosci* **2020,** *20* (1), e1900221.
109. C R Hopkins, I. S. T., Internalization and processing of transferrin and the transferrin receptor in human carcinoma A431 cells. *J Cell Biol.* **1983,** *97* (2), 581-21.
110. Mitchell, M. J.; Billingsley, M. M.; Haley, R. M.; Wechsler, M. E.; Peppas, N. A.; Langer, R., Engineering precision nanoparticles for drug delivery. *Nat Rev Drug Discov* **2021,** *20* (2), 101-124.
111. Xu, M.; Soliman, M. G.; Sun, X.; Pelaz, B.; Feliu, N.; Parak, W. J.; Liu, S., How Entanglement of Different Physicochemical Properties Complicates the Prediction of in Vitro and in Vivo Interactions of Gold Nanoparticles. *ACS Nano* **2018,** *12* (10), 10104-10113.
112. Li, Y.; Monteiro-Riviere, N. A., Mechanisms of cell uptake, inflammatory potential and protein corona effects with gold nanoparticles. *Nanomedicine (Lond)* **2016,** *11* (24), 3185-3203.
113. Ma, X.; Hartmann, R.; Jimenez de Aberasturi, D.; Yang, F.; Soenen, S. J. H.; Manshian, B. B.; Franz, J.; Valdeperez, D.; Pelaz, B.; Feliu, N.; Hampp, N.; Riethmuller, C.; Vieker, H.; Frese, N.; Golzhauser, A.; Simonich, M.; Tanguay, R. L.; Liang, X. J.; Parak, W. J., Colloidal Gold Nanoparticles Induce Changes in Cellular and Subcellular Morphology. *ACS Nano* **2017,** *11* (8), 7807-7820.
114. Bastus, N. G.; Comenge, J.; Puntes, V., Kinetically controlled seeded growth synthesis of citrate-stabilized gold nanoparticles of up to 200 nm: size focusing versus Ostwald ripening. *Langmuir* **2011,** *27* (17), 11098-105.
115. Schulz, F.; Homolka, T.; Bastus, N. G.; Puntes, V.; Weller, H.; Vossmeyer, T., Little adjustments significantly improve the Turkevich synthesis of gold nanoparticles. *Langmuir* **2014,** *30* (35), 10779-84.
116. Jessica Rodríguez-Fernández, J. P.-J., F Javier García de Abajo, Luis M Liz-Marzán, Seeded growth of submicron Au colloids with quadrupole plasmon resonance modes. *Langmuir* **2006 Aug,** *22, 7007-7010*.
117. Xiaohui Ji, X. S., Jun Li, Yubai Bai, Wensheng Yang, and Xiaogang Peng, Size Control of Gold Nanocrystals in Citrate Reduction: The Third Role of Citrate. *J. AM. CHEM. SOC.* **2007,** *129, 13939-13948*.
118. Wolfgang Haiss, †,‡ Nguyen T. K. Thanh,†,‡ Jenny Aveyard,† and David G. Fernig‡, determination of size and concentration of gold nanoparticles from UV-vis spectra. *Anal. Chem.* **2007,** *79, 4215-4221*.
119. Bastús, N. G.; Merkoçi, F.; Piella, J.; Puntes, V., Synthesis of Highly Monodisperse Citrate-Stabilized Silver Nanoparticles of up to 200 nm: Kinetic Control and Catalytic Properties. *Chemistry of Materials* **2014,** *26* (9), 2836-2846.
120. Jin, T.; Guo, S.; Zuo, J. L.; Sun, S., Synthesis and assembly of Pd nanoparticles on graphene

for enhanced electrooxidation of formic acid. *Nanoscale* **2013,** *5* (1), 160-3.
121. Hühn, J.; Carrillo-Carrion, C.; Soliman, M. G.; Pfeiffer, C.; Valdeperez, D.; Masood, A.; Chakraborty, I.; Zhu, L.; Gallego, M.; Yue, Z.; Carril, M.; Feliu, N.; Escudero, A.; Alkilany, A. M.; Pelaz, B.; del Pino, P.; Parak, W. J., Selected Standard Protocols for the Synthesis, Phase Transfer, and Characterization of Inorganic Colloidal Nanoparticles. *Chemistry of Materials* **2016,** *29* (1), 399-461.
122. Park, J. W.; Shumaker-Parry, J. S., Structural study of citrate layers on gold nanoparticles: role of intermolecular interactions in stabilizing nanoparticles. *J Am Chem Soc* **2014,** *136* (5), 1907-21.
123. Jokerst, J. V.; Lobovkina, T.; Zare, R. N.; Gambhir, S. S., Nanoparticle PEGylation for imaging and therapy. *Nanomedicine (Lond)* **2011,** *6* (4), 715-28.
124. Lv, R.; Feng, M.; Parak, W. J., Up-Conversion Luminescence Properties of Lanthanide-Gold Hybrid Nanoparticles as Analyzed with Discrete Dipole Approximation. *Nanomaterials (Basel)* **2018,** *8* (12).
125. Stepanenko, A. A.; Dmitrenko, V. V., Pitfalls of the MTT assay: Direct and off-target effects of inhibitors can result in over/underestimation of cell viability. *Gene* **2015,** *574* (2), 193-203.
126. O'Brien, J.; Wilson, I.; Orton, T.; Pognan, F., Investigation of the Alamar Blue (resazurin) fluorescent dye for the assessment of mammalian cell cytotoxicity. *Eur J Biochem* **2000,** *267* (17), 5421-6.
127. Yang, H.; Wang, M.; Zhang, Y.; Li, F.; Yu, S.; Zhu, L.; Guo, Y.; Yang, L.; Yang, S., Conformational-transited protein corona regulated cell-membrane penetration and induced cytotoxicity of ultrasmall Au nanoparticles. *RSC Adv* **2019,** *9* (8), 4435-4444.
128. Sousa de Almeida, M.; Susnik, E.; Drasler, B.; Taladriz-Blanco, P.; Petri-Fink, A.; Rothen-Rutishauser, B., Understanding nanoparticle endocytosis to improve targeting strategies in nanomedicine. *Chem Soc Rev* **2021,** *50* (9), 5397-5434.
129. Li, Y.; Kroger, M.; Liu, W. K., Endocytosis of PEGylated nanoparticles accompanied by structural and free energy changes of the grafted polyethylene glycol. *Biomaterials* **2014,** *35* (30), 8467-78.
130. Nold, P.; Hartmann, R.; Feliu, N.; Kantner, K.; Gamal, M.; Pelaz, B.; Huhn, J.; Sun, X.; Jungebluth, P.; Del Pino, P.; Hackstein, H.; Macchiarini, P.; Parak, W. J.; Brendel, C., Optimizing conditions for labeling of mesenchymal stromal cells (MSCs) with gold nanoparticles: a prerequisite for in vivo tracking of MSCs. *J Nanobiotechnology* **2017,** *15* (1), 24.
131. Sun, X.; Gamal, M.; Nold, P.; Said, A.; Chakraborty, I.; Pelaz, B.; Schmied, F.; von Pückler, K.; Figiel, J.; Zhao, Y.; Brendel, C.; Hassan, M.; Parak, W. J.; Feliu, N., Tracking stem cells and macrophages with gold and iron oxide nanoparticles – The choice of the best suited particles. *Applied Materials Today* **2019,** *15*, 267-279.
132. Bissardon, C.; Reymond, S.; Salome, M.; Andre, L.; Bayat, S.; Cloetens, P.; Bohic, S., Cell Culture on Silicon Nitride Membranes and Cryopreparation for Synchrotron X-ray Fluorescence Nano-analysis. *J Vis Exp* **2019,** (154).
133. Kurosaki, T.; Kitahara, T.; Kawakami, S.; Higuchi, Y.; Yamaguchi, A.; Nakagawa, H.; Kodama, Y.; Hamamoto, T.; Hashida, M.; Sasaki, H., Gamma-polyglutamic acid-coated vectors for effective and safe gene therapy. *J Control Release* **2010,** *142* (3), 404-10.
134. Jin, Q.; Paunesku, T.; Lai, B.; Gleber, S. C.; Chen, S. I.; Finney, L.; Vine, D.; Vogt, S.; Woloschak, G.; Jacobsen, C., Preserving elemental content in adherent mammalian cells for analysis by synchrotron-based x-ray fluorescence microscopy. *J Microsc* **2017,** *265* (1), 81-93.
135. Schroer, C. G.; Boye, P.; Feldkamp, J. M.; Patommel, J.; Samberg, D.; Schropp, A.; Schwab, A.; Stephan, S.; Falkenberg, G.; Wellenreuther, G.; Reimers, N., Hard X-ray nanoprobe at beamline P06 at PETRA III. *Nuclear Instruments and Methods in Physics Research Section A: Accelerators, Spectrometers, Detectors and Associated Equipment* **2010,** *616* (2-3), 93-97.

136. Mosquera, J.; Garcia, I.; Liz-Marzan, L. M., Cellular Uptake of Nanoparticles versus Small Molecules: A Matter of Size. *Acc Chem Res* **2018,** *51* (9), 2305-2313.
137. Oh, N.; Park, J. H., Endocytosis and exocytosis of nanoparticles in mammalian cells. *Int J Nanomedicine* **2014,** *9 Suppl 1* (Suppl 1), 51-63.
138. Kim, J. A.; Aberg, C.; Salvati, A.; Dawson, K. A., Role of cell cycle on the cellular uptake and dilution of nanoparticles in a cell population. *Nat Nanotechnol* **2011,** *7* (1), 62-8.
139. Park, N. O. a. J.-H., Surface Chemistry of Gold Nanoparticles Mediates Their Exocytosis in Macrophages. *ACS Nano* **2014,** *8* (6), 6232–6241.
140. Zhu, Y.; Earnest, T.; Huang, Q.; Cai, X.; Wang, Z.; Wu, Z.; Fan, C., Synchrotron-based X-ray-sensitive nanoprobes for cellular imaging. *Adv Mater* **2014,** *26* (46), 7889-95.
141. Zhu, Y.; Zhang, J.; Li, A.; Zhang, Y.; Fan, C., Synchrotron-based X-ray microscopy for sub-100nm resolution cell imaging. *Curr Opin Chem Biol* **2017,** *39*, 11-16.
142. Kong, H.; Zhang, J.; Li, J.; Wang, J.; Shin, H. J.; Tai, R.; Yan, Q.; Xia, K.; Hu, J.; Wang, L.; Zhu, Y.; Fan, C., Genetically encoded X-ray cellular imaging for nanoscale protein localization. *Natl Sci Rev* **2020,** *7* (7), 1218-1227.
143. Kikongi, P.; Salvas, J.; Gosselin, R., Curve-fitting regression: improving light element quantification with XRF. *X-Ray Spectrometry* **2017,** *46* (5), 347-355.
144. McRae, R.; Lai, B.; Vogt, S.; Fahrni, C. J., Correlative microXRF and optical immunofluorescence microscopy of adherent cells labeled with ultrasmall gold particles. *J Struct Biol* **2006,** *155* (1), 22-9.
145. Meyer-Ilse, W.; Hamamoto, D.; Nair, A.; Lelievre, S. A.; Denbeaux, G.; Johnson, L.; Pearson, A. L.; Yager, D.; Legros, M. A.; Larabell, C. A., High resolution protein localization using soft X-ray microscopy. *J Microsc* **2001,** *201* (Pt 3), 395-403.
146. Paunesku, T.; Vogt, S.; Maser, J.; Lai, B.; Woloschak, G., X-ray fluorescence microprobe imaging in biology and medicine. *J Cell Biochem* **2006,** *99* (6), 1489-502.
147. Paunesku, T.; Rajh, T.; Wiederrecht, G.; Maser, J.; Vogt, S.; Stojicevic, N.; Protic, M.; Lai, B.; Oryhon, J.; Thurnauer, M.; Woloschak, G., Biology of TiO2-oligonucleotide nanocomposites. *Nat Mater* **2003,** *2* (5), 343-6.
148. Brown, K.; Thurn, T.; Xin, L.; Liu, W.; Bazak, R.; Chen, S.; Lai, B.; Vogt, S.; Jacobsen, C.; Paunesku, T.; Woloschak, G. E., Intracellular in situ labeling of TiO(2) nanoparticles for fluorescence microscopy detection. *Nano Res* **2018,** *11* (1), 464-476.
149. Zhang, J.; Cai, X.; Zhang, Y.; Li, X.; Li, W.; Tian, Y.; Li, A.; Yu, X.; Fan, C.; Huang, Q., Imaging cellular uptake and intracellular distribution of TiO2 nanoparticles. *Analytical Methods* **2013,** *5* (23).
150. Yi, P.; Chen, G.; Zhang, H.; Tian, F.; Tan, B.; Dai, J.; Wang, Q.; Deng, Z., Magnetic resonance imaging of Fe3O4@SiO2-labeled human mesenchymal stem cells in mice at 11.7 T. *Biomaterials* **2013,** *34* (12), 3010-9.
151. Tian, F.; Chen, G.; Yi, P.; Zhang, J.; Li, A.; Zhang, J.; Zheng, L.; Deng, Z.; Shi, Q.; Peng, R.; Wang, Q., Fates of Fe3O4 and Fe3O4@SiO2 nanoparticles in human mesenchymal stem cells assessed by synchrotron radiation-based techniques. *Biomaterials* **2014,** *35* (24), 6412-21.
152. Wei, Y.; Chen, Q.; Wu, B.; Zhou, A.; Xing, D., High-sensitivity in vivo imaging for tumors using a spectral up-conversion nanoparticle NaYF4: Yb3+, Er3+ in cooperation with a microtubulin inhibitor. *Nanoscale* **2012,** *4* (13), 3901-9.
153. Huang†, M. Y. F. L. Z. C. H. H. C. Z. H. Y. C., Laser Scanning Up-Conversion Luminescence Microscopy for Imaging Cells Labeled with Rare-Earth Nanophosphors. *Analytical Chemistry* **2009,** *81* (3), 930-935.
154. Roy, P. S.; Saikia, B. J., Cancer and cure: A critical analysis. *Indian J Cancer* **2016,** *53* (3), 441-442.
155. Hausman, D. M., What Is Cancer? *Perspect Biol Med* **2019,** *62* (4), 778-784.

156. Ioanna Andreadou, W. M. P. B. M., Jan N. M. Commandeur, Eduard A. Worthington, and Nico P. E. Vermeulen, Synthesis of Novel Se-Substituted Selenocysteine Derivatives as Potential Kidney Selective Prodrugs of Biologically Active Selenol Compounds: Evaluation of Kinetics of β-Elimination Reactions in Rat Renal Cytosol. *J. Med. Chem.* **1996,** *39* (2040-2046S0022-2623).
157. Tan, C. P.; Lu, Y. Y.; Ji, L. N.; Mao, Z. W., Metallomics insights into the programmed cell death induced by metal-based anticancer compounds. *Metallomics* **2014,** *6* (5), 978-95.
158. Todd, R. C.; Lippard, S. J., Consequences of cisplatin binding on nucleosome structure and dynamics. *Chem Biol* **2010,** *17* (12), 1334-43.
159. LIPPARD, S. M. C. A. S. J., Cisplatin: From DNA Damage to Cancer Chemotherapy. *Progress in Nucleic Acid Research and Molecular Biolog* **2001,** *67*, 93-130.
160. Pons, D. G.; Moran, C.; Alorda-Clara, M.; Oliver, J.; Roca, P.; Sastre-Serra, J., Micronutrients Selenomethionine and Selenocysteine Modulate the Redox Status of MCF-7 Breast Cancer Cells. *Nutrients* **2020,** *12* (3).
161. Zhang, G.; Nitteranon, V.; Guo, S.; Qiu, P.; Wu, X.; Li, F.; Xiao, H.; Hu, Q.; Parkin, K. L., Organoselenium compounds modulate extracellular redox by induction of extracellular cysteine and cell surface thioredoxin reductase. *Chem Res Toxicol* **2013,** *26* (3), 456-64.
162. Yamashita, M., Auranofin: Past to Present, and repurposing. *Int Immunopharmacol* **2021,** *101* (Pt B), 108272.
163. Curbo, S.; Gaudin, R.; Carlsten, M.; Malmberg, K. J.; Troye-Blomberg, M.; Ahlborg, N.; Karlsson, A.; Johansson, M.; Lundberg, M., Regulation of interleukin-4 signaling by extracellular reduction of intramolecular disulfides. *Biochem Biophys Res Commun* **2009,** *390* (4), 1272-7.
164. Schneider, W. K. P. W., Chemistry of X-Ray Contrast Agents. In Contrast Agents II: Optical, Ultrasound, X-Ray and Radiopharmaceutical Imaging, . *Springer Berlin Heidelberg: Berlin, Heidelberg,* **2002**, 107-150.

Acknowledgements

Time flies, and my doctoral training is coming to an end. At this moment, sincerely thanks to Prof. Wolfgang Parak for giving me the opportunity to work in his group for my PhD study in center for hybrid nanostructure, chemistry department in Hamburg University. Thank him for his valuable advice and professional guidance in my research.

Besides, I also would like to thank Prof. Alf Mews and Prof. Tobias Beck as my co-supervisor from chemistry department, for giving me opportunity to do a poster presentation to practice my orally expression, and give me kind suggestions for my PhD study. I also want to thank Prof. Neus Feliu for offering continuous professional guidance in our cell experiments and some advice in capsule study. Thanks for Prof. Dr.Gerald Falkenberg for helping XFI.

I am also thanks to University of Hamburg for hiring a student assistant to support my PhD study during my pregnant period which help me develop my second project.

I would like to thank Leroy Neck for teaching me about synthesize iron oxide nanoparticles and capsules in my first year in our lab; also, thanks to Marvin Skiba helping me do X-ray fluoresce imaging in P06 in DESY. thanks to Dr. Dingcheng Zhu always for supporting in the experiment operation and suggestion. And thanks for Dr. Ruixia Wang always for supporting in the XFI project.

Thanks to all the colleagues in the group for their help and tolerance, which make me feel the relaxed working atmosphere and it let me feel I not lonely. This is an international team has many advanced instruments and students from various research background and different country, and it is my great honor to be a member of this group.

I am sincerely grateful to the Chinses Scholarship Council (CSC) for the financial support for my overseas studies. I will never be thankful enough to them.

Last but not the least, I am thanks to my mother-in-law, her take care of my child, let me have time to do my research. Also, thanks to my parents and husband for help me in life, always take care of me.

List of publication

1. Abdullah A. A. Ahmed, Nuria Alegret, Bethany Almeida, Ramón Alvarez-Puebla, Anne M. Andrews, Laura Ballerini, Juan J. Barrios-Capuchino1, Charline Becker, Robert H. Blick1, Shahin Bonakdar, Indranath Chakraborty, Xiaodong Chen, Jinwoo Cheon, Gerwin Chilla1, Andre Luiz Coelho Conceicao, James Delehanty, Martin Dulle, Alexander L. Efros, Matthias Epple, Mark Fedyk, Neus Feliu, Miao Feng, Rafael Fernández-Chacón, Irene Fernandez-Cuesta1, Niels Fertig, Stephan Förster, Jose A. Garrido6, Michael George, Andreas H. Guse, Norbert Hampp, Jann Harberts, Jili Han, Hauke R. Heekeren, Ulrich G. Hofmann, Malte Holzapfe, Hessam Hosseinkazemi, Yalan Huang, Patrick Huber, Taeghwan Hyeon, Sven Ingebrandt, Marcello Ienca, Armin Iske, Yanan Kang, Gregor Kasieczka, Dae-Hyeong Kim, Kostas Kostarelos, Jae-Hyun Lee, Kai-Wei Lin, Sijin Liu, Xin Liu, Yang Liu, Christian Lohr, Volker Mailänder, Laura Maffongelli, Saad Megahed, Alf Mews, Marina Mutas, Leroy Nack, Nako Nakatsuka, Thomas G. Oertner, Andreas Offenhäuser, Martin Oheim, Ben Otange, Ferdinand Otto, Enrico Patrono, Bo Peng, Alessandra Picchiotti, Filippo Pierini, Monika Pötter-Nerger, Maria Pozzi, Arnd Pralle, Maurizio Prato, Bing Qi, Pedro Ramos-Cabrer, Ute Resch Genger, Norbert Ritter, Marten Rittner, Sathi Roy, Francesca Santoro, Nicolas W. Schuck, Florian Schulz, Erkin Şeker, Marvin Skiba, Martin Sosniok, Holger Stephan, Ruixia Wang, Ting Wang, K. David Wegner, Paul S. Weiss, Ming Xu, Chenxi Yang, Seyed Shahrooz Zargarian, Yuan Zeng, Yaofeng Zhou, Dingcheng Zhu, Robert Zierold, Wolfgang J. Parak. Interfacing with the Brain: How Nanotechnology Can Contribute. ACS Nano. 2024 Aug 02. (Manuscript ID: nn-2024-105257, Review)

2. A significant part of this work is in preparation for submission: Bo Peng, Wolfgang Parak. Application of Polyelectrolyte magnetic capsule for target cells sorting. (In preparation)

3. X-Ray Fluorescence-Driven 2D and 3D Cellular Discrimination Using Inorganic Nanoparticle Tags, Ruixia Wang, Marvin Skiba, Bjorn De Samber, Bo Peng, Gerald Falkenberg, Neus Feliu Torres, Wolfgang Parak. (In preparation)

4. Different metal-based drug label cells for X-ray Fluorescence imaging. Marvin Skiba, Ruixia Wang, Bo Peng, Wolfgang Parak. (In preparation)

other contribution:

1. “Assemblies of Hybrid Nanostructures”, Charline Becker, Bo Peng, Wolfgang Parak. Conference of DFG in Hamburg. [Poster]

2. GIRLS DAY 25.4.2024 "Einblick in die Nanowissenschaften", as a part to organize “Wir kochen Nanopartikel”.

List of Hazardous substances

Sbustance	Signal word	GHS-symbols	Hazard statements	Precautionary statements
Sulfo-Cyanin5	Not hazardous substance			
oleic acid	Not hazardous substance			
Dulbecco's modified eagle medium-High glucose	Not hazardous substance			
RPMI 1640 medium	Not hazardous substance			
Phosphate buffered saline	Not hazardous substance			
0.05% trypsin/EDTA	Not hazardous substance			
Fetal bovine serum	Not hazardous substance			
Calcium chloride	warning		H319	P264+P265, P280,P305+P351+P338, P337+P317
sodium carbonate	warning		H319	P264+P265, P280,P305+P351+P338, P337+P317
bovine serum albumin	Warning		H302	P264, P270, P301+P312, P330, P501
Calcein	Warning		H302, H312, H315, H319, H332, H335	P261+ P264 +P280
poly (sodium 4-styrenesulfonate)	warning		H332	P261, P271,P304+P340, P317
poly (allylamine hydrochloride)	warning		H302, H317	P261, P264, P270,P272, P280,P301+P317,P302+P352, P321,P330, P333+P313,P362+P364, P501
ethylenediaminetetraacetic acid disodium salt	warning		H302, H312, H315, H319,	P260, P261, P264+P265,

dihydrate			H332, H335, H373, H412	P270,P271, P273, P280,P301+P317,P302 +P352,P304+P340,P30 5+P351+P338,P317, P319, P321,P330, P332+P317, P362+P364,P403+P23 3, P405, P501
Benzyl ether	warning		H317, H410	P261, P272, P273, P280, P302+P352, P333+P313
biphenyl-4-carboxylic acid	warning		H319	P264, P280, P305+P351+P338, P337+P313,
iron (III) acetylacetonate	warning		H302, H312, H332, H318	P261, P280, P301+P312, P304+P340+P312, P305+P351+P338
Gold (III) chloride trihydrate	danger		H314-H317	P305 + P351 + P338 P260, P264, P272, P280, P301, P330, P331, P303, P361, P353, P304, P340, P310, P305, P351,135 P338, P310, P333, P313, P362,P364, P405, P501
Sodium citrate	Not hazardous substance			
tannic acid	Not hazardous substance			
Silver nitrate	Warning, danger		H272+H314+ H400+H410	P210, P220, P221, P260,P264, P273, P280,P301+P330+P33 1,P303+P361+P353,P3 04+P340,P305+P351+ P338, P310,P321, P363, P370+P378,P391, P405, P501
poly (isobutylene-alt-maleic anhydride)	Not hazardous substance			

tetrahydrofuran	danger		H225, H302, H319, H335, H336, H351	P201, P202, P210, P233, P240, P241, P243, P261, P264, P270, P271, P280, P301+P312+P330, P303+P361+P353, P304+P340+P312, P305+P351+P338, P308+P313, P337+P313, P370+P378, P403+P233, P403+P235, P405, P501
dodecylamine	danger		H304, H314,H335, H373,H410	P260, P264, P271, P273, P280, P301+P310, P301+P330+P331, P303+P361+P353, P304+P340+P310, P305+P351+P338+P310, P314, P363, P391, P403+P233, P405, P501
chloroform	danger		H302, H315,H319, H331,H336, H351,H361, H372,H412	P201, P202, P260, P264, P270, P271, P273, P280, P301+P312+P330, P302+P352, P304+P340+P338, P308+P313, P332+P313, P337+P313, P362+P364, P403+P233, P405, P501
SH-PEG-CH_3O	warning		H302	P264, P270, P301+P312, P330, P501
Ethanol	danger		H225, H319	P210, P305+P351+P338, P337+P313, P403+P235
Methanol	danger		H225, H301+H311+ H331, H370	P210, P233, P280, P301+P310, P303+P361+P353, P304+P340+P311

acetone	danger		H225, H319, H336, H373	210,240, 305+351+338, 403+233
Resazurin	Not hazardous substance			
Poly-L-lysine hydrobromide	Not hazardous substance			
Sodium chloride	Not hazardous substance			
DMSO	Not hazardous substance			
Sodium Hydroxide	danger		H290, H314,H402	P234, P260, P264, P273, P280, P301+P330+P331, P303+P361+P353, P304+P340+P310, P305+P351+P338, P337+P313, P363, P390, P405,P501
Hydrochloric Acid	danger		H2901, H314,H335	P234, P261, P271, P280, P303+P361+P353, P305+P350+P338
Nitric Acid	danger		H272, H290, H314, H331	P210, P220, P280, P303 + P361 + P353, P304 + P340 + P310, P305 + P351 + P338
(n-) Hexane	danger		H225, H304, H361f, H373, H315, H336, H411	P210, P240, P273, P301+P310, P331, P302+P352, P403+P235

Declaration on oath

I hereby declare and affirm that this doctoral dissertation is my own work and that I have not used any aids and sources other than those indicated. If electronic resources based on generative artificial intelligence (gAI) were used in the course of writing this dissertation, I confirm that my own work was the main and value adding contribution and that complete documentation of all resources used is available in accordance with good scientific practice. I am responsible for any erroneous or distorted content, incorrect references, violations of data protection and copyright law or plagiarism that may have been generated by the gAI.

Date: 15. Sep. 2024

Signature: Bo PENG